10-16-2023

Mammalian Dihydropyrimidine Dehydrogenase: Employing Transient State Kinetic Methods to Determine Catalytic and Inhibitory Mechanisms

Dariush Forouzesh
Loyola University of Chicago Graduate School

LOYOLA UNIVERSITY CHICAGO

MAMMALIAN DIHYDROPYRIMIDINE DEHYDROGENASE: EMPLOYING TRANSIENT STATE KINETIC METHODS TO DETERMINE CATALYTIC AND INHIBITORY MECHANISMS

A DISSERTATION SUBMITTED TO
THE FACULTY OF THE GRADUATE SCHOOL
IN CANDIDACY FOR THE DEGREE OF
DOCTOR OF PHILOSOPHY

PROGRAM IN CHEMISTRY AND BIOCHEMISTRY

BY

DARIUSH C. FOROUZESH
CHICAGO, IL

AUGUST 2023

ACKNOWLEDGMENTS

I would like to thank everyone who made this dissertation possible, first with Dr. Graham Moran for my researcher education and the opportunity to work on this project. Thank you to Dr.'s Brett Beaupre and Joe Roman, who carried the project before I joined and demonstrated various research techniques. Thank you to Dr.'s Dali Liu and Arseniy Butrin, for collecting and refining the structural data in addition to offering insight during the analysis in this collaborative effort. I would also thank my lab colleague Madison Smith for her contributions to and continuing the project with my departure.

Thank you to the Arthur J. Schmitt Foundation for financial support during my dissertation year. Lastly, I would like to thank my parents and family for their patience and support during this entire endeavor.

TABLE OF CONTENTS

ACKNOWLEDGMENTS iii

LIST OF FIGURES AND SCHEMES vii

LIST OF TABLES x

CHAPTER 1: TRANSIENT STATE ANALYSIS OF PORCINE DIHYDROPYRIMIDINE DEHYDROGENASE REVEALS REDUCTIVE ACTIVATION BY NADPH 1
Introduction 1
Materials and Methods 6
Materials, Quantitation and Reaction Conditions 6
Expression and Purification of DPD 7
Anaerobic Methods for Transient State Observations 10
Steady-State Assay Methods 11
Evaluation of DPD Reaction Thermodynamics 12
Ligand Binding Isotherms 13
The Reaction of DPD with NADPH in the Absence of Pyrimidines 13
Single Turnover with Limiting NADPH 14
Turnover with Limiting Pyrimidine 15
HPLC Stoichiometric Analysis of Single-Turnover Reactions with Limiting NADPH 16
Results 18
Steady-State Kinetics 18
Thermodynamic Evaluation of the DPD Reaction 19
Ligand Binding Isotherms 21
Reduction of WT DPD by NADPH in the Absence of Pyrimidines 22
Single-Turnover Analysis of DPD WT and the C671S Variant 23
Discussion 32
Conclusive Remarks 42

CHAPTER 2: THE INTERACTION OF DIHYDROPYRIMIDINE DEHYDROGENASE WITH THE CHEMOTHERAPY SENSITIZER 5-ETHYNYLURACIL 43
Introduction 43
Materials and Methods 49
Materials and Quantitation 49
Expression and Purification of DPD Wild Type and Variants 50
Determination of 5EU Extinction Coefficient 51
Dissociation Constant for WT and Cys671Ser Variant

DPD•Pyrimidine Complexes 52
DPD Activity Assay 53
Anaerobic Methods for Transient-State Observations 54
Measurement of the Rate Constant for DPD Inactivation by 5EU 55
The Influence of NADP Binding on 5EU Inactivation 56
Transient-State Measurement of NADPH Oxidation Associated with 5EU Inactivation 56
Crystallization and Structure Determination of DPD•5EU Complexes 58
Model Building and Refinement 60
Results 62
Dissociation Constant for the DPD•5EU Complex 62
Measurement of the Rate Constant for DPD Inactivation by 5EU 63
The Influence of NADP Binding on 5EU Inactivation 64
Transient-State Measurements of NADPH Oxidation Associated with 5EU Inactivation 65
The Interaction of 5EU with the Cys671Ser Variant 69
Structures of DPD•5EU Complexes 70
Discussion 74
Conclusive Remarks 79

CHAPTER 3: PERTURBING THE MOVEMENTS OF HYDROGENS TO DELINEATE AND ASSIGN EVENTS IN THE REDUCTIVE ACTIVATION AND TURNOVER OF PORCINE DIHYDROPYRIMIDINE DEHYDROGENASE 81
Introduction 81
Materials and Methods 85
Materials, Quantitation and Reaction Conditions 85
Preparation of DPD and Experimental Protocols 86
Steady-State Observations of DPD Catalysis 87
Transient-State Observations 91
The Crystal Structures of the Activated C671S and C671A Variants 94
Results 98
Steady-State Rate Dependence on pH and Solvent Deuterium Fraction 98
Transient-State pH Effects on the Reductive Activation of the DPD C671S Variant 101
Spectrophotometric Deconvolution of DPD Reductive Activation 103
Structural Evidence for the Activated State of DPD 107
Transient-State Kinetic Isotope Effects 110
Discussion 112

CHAPTER 4: MAMMALIAN DIHYDROPYRIMIDINE DEHYDROGENASE 119

Introduction 119
Clinical Significance 120
Structure of DPD 123
The Interactions of Substrates within the Active Sites 129
Mechanistic Studies of DPD 132
Recent Findings that Reframe the Catalytic Mechanism of DPD 137
Reductive Activation 139
Pyrimidine Reduction 144
Conclusive Remarks 147

APPENDIX A: COMPARISON OF THE MOBILE LOOP POSITIONS IN THE DPD•5EU$_{OPEN}$ AND DPD•5EU•NADP(H)$_{CLOSED}$ COMPLEXES 155

APPENDIX B: THE NADPH BINDING POSE OF THE DPD•5EU•NADP(H)$_{CLOSED}$ COMPLEX 157

APPENDIX C: THE URACIL BINDING ISOTHERM FOR DPD COVALENTLY ACTIVATED BY 5EU 159

APPENDIX D: CRYSTAL STRUCTURE OF THE ACTIVATED FORM OF THE DPD C671A VARIANT DPD-FMN(H_2) IN THE PRESENCE OF THYMINE AND NADPH 161

REFERENCE LIST 163

VITA 176

LIST OF FIGURES AND SCHEMES

Figure 1. The Chemistry Catalyzed by DPD 1

Figure 2. The Structure of the DPD Dimer (PDB ID: 1H7X) 3

Figure 3. The DPD Hydride Transfer Reactions 4

Figure 4. Minimal Reaction Model of DPD Reductive Activation and Pyrimidine Reduction 15

Figure 5. Spectrophotometric Evidence of Anaerobic DPD Reaction Equilibrium 20

Figure 6. Ligand Dissociation Constants for DPD 22

Figure 7. Anaerobic Wild-Type DPD Reacting with NADPH 23

Figure 8. Comparison of Net Single-Turnover Reactions of Wild-Type and C671S Variant DPD 24

Figure 9. Pyrimidine Concentration Dependence on Amplitude of the Observed Second Phase in Reaction 26

Figure 10. Singular Value Decomposition Difference Spectra from the CCD data of the DPD C671S Variant in Single Turnover 27

Figure 11. C671S Variant DPD Single Turnover with Varying NADPH Concentration 29

Figure 12. Acid Quench HPLC Analysis of C671S DPD Single Turnover Reactions with Uracil or Thymine and Limiting NADPH 32

Figure 13. The Observed Positions of C671 in the Presence of 5IU alone (PDB ID: 1GTE, grey) and 5IU with NADPH (PDB ID: 1GTH, green) 37

Figure 14. Kinetic Model for DPD C671S Accounting for 2:1 Stoichiometry Observed in Limiting NADPH Single Turnover with Uracil 40

Figure 15. Chemistry Catalyzed by DPD and Cofactors Employed by the Functional DPD Dimer 44

Figure 16. Determination of the DPD•5EU Complex Dissociation Constant 65

Figure 17. The Rate and Ligand Dependence of Inactivation of DPD 64

Figure 18. Ligand-Dependent Inactivation of DPD by 5EU 65

Figure 19. 5EU Dependent Oxidation of NADPH by DPD 67

Figure 20. Spectrophotometric Evidence that Electrons Taken up during 5EU-Dependent Inactivation of DPD from NADPH Reside on a Flavin Cofactor 68

Figure 21. The Interaction of 5EU with the C671S Variant of DPD 70

Figure 22. Structural Analysis of DPD•5EU Complexes 71

Figure 23. The Proposed Chemistry of 5EU DPD Inhibition 76

Figure 24. The Chemistry Catalyzed by DPD 81

Figure 25. The Structure of Porcine Dihydropyrimidine Dehydrogenase 83

Figure 26. pH Dependence for DPD WT and C671S and Steady-State Solvent Isotope Effects for DPD WT 99

Figure 27. The Effect of pH on the Activation Phase of C671S DPD 102

Figure 28. Deconvolution of DPD C671S and C671A Activation Events 104

Figure 29. Crystal Structure of the Activated (DPD-$FMNH^-$) Form of the DPD C671S Variant in the Presence of Thymine and NADPH (PDB ID: 7M31) 108

Figure 30. Transient State Kinetic Isotope Effects on C671S DPD 111

Figure 31. Observed and Inferred Steps in DPD C671S Activation and Turnover with Thymine 117

Figure 32. Pyrimidine Catabolism 119

Figure 33. Metabolism of 5-Fluroruacil 121

Figure 34. Proposed Mechanisms for Inactivation of DPD by 5-Ethynyluracil and 5-Iodouracil 123

Figure 35. The Domains of DPD 125

Figure 36. The Conserved Electron Insertion Module 126

Figure 37. The Proposed Electron Transfer Path and Reaction Sequence of DPD 128

Figure 38. The FAD/NADPH Active Site Ligand Interactions of DPD 129

Figure 39. The $FMNH_2$/Pyrimidine Active Site Ligand Interactions of DPD 130

Figure 40. The Proposed Steps in Reductive Activation and Turnover of DPD 138

LIST OF TABLES

Table 1. Apparent Steady State Parameters of Wild-Type DPD and C671S variant DPD 18

Table 2. Crystallographic Data Collection and Model Refinement Statistics for the DPD•5EU Complexes 61

Table 3. Crystallographic Data Collection and Model Refinement Statistics for the DPD Variant Complexes 97

CHAPTER 1

TRANSIENT STATE ANALYSIS OF PORCINE DIHYDROPYRIMIDINE DEHYDROGENASE REVEALS REDUCTIVE ACTIVATION BY NADPH

Introduction

Uracil and thymine bases are the oxidant substrates for dihydropyrimidine dehydrogenase (DPD). DPD reduces the pyrimidine 5,6-vinylic bond with electrons derived from NADPH (Figure 1).

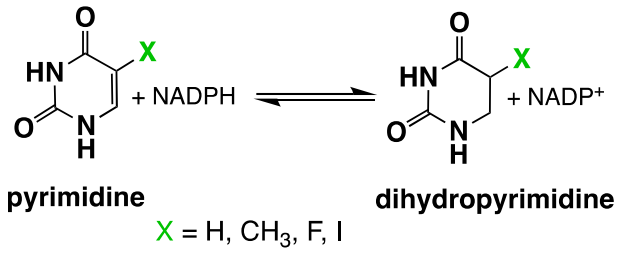

Figure 1. The Chemistry Catalyzed by DPD

This reaction is reversible and reported to be the rate-limiting step in the catabolism of pyrimidines to aminoisobutyrate (thymine) or beta-alanine (uracil)[1-5]. In addition to native pyrimidines, DPD will reduce a variety of 5-substituted uracils[1, 6, 7] including one of the most commonly prescribed cytotoxic agents used in the treatment of cancer, 5-fluorouracil (5FU). 5FU was offered as a potential tumor cell toxicant in the late 1950's in response to the discovery that rat liver tumor cells sequestered uracil at a higher rate than normal cells [8-11]. Nearly isosteric with uracil, 5FU is incorporated into

both RNA and DNA where it disrupts post-transcriptional modifications and interferes with replication[11, 12]. However, its primary mode of action is via 5FdUMP, a potent inhibitor of thymidylate synthase (TS)[13, 14]. Inhibition of TS hinders DNA synthesis and repair dictating that 5FU toxicity is heightened for cells undergoing rapid growth and division[15]. The pharmacokinetic rate of 5FU detoxification by DPD is rapid with a half-life of ~ 20 minutes[16, 17]. DPD therefore undermines the antineoplastic potential of 5FU and is a central mitigating factor in the treatment of numerous cancers[15, 18]. Modulation of DPD activity by inhibition therefore has stood as a promising path to enhanced fluoropyrimidine efficacy[15, 17-22].

Despite the importance of DPD with regard to the efficacy potential of 5FU, relatively little definitive data has been published that accounts for its catalytic behavior or inhibition, a point noted by Schnackerz et al. in the most recent review available[23]. In nature the type of chemistry catalyzed by DPD is more often catalyzed by a flavoprotein that has a single ligand binding cavity and exhibits what is known as a ping-pong kinetic mechanism. In such a mechanism the enzyme initially binds NAD(P)H and accepts a hydride. Upon the release of $NAD(P)^+$ the enzyme then acquires and reduces an oxidant substrate[24-26]. DPD accomplishes each of these steps but utilizes two ligand binding sites ~56 Å apart that each have a flavin cofactor.

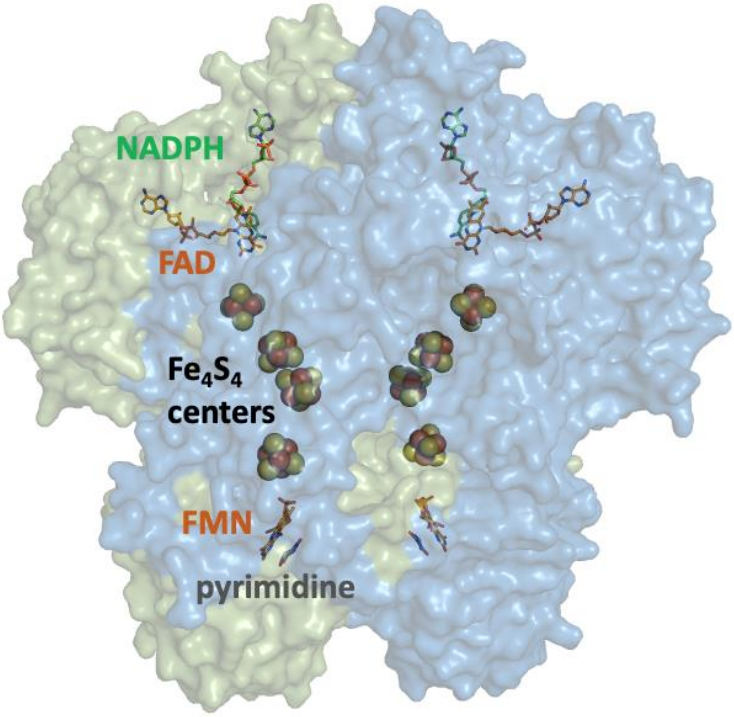

Figure 2. The structure of the DPD dimer (PDB ID: 1H7X)

The flavins of DPD are connected by an apparent wire composed of four Fe_4S_4 centers[7, 27]. The quaternary structure is a head-to-head homodimer with a large buried interface of ~10,800 $Å^2$. Each subunit has an FAD site that binds NADPH and an FMN site that binds pyrimidine bases (Figure 2). The enzyme is a functional dimer; each protomer has four Fe_4S_4 centers but each provides two of the four centers that complete the conduit in the other subunit[27]. Given the simplicity of the chemistry catalyzed, the DPD architecture is seemingly unnecessarily elaborate. Nonetheless, the enzyme's structure does not by itself indicate that the mechanism at work is anything more complex than a linear transfer of electrons from NADPH to

the pyrimidine base. What is not apparent from the structure or in any published work is where electrons reside at intervening stages of catalysis.

Much of the biochemical data published for DPD describes purification and rudimentary characterization of various homologs[1, 4, 5, 28, 29]. Two structural studies of the enzyme have been published both of which include structures of ternary complexes with NADPH and a form of pyrimidine bound[7, 27]. These ternary complex structures (PDB IDs: 1H7X, 1GT8 & 1GTH) have the ligands positioned appropriately for hydride transfer to and from the N5 of the flavins and so provide a clear understanding of the active site interactions. This has led directly to a hypothetical chemical mechanism (Figure 3)[30].

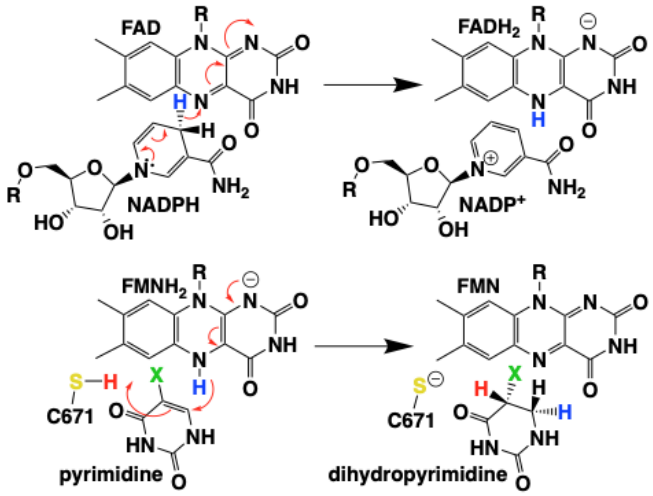

Figure 3. The DPD hydride transfer reactions

Under steady-state conditions, specific forms of DPD produce parallel lines in Lineweaver-Burk plots with respect to both substrates; traditionally interpreted as ping-pong kinetics [5, 29]. For DPD, such a mechanism suggests

an intervening reduced state of the enzyme. However, bacterial and bovine DPD exhibited steady-state kinetic patterns consistent with a rapid equilibrium random mechanism that predicts both substrates are bound prior to the chemistry[4, 31]. These apparent homolog-dependent kinetic mechanism differences are, from a chemical mechanism standpoint, not mutually exclusive and likely reflect different ligand-gated contingencies for electron transfer between the active sites. However, it is of note that by themselves, these designations or categories do not reveal specific mechanistic details. In addition, none of the steady-state analyses for DPD have considered the potential for dioxygen reactivity of reduced flavins [1, 2, 4-6, 19, 22, 28, 29, 31-35].

In 1998, Rosenbaum et al. published transient state data for DPD that were consistent with a sequential rapid-equilibrium kinetic mechanism. This study measured ligand binding equilibria and included a preliminary examination of what was described as the transient state reductive half-reaction[30]. The ligand binding data indicated low micromolar dissociation constants for uracil and NADPH. For the reductive reaction (carried out under anaerobic conditions) it was concluded that while NADPH binds and reduces the enzyme, the $NADP^+$ formed was inhibitory and prevented the rapid reduction of the majority fraction of one flavin equivalent per protomer. In the presence of uracil, the reductive reaction was said to be approximately two orders of magnitude more rapid, leading to the conclusion that pyrimidine base occupancy at the FMN site enhances the capacity for hydride

transfer at the FAD site (56 Å distant). The data from this study were not pursued in a systematic manner that would have enabled more substantial mechanistic conclusions to be drawn.

It therefore remains reasonable to state that the mechanistic understanding of DPD lags behind its therapeutic relevance and biochemical importance. Almost universally, traditional enzymological approaches based on aerobic steady-state turnover have been used to fashion a descriptive understanding of the kinetic mechanism. Here we show, using primarily transient state observations under anaerobic conditions (where appropriate), that DPD requires activation by two electrons from NADPH to constitute the catalytically active state of the enzyme. Importantly, this two-electron reduced form of DPD persists in the absence of NADPH and in the presence of pyrimidine substrate under anaerobic conditions. In the active state, occupancy of the pyrimidine and NADPH binding sites induces transmission of electrons from NADPH to the pyrimidine without evidence of the accumulation of an intervening reduced state of the enzyme. In the absence of the pyrimidine, DPD can be observed to reduce, but at a rate ~10 to 20-fold lower than the turnover number with native substrates.

Materials and Methods

Materials, Quantitation and Reaction Conditions

Competent BL21 (DE3) cells were obtained from New England Biolabs. Tris(hydroxymethyl)aminomethane (Tris), dipotassium hydrogen phosphate

(KPi), 5,6-dihydro uracil (DHU), 5,6-dihydro-5-methyluracil (DHT), ethylenediaminetetraacetic acid (EDTA), oxidized nicotinamide adenine dinucleotide phosphate ($NADP^+$), ammonium sulfate, the Miller formulation of lysogeny broth (LB) powder, ammonium acetate, sodium dodecyl sulfate (SDS), methanol, acetonitrile and trichloroacetic acid were purchased from Fisher Scientific. Dithiothreitol (DTT) and reduced nicotinamide adenine dinucleotide phosphate (NADPH) were purchased from RPI Research Products. The sodium salt of ampicillin and dextrose powder were purchased from Spectrum Chemical. 5-Methyluracil (thymine), uracil (U), and glucose oxidase were obtained from Sigma-Millipore. Streptomycin sulfate powder was made by Gibco.

All concentrations of DPD substrates and products were determined spectrophotometrically using known extinction coefficients (NADPH; ε_{340} = 6,220 $M^{-1}cm^{-1}$, $NADP^+$; ε_{260} = 17,800 $M^{-1}cm^{-1}$, uracil; ε_{260} = 8,200 $M^{-1}cm^{-1}$, dihydrouracil; ε_{225} = 1,280 $M^{-1}cm^{-1}$, thymine; ε_{264} = 7,860 $M^{-1}cm^{-1}$, dihydrothymine; ε_{225} = 1,670 $M^{-1}cm^{-1}$). All kinetic experiments were undertaken in reaction buffer (30 mM KPi, 2 mM DTT, pH 7.4) at 20°C.

Expression and Purification of DPD

The methods for expression and purification of porcine DPD was from Beaupre et al.[36]. The gene for porcine (*Sus scrofa*) dihydropyrimidine dehydrogenase (DPD) codon-optimized for heterologous expression in *E. coli*

was synthesized and subcloned by Genscript. The gene was cloned into the expression plasmid pET17b utilizing the Nde I and Xho I restriction sites. Mutation of this plasmid to produce a construct for expression of the C671S variant was also carried out by Genscript. The resulting plasmids, pSsDPD and pSsDPDC671S were transformed into *E. coli* BL21 DE3 cells, plated onto LB agar containing 100 µg/mL ampicillin and grown for 16 hours at 37 °C. Cell stocks of WT and variant forms of DPD were prepared from an isolated colony used to inoculate ~20 mL of LB broth and cultured at 37 °C with 220 rpm agitation until early log phase growth was reached. Cells in broth were added to sterile glycerol (20 % final) and were aliquoted and stored at -80 °C.

Expression of both WT and variant forms of DPD was carried out by thawing a cell stock and spread plating 100 µL onto LB agar, 100 µg/mL ampicillin (2 plates per liter of culture) and incubation for 16 hours at 37 °C. The resulting cell lawn was suspended into LB broth using a plate spreader and was used to inoculate 1 L of pre-warmed LB broth, 100 µg/mL ampicillin. Cell cultures were grown at 37 °C with shaking (220 rpm) until late log phase growth (OD_{600nm} = 0.6). The temperature was then decreased to 30 °C and left to equilibrate for 1 hour and then 100 µM iron sulfate and 1 mM sodium sulfate was added. The culture was induced with 100 µM isopropyl-β-D-1-thiogalactopyranoside and incubated at 30 °C with shaking for an additional ~20 hours.

All purification steps were undertaken at 4 °C. Cell cultures were harvested by centrifugation (4000 g for 30 min) and resuspended in 30 mM Tris, 2 mM DTT, pH 8.0 (buffer A, ~20 mL per L of culture) and placed in a stainless-steel beaker. Before sonication, FAD and FMN were each added to a final concentration of 50 μM. The slurry was then lysed with two 4 min periods of sonication using a Branson 450 sonifier set to provide 50 W of power. Lysed cells were centrifuged at 10,000 g for 45 min to pellet the cell debris. The crude supernatant was fractionated with ammonium sulfate and centrifuged at 10,000 g for 15 min. DPD was observed to precipitate between 35% and 55% ammonium sulfate saturation. The 55% ammonium sulfate pellet was re-dissolved in buffer A and diluted until conductivity was equal to or less than 6 mS. The dilute crude sample was loaded at 1 mL/min onto a 2.5 x 20 cm High Q support anion exchange column (Bio-Rad) that had been pre-equilibrated in buffer A. The column was then washed with 200 mL of buffer A before fractionation using a 400 mL gradient from 0 to 300 mM NaCl in buffer A. Eluted protein was collected as 5 mL fractions. Fractions containing DPD were pooled and concentrated using a 10 kDa nominal molecular weight cutoff centrifugal concentrator (Millipore, Amicon) until the volume was equal to or less than 2 mL. The concentrated sample was then subject to size exclusion chromatography by loading onto a 2.5 x 100 cm Sephacryl S-200, high resolution column (Pharmacia Biotech) equilibrated with 30 mM Tris, 2 mM DTT, pH 8.0. DPD was eluted with 200

mL of 30 mM KPi, 2 mM DTT, pH 7.4 (reaction buffer) and collected as 5 mL fractions. Fractions that contained pure DPD (as judged by a 280 nm:380 nm absorbance ratio of ≤ 3.5) were pooled, and concentrated. The enzyme was quantified using an extinction coefficient at 426 nm of 75,000 $M^{-1}cm^{-1}$ [36]. Aliquots of purified, concentrated DPD were stored at -80 °C.

Anaerobic Methods for Transient State Observations

All transient state observations were made using a TgK stopped-flow instrument equipped with ceramic valves and PEEK flow circuit. A 1:1 mixing ratio and a 1 cm pathlength was used for all experiments. All stated concentrations pertaining to transient state observations are post mixing. The instrument was made anaerobic by the introduction of an anaerobic solution of 20 mM KPi, 10 mM dextrose pH 7.0 with glucose oxidase (10 U/mL) for a minimum of three hours prior to experiments. Enzyme solutions were prepared anaerobically in tonometers and other glass vessels attached to a Schlenck line. Enzyme solutions were subject to 36 alternating cycles of mild vacuum (~730 mmHg) and 5 psi argon. Glucose oxidase (1 U/mL) was added from the sidearm of the tonometer. Tonometers were then mounted onto the stopped-flow instrument and mixed with substrate solutions. Anaerobic substrate solutions in reaction buffer contained 1 mM dextrose and were made anaerobic by sparging with purified argon gas for five minutes at which time 1 U/mL glucose oxidase was added and the sample mounted to the stopped-flow instrument [37].

Steady-State Assay Methods

Aerobic steady-state kinetics for DPD were determined under saturating conditions of pyrimidine (200 μM) or NADPH (200 μM) while varying the other substrate. All aerobic spectrophotometric assays were monitored with a Shimadzu UV-2600 spectrophotometer and were carried out at 20 °C in reaction buffer. Assays were initiated with the addition of DPD (0.4-1.5 μM). Reactions where quantified by observing the oxidation of NADPH at 340 nm over a period of 200 seconds, the linear rate of which was typically measured between 20 and 60 seconds.

Anaerobic steady-state parameters were measured using a stopped-flow spectrophotometer. DPD (0.92 μM) was prepared anaerobically in a tonometer. The enzyme and substrates were then combined by rapid mixing and the oxidation of NADPH observed at 340 nm and fit as above to determine rates. In these experiments, one of the two substrates was varied whilst the other was held constant and saturating. The saturating concentrations used were 75 μM U and 112 μM NADPH.

Dioxygen was also assessed as an oxidant in the steady-state. In this case the rate of turnover was measured using a Clark-type Hansetech Oxygraph electrode. The low rate of oxygen reactivity necessitated the use of relatively high DPD concentrations (4.5 μM). The 1 mL reaction contained NADPH (0-1 mM) in the presence or absence of 250 μM U and the reaction was monitored for oxygen consumption over 200 seconds. All assays were

carried out under aerobic conditions (~250 μM O_2) at 20 °C in reaction buffer. Steady state rates were measured from the data collected in the first 35 seconds.

For each steady-state experiment, the Michaelis constant (K_m) and the turnover number (k_{cat}) were determined from the fit of the initial rate dependence data to the Michaelis-Menten equation (Equation 1). To avoid unnecessary propagation of errors, the catalytic efficiency (k_{cat}/K_m) was calculated from a modified version of the Michaelis-Menten equation (Equation 2). All steady-state data dependencies were fit using the Marquardt-Levenberg least-squares routine available in KaleidaGraph Software (Synergy).

Equation 1. $$\frac{v}{e} = \frac{k_{cat}[S]}{K_m + [S]}$$

Equation 2. $$\frac{v}{e} = \frac{k_{cat}[S]}{k_{cat}/\frac{k_{cat}}{K_m} + [S]}$$

Evaluation of DPD Reaction Thermodynamics

The equilibrium position of the DPD reaction was assessed in the forward (U or T and NADPH) and the reverse (DHU or DHT and $NADP^+$) directions. The assessment was made under anaerobic conditions monitoring the consumption or formation of NADPH at 340 nm. DPD (2.43 μM for U:NADPH and for T:NADPH) was prepared anaerobically in a tonometer in a solution of reaction buffer with 1 mM dextrose. Glucose oxidase (1 U/mL) was added from the tonometer side arm prior to mounting on the stopped-

flow instrument. Substrate concentrations were each 100 μM and were prepared in reaction buffer anaerobically as described above and mounted to the stopped-flow instrument. After mixing, absorbance traces were recorded at 340 nm until the changes in absorption ceased (~2000 seconds). The data reported from these experiments were the average of three observations.

Ligand Binding Isotherms

Binding isotherms for DPD substrate and product ligands were based on perturbation of the absorption spectrum of DPD. DPD was titrated with ligand and the absorption spectra between 250 and 850 nm were recorded using a Shimadzu-2600 spectrophotometer. All spectra were corrected for dilution and the fractional changes in the absorption at 500 nm were used as a measure of the DPD•ligand ([DPD•L]) concentration. The changes in absorption were fit to the quadratic form of the single site binding equation (Equation 3) in which [DPD] is the DPD concentration, [L] is the ligand concentration, K_L is the dissociation constant of the DPD•ligand complex.

Equation 3. $$[\mathrm{DPD} \bullet \mathrm{L}] = \frac{([\mathrm{L}]+[\mathrm{DPD}]+ \mathrm{K}_L)-\sqrt{([\mathrm{L}]+[\mathrm{DPD}]+ \mathrm{K}_\mathrm{L})^2-(4[L]+[DPD])}}{2}$$

The Reaction of DPD with NADPH in the Absence of Pyrimidine

The pyrimidine independent reaction of DPD with NADPH under anaerobic conditions was observed using stopped-flow spectrophotometry. DPD in reaction buffer with 1 mM dextrose was prepared in a tonometer as

described above. This solution was then mixed with varied concentrations of NADPH (1 to 256 μM) also prepared anaerobically. The solutions were mixed and the reduction of the cofactors of DPD was monitored at 440 nm. Data obtained from pseudo-first order reactant ratios were fit to a linear combination of two exponentials according to Equation 4, where k_{obs1} and k_{obs2} are the respective observed rate constants for the two phases, ΔA_1 and ΔA_2 are the amplitudes associated with each rate constant, and C is the absorbance endpoint.

Equation 4. $$A_{Xnm} = \Delta A_1(e^{-k_{obs1}t}) + \Delta A_2(e^{-k_{obs2}t}) + C$$

Single Turnover with Limiting NADPH

Single-turnover experiments in the presence of excess saturating pyrimidine and limiting NADPH with respect to the enzyme concentration, were carried out under anaerobic conditions using stopped-flow methods. Reactions were monitored by absorption using either a charge coupled device (CCD) to gather spectra between 300 and 800 nm or by photomultiplier at 340 or 450 nm. For single-wavelength detection these positions primarily report absorption changes associated with NADPH and DPD respectively. In these experiments a tonometer containing wild-type or the C671S variant of DPD in reaction buffer with 1 mM dextrose was made anaerobic as described above and mounted onto the stopped-flow spectrophotometer. Kinetic data were the average of three observations. Reactions monitored using the CCD were collected for both short and long

time-bases to obtain optimal time resolution for successive fast and slow steps. Data were averaged from five separate observations for both time frames. These data were then stitched together into one dataset using excel software (Microsoft Corp.). The CCD data were analyzed using the SpectraFit singular value decomposition (SVD) routine available within KinTek Explorer Software (KinTek Ltd). The model free eigenvectors were used to conform the data to the minimal model shown in Figure 4 that describes three species and two successive irreversible events, by eliminating the portion of the data deemed to be noise. In this scheme the first step represents the activation of the enzyme the second step represents the concomitant consumption of NADPH and formation of dihydropyrimidine. None of the complexity associated with the exchange of ligands between these states was included as these data contain only evidence of two first order events.

Figure 4. Minimal reaction model of DPD reductive activation and pyrimidine reduction

Turnover with Limiting Pyrimidine

Transient state analysis of NADPH oxidation in the presence of limiting uracil was used to assess the dependence of the amplitudes of both phases observed at 340 nm on the pyrimidine concentration. A solution of DPD C671S variant in reaction buffer with 1 mM dextrose was prepared

anaerobically as described above and mounted onto the stopped-flow spectrophotometer. Multiple concentrations of limiting uracil (5 to 40 μM) were prepared anaerobically in reaction buffer containing 1 mM dextrose and 50 μM NADPH as described above. The solutions containing the substrates were mounted to the instrument and mixed with the enzyme. Reactions were monitored at 340 nm following the absorption changes relative to the NADPH oxidation extinction coefficient change (6,220 $M^{-1}cm^{-1}$). The amount of NADPH oxidized in each phase was estimated from the amplitudes of the absorbance changes of both phases.

HPLC Stoichiometric Analysis of Single-Turnover Reactions with Limiting NADPH

Stoichiometry of NADPH oxidation and pyrimidine reduction (uracil or thymine) during each phase of the events observed in single-turnover reactions was assessed using the C671S variant as this form of the enzyme exhibits marked separation of what are described here as successive activation and catalytic phases. HPLC product analysis conducted after the reactions were quenched at predetermined timepoints (10, 100 and 600 seconds for uracil and 10 and 80,000 seconds for thymine) was used to assess relative NADPH and pyrimidine consumption. A solution representative of time zero was made by substituting the addition of DPD with reaction buffer. This experiment used reactant ratios that support both activation and subsequent single turnover (C671S DPD (50 μM), thymine or

uracil (80 μM) and NADPH (40 μM)). The reaction also included an inert internal standard of tryptophan (100 μM) to allow normalization of the HPLC data. With the exception of the longest time point for thymine (which was prepared in a more an anaerobic cuvette), the reaction was prepared in an anaerobic vessel with a port covered by a rubber septum. Enzyme in reaction buffer with 1 mM dextrose was made prepared as described above. After anaerobic conditions were achieved, glucose oxidase (1 U/mL) was added to remove any residual oxygen. The reaction was initiated by the injection of 250 μL of an anaerobic solution giving a final concentration of 40 μM NADPH, 80 μM pyrimidine and 100 μM tryptophan. To terminate the reaction at the desired time, magnetic stirring was initiated and a 1:1 ratio of anaerobic 1 M trichloroacetic acid with 1 mM EDTA was added to the reaction vessel via the septum. The substrate and acid solution were made anaerobic by sparging with pure argon for ~5 minutes as described above. The samples were then removed from the vessel, vortexed for 2 minutes, and then centrifuged for 10 minutes at 10,000 g at 4 °C to pellet the denatured enzyme. The supernatant was collected and neutralized by titration with 3M NaOH until a pH of ~7 was recorded on litmus paper and immediately frozen at -80 °C. A 20 μL aliquot was injected onto a C18 column (Xterra 5 μm, 4.6 x 250 mm) pre-equilibrated in 10 mM ammonium acetate, 15 mM triethylamine with 1 % acetonitrile, pH 6.5 (titrated with acetic acid). The sample was eluted under isocratic conditions at 1 mL/min

and monitored simultaneously at 260 and 300 nm. On the day of analysis, a standard curve was acquired for $NADP^+$, tryptophan, and pyrimidine (thymine or uracil) and the linear dependencies were used to quantify the amount of NADPH oxidized and pyrimidine reduced during the reaction. Dihydrothymine and dihydrouracil were not quantified due to their low extinction coefficients in the near-UV region of the spectrum. NADPH was not quantified due to denaturation in acid.

Results

Steady-State Kinetics

In this study steady state kinetic experiments were used primarily to compare apparent k_{cat} values to the rate constants measured in transient state experiments. Table 1 summarizes steady-state kinetics observed for WT and the C671S variant of DPD. These data indicate k_{cat} and K_m values for the WT that are comparable to those previously published for the porcine homolog[34].

	aerobic				anaerobic						dioxygen consumption	
	WT DPD			C671S DPD	WT DPD			C671S DPD			WT DPD	
	NADPH (200 µM U)	Uracil (200 µM NADPH)	Thymine (200 µM NADPH	Uracil (200 µM NADPH)	NADPH (75 µM U)	Uracil (112 µM NADPH)	Thymine (200 µM NADPH)	NADPH (100 µM U)	Uracil (150 µM NADPH)	Thymine (150 µM NADPH)	NADPH (250 µM O_2)	NADPH (250 µM O_2, 250 µM U)
k_{cat} (s^{-1})	0.65 ±0.01	0.73 ±0.01	0.42 ±0.02	0.030 ±0.001	0.85 ±0.01	0.78 ±0.01	0.39 ±0.01	0.015 ±0.001	0.015 ±0.001	0.00024*	0.043 ±0.001	0.015 ±0.003
K_m (µM)	5.4 ±0.7	6.3 ±0.7	4.6 ±0.6	1.48 ±0.35	2.3 ±0.09	0.87 ±0.5	0.79 ±0.1	9.31 ±0.02	5.48 ±0.09	NM	NM	NM
K_{cat}/K_m ($\mu M^{-1}s^{-1}$)	0.12 ±0.01	0.11 ±0.01	0.09 ±0.01	0.02 ±0.01	0.36 ±0.08	0.90 ±0.08	0.50 ±0.07	0.002 ±0.001	0.003 ±0.001	NM	NM	NM

*taken from Figure 5, NM – not measured

Table 1. Apparent steady state parameters of wild type and C671S variant DPD

The steady-state parameters were similar when comparing those data collected under anaerobic and aerobic conditions, suggesting that dioxygen is not a significant oxidant for reduced forms of DPD in the presence of native substrates. Using dioxygen as the exclusive oxidant revealed a rate of turnover ~1/17th that observed with uracil as the oxidant. In addition, the consumption of dioxygen was suppressed by three-fold when excess uracil was added to the reaction, suggesting that electrons lost to dioxygen most often exit the enzyme through the FMN cofactor. This indicates that DPD is relatively unreactive with dioxygen and that prior steady-state observations made in atmosphere were not significantly undermined by loss of electrons via this route[1, 2, 4-6, 19, 22, 28, 29, 31-35]. The k_{cat} values are of prime relevance to this study as we have previously demonstrated that the enzyme is fully active and the turnover number will therefore correspond with the slowest step(s) observed in transient state[36]. For the wild type enzyme this value was observed to be ~0.8 s^{-1} with uracil and ~0.4 s^{-1} for thymine. The k_{cat} of the C671S variant was significantly lower and was more dependent on the identity of the oxidant substrate in that the k_{cat} with thymine, estimated at 0.00024 s^{-1} is ~60-fold lower than that with uracil at 0.015 s^{-1}.

Thermodynamic Evaluation of the DPD Reaction

While it is widely reported that the DPD reaction is reversible[1-5], the free energy change of the reaction has not been previously determined. Such a determination requires strict anaerobic conditions to avoid skewing

the measurement by incorporating the highly endergonic reduction of dioxygen. To measure the equilibrium position of the DPD reaction equimolar concentrations of pyrimidines and NADPH or dihydropyrimidines and $NADP^+$ were combined under anaerobic conditions and the consumption or production of NADPH was observed (Figure 5).

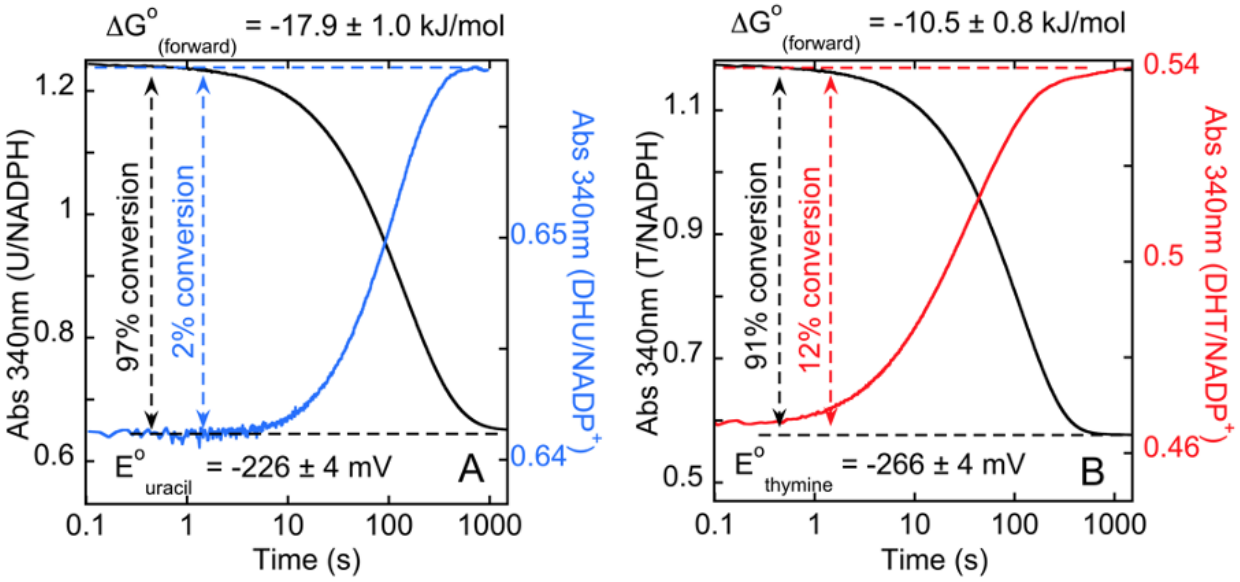

Figure 5. Spectrophotometric evidence of anaerobic DPD reaction equilibrium. A. DPD (2.43 µM) was combined in a stopped-flow spectrophotometer with either 100 µM of both NADPH and uracil (black) or $NADP^+$ and dihydrouracil (blue). B. DPD (2.43 µM) was combined in a stopped-flow spectrophotometer with either 100 µM of both NADPH and thymine (black) or $NADP^+$ and dihydrothymine (red). Data for both reactions was recorded at 340 nm for 2000 seconds. Each trace is the average of three observations.

For the U:NADPH reaction, the forward reaction was observed to be 97% converted at equilibrium. Similarly, for the reverse reaction, equilibrium was attained at 2% completion. These data indicate that the average ΔG° of the U:NADPH reaction in the forward direction is -17.9 ± 1.0 kJ/mol and that the two-electron reduction potential of the U:DHU couple is -226 ± 4 mV. For the T:NADPH reaction the forward reaction was observed to be 91%

converted at equilibrium and for the reverse reaction equilibrium was attained at 12% completion. These data indicate that the average ΔG^o of the T:NADPH reaction in the forward direction is -10.5 ± 0.8 kJ/mol and that the two-electron reduction potential of the T:DHT couple is -266 ± 4 mV. These values compare favorably with the ΔG^o of -13.3 kJ/mol for the reaction in the same direction of dihydroorotate dehydrogenase and the orotate:dihydroorotate couple of -252 mV determined by Krakow and Vennesland [38]. Sources of additional error in this data arise from changes in the spectrum of the enzyme that occur with pre-activation (see below) and varied spectral perturbation as the pyrimidine:dihydropyrimidine ratio changes. This latter complication is not significant for T/DHT but may be a small source of error for U/DHU (see Figure 6 below).

Ligand Binding Isotherms

The association of substrate and product ligands perturbs the DPD absorption spectrum providing a simple means of measuring dissociation constants for the enzyme. These values were used to define saturating ligand concentrations in transient state experiments. The K_d values measured for oxidized DPD indicate low micromolar binding for substrate pyrimidines and 4 to 20-fold weaker binding for dihydropyrimidines (Figure 6). $NADP^+$ is also observed to bind to DPD with high affinity, with a K_d of 1.6 μM (data not shown). This K_d is consistent with prior reports that show DPD reduction is hindered by $NADP^+$ that accumulates with oxidation of NADPH

and that this inhibition can be alleviated to some degree by the addition of an enzyme that reduces $NADP^+$ to NADPH[30].

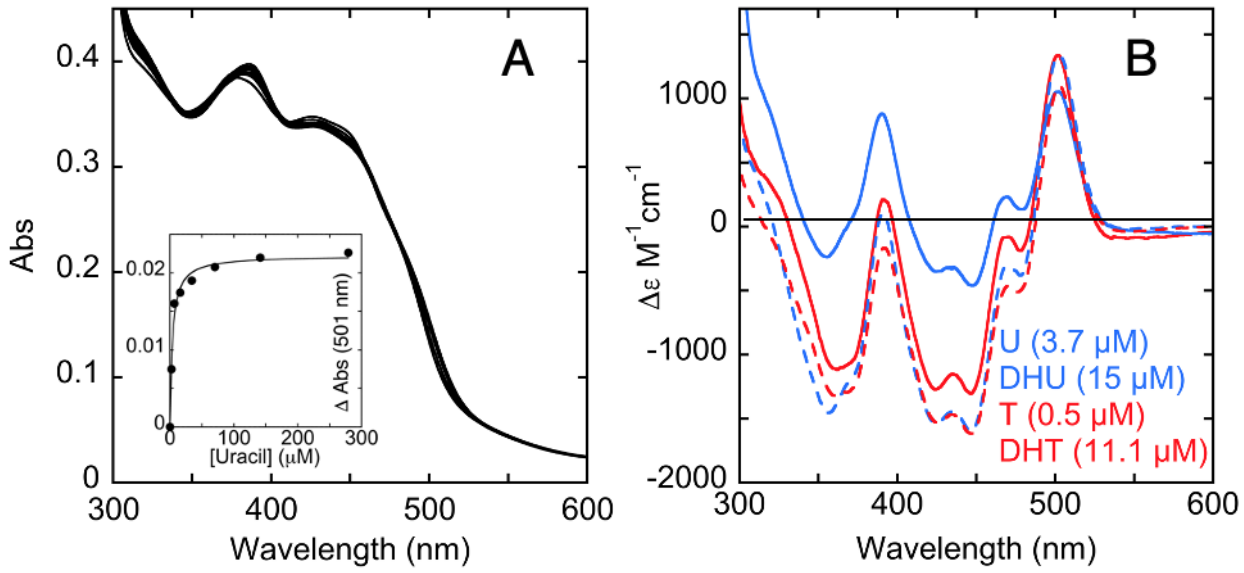

Figure 6. Ligand dissociation constants for DPD. Ligand dissociation constants were determined from perturbation of the DPD spectrum. A. Example titration of 4.5 μM DPD with uracil (0 – 256 μM). Inset depicts the change in absorbance at 501 nm plotted against the concentration of uracil and fit to Equation 3. B. The binding difference spectra observed for saturating ligands associating with DPD. Dissociation constants for the DPD•L complexes are shown in the bottom right. Uracil and thymine are depicted with solid lines while their respective products are shown in dashed lines.

Reduction of WT DPD by NADPH in the Absence of Pyrimidines

For flavoprotein dehydrogenases, it is generally possible to observe reduction of the flavin by NADPH independently by excluding the oxidizing substrate (and dioxygen). For DPD, the reduction of the enzyme was evident as modest extinction coefficient changes between 380 and 460 nm upon titration of NADPH under anaerobic conditions (Figure 7). The kinetic traces for 440 nm that were pseudo-first-order with respect to the concentration of the enzyme were fit to Equation 4. The fit to this equation returned a k_{obs1} = 2 s^{-1} for the initial phase followed by a slower phase with a rate constant

k_{obs2} = 0.04 s^{-1}. This latter phase accounted for ~75% of the overall amplitude change at 440 nm. The slow phase is 10 to 20-fold lower than the observed turnover number and thus is not catalytically relevant. The overall change in extinction coefficient for both phases was ~ 6,500 $M^{-1}cm^{-1}$, approximately equivalent to the reduction of one flavin per subunit at this wavelength. The extent of the reaction titrated with NADPH concentration indicating an equilibrium reduction process.

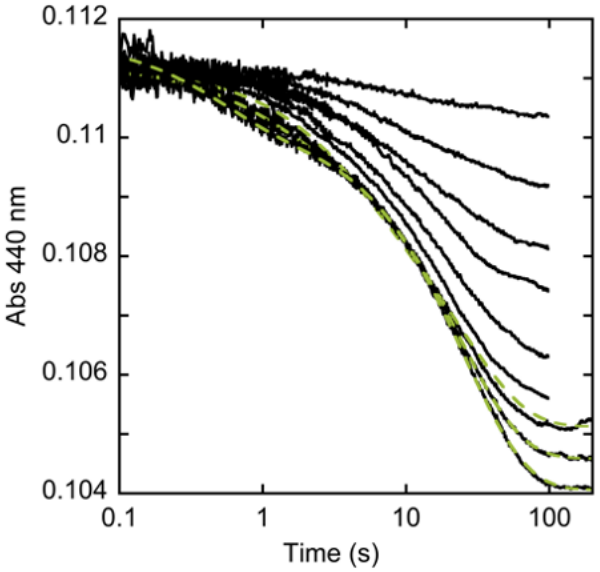

Figure 7. Anaerobic wild-type DPD reacting with NADPH. Reduction of 1.7 µM DPD when titrated with NADPH monitored at 440 nm. Traces shown top to bottom are for 1, 2, 4, 8, 16, 32, 64, 128, and 256 µM NADPH. Data for NADPH concentrations that were pseudo first order to the enzyme concentration (64, 128 and 256 µM) were fit to Equation 4.

Single-Turnover Analysis of DPD WT and the C671S Variant

Turnover of DPD in the presence of saturating oxidant pyrimidine and limiting NADPH with respect to the enzyme concentration was monitored at 340 nm using photomultiplier and/or using CCD detection (Figure 8). In all experiments, observation at 340 nm reveals two phases of decreasing absorption, similar to those seen in reductive half reaction experiments in the absence of the pyrimidine (Figure 7).

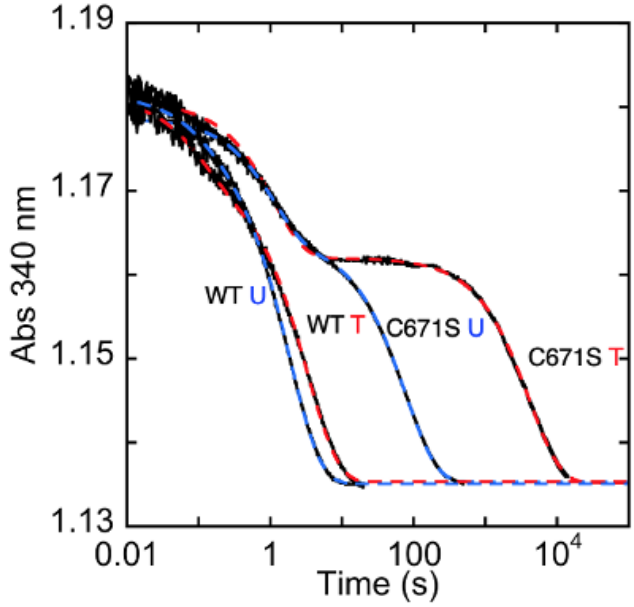

Figure 8. Comparison of net single-turnover reactions of wild-type and C671S variant DPD. Amplitudes of reaction traces were normalized to equate to 10 µM NADPH consumption. The data were fit to Equation 4 to derive estimates of the rate constants for the two phases observed. Fits are shown as individually colored dashed lines. The actual concentrations used were as follows: WT U, 12.8 µM DPD, 100 µM uracil, 7.5 µM NADPH, WT T, 12.8 µM DPD, 100 µM thymine, 7.5 µM NADPH, C671S U, 12.0 µM DPD, 100 µM uracil, 9.6 µM NADPH, C671S T, 12.0 µM DPD, 100 µM thymine, 10.0 µM NADPH.

In Figure 8, the dependence of the two phases observed in single turnover with limiting NADPH on the form of the enzyme and the substrate are compared. These data show that the rate of the first phase is dependent on the enzyme form (WT vs C671S) and that the rate of the second phase is dependent both on the form of the enzyme and on the pyrimidine substrate (U vs T). When fit to Equation 4, the first phase for the WT enzyme returned an average rate constant of 9.0 ± 0.7 s^{-1}. The first phase for the C671S variant enzyme fit to the same equation gave a rate constant ten-fold lower at 0.91 ± 0.01 s^{-1}. The second phase returned rate constants that indicate a greater dependence on the identity of the substrate pyrimidine. For WT DPD this phase was fit to 0.54 ± 0.01 s^{-1} for uracil, while for thymine the fit returned a value approximately two-fold lower of 0.31 ± 0.01 s^{-1}. The latter of these values qualitatively agrees with the measured turnover number for

this substrate with the WT enzyme (Table 1). The ~30% discrepancy in the measured rate constant and the k_{cat} value for the uracil substrate is likely a limitation of analytical fitting to exponentials. The fact that the two events captured in this trace are poorly delineated dictates that the confidence interval of the rate constants will be large relative to the fit error. When fixed to match the k_{cat} value measured in the steady state, the fit conforms to the line, but returns greater error for the parameters determined. For the C671S variant the second phase was fit to rate constants of 0.013 ± 0.001 s^{-1} and 0.00024 ± 0.00001 s^{-1} for uracil and thymine respectively; the former of which correlates well to the measured turnover number (Table 1). Interestingly, the turnover number for this variant measured under aerobic conditions is additive with the aerobic rate of dioxygen consumption in the presence of uracil for the WT enzyme, suggesting that the apparent aerobic turnover number (based on NADPH oxidation) for this variant is elevated by the reduction of dioxygen. These data show a 55-fold influence of the variant serine the thymine substrate, considerably larger than the dependence observed for the WT enzyme.

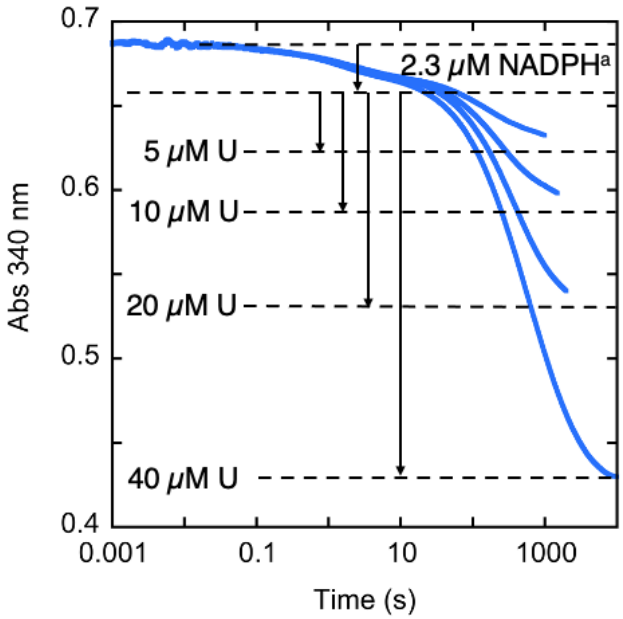

Figure 9. Pyrimidine concentration dependence on amplitude of the observed second phase in reaction. DPD C671S variant (4.2 μM) with NADPH (50 μM) was titrated with uracil (5, 10, 20, 40 μM) and monitored at 340 nm. The amplitudes of both phases of each trace are evaluated relative to the extinction coefficient change for the oxidation of NADPH (6,220 $M^{-1}cm^{-1}$) indicated as dashed lines.

In Figure 9 the amplitudes of the two phases observed were evaluated with respect to limiting pyrimidine concentration. In this experiment each uracil concentration was limiting and the amplitudes of the second phase titrated with the pyrimidine concentration indicating that uracil reduction is occurring in this phase. These traces do not end cleanly due to the ensuing slow reduction of the enzyme in the presence of excess NADPH (Figure 7) and so the traces were truncated to an early indication of slowing curvature. Data of this type was observed previously by Rosenbaum et al. [30]. The purpose of this experiment is demonstrative and so the data were not fit either analytically or to an encompassing model. The first phase is unchanging for each uracil concentration indicating that the amplitude and rate constant of this phase is independent of the uracil concentration.

Together these observations indicate that only the second phase includes reduction of the pyrimidine substrate.

In order to define the net spectrophotometric changes occurring in each the observed phases in single-turnover reactions, the C671S variant of DPD was mixed with saturating uracil and limiting NADPH and time-dependent spectral data were collected using CCD.

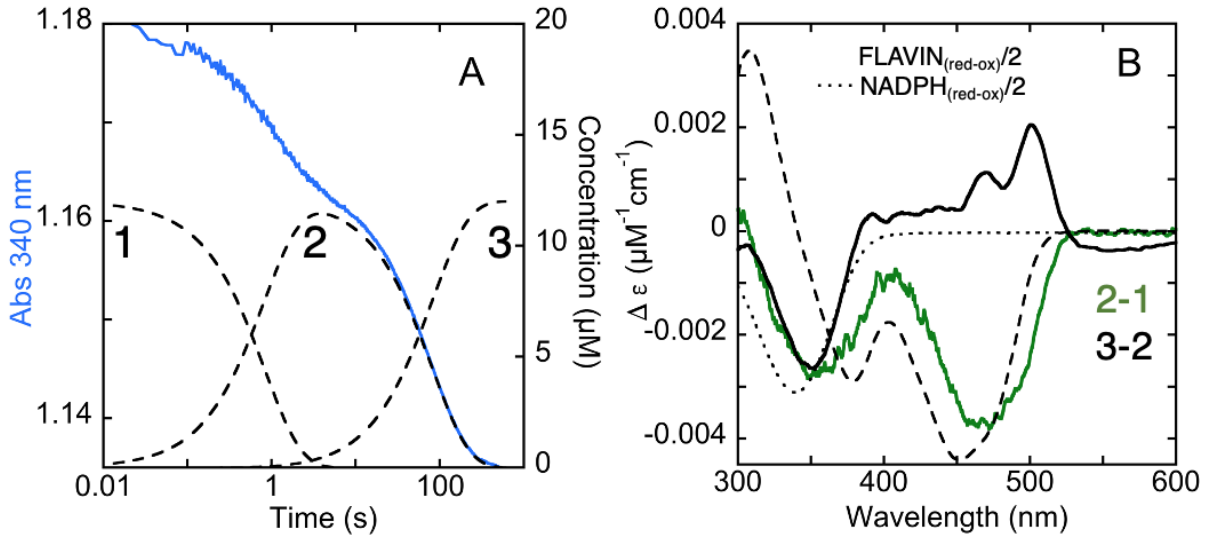

Figure 10. Singular value decomposition difference spectra from CCD data of the DPD C671S variant in single turnover. A. Representative single wavelength trace (340 nm). The C671S variant DPD (12 μM) was mixed with saturating uracil (100 μM) and limiting NADPH (10 μM) and monitored using CCD. B. Difference spectra computed from SVD deconvoluted data from CCD for species indicated as 1, 2, and 3 in A. The positions of these numbers correspond to the time of maximal concentration of each species as shown. Reference spectra for assignment of difference spectrum 2-1 are overlaid in B. These are one half equivalent for reduction of a flavin (dashes) and oxidation of one half equivalent NADPH (dots).

This experiment used the variant form of the enzyme as the two phases under study are more clearly delineated (Figure 8). Moreover, the single-turnover kinetics observed for the C671S variant with uracil is more amenable to observation within the timescales available for the stopped-flow instrument compared to the kinetics of the reaction with thymine. This dataset was deconvoluted using SVD analysis which resulted in clearly

resolved spectra for each of the three species observed. The deconvoluted spectra were used to calculate difference spectra representing the net absorption changes in both phases. The difference spectrum representative of the changes that occur in first phase (2-1 in Figure 10) indicates a decrease in extinction coefficient of ~2,800 $M^{-1}cm^{-1}$ at 340 nm and ~3,700 $M^{-1}cm^{-1}$ at 480 nm. Both of these changes are consistent with partial reduction of DPD in the first phase. Furthermore, the difference spectrum is similar in shape and intensity to one half the difference spectrum for reduction of a red-shifted flavin isoalloxazine, accounting for reduction of one flavin per dimer. The difference spectrum of the second phase (3-2 in Figure 10B) has characteristics that represent the spectral properties of both pyrimidine ligand association at 500 nm (Figure 3) and NADPH oxidation at 340 nm. Interestingly the magnitude of the change at 340 nm is similar to that observed in the first phase (2-1). This was interpreted as the difference-difference spectrum of uracil vs dihydrouracil binding that arises as this product is formed in this phase. When the final spectrum is subtracted from the initial (3-1) the difference in extinction coefficient change at 340 nm is consistent with the overall oxidation of NADPH (10 μM) expected in this reaction (not shown). However, that half this concentration was consumed in the first phase, suggests that a reductive activation of the enzyme precedes catalytic turnover. In addition, the spectral change centered around 480 nm in the first phase (2-1) does not have an equivalent

opposite change in the subsequent phase (3-2) even in the presence of excess uracil. This reveals that the changes imparted in the first phase remain in the final state, suggesting that the redox state of the enzyme at position 2 is the same as at position 3.

Figure 11A shows four single-turnover traces at 340 nm for the C671S variant reacting with excess saturating uracil and four concentrations of NADPH, each less than the enzyme concentration.

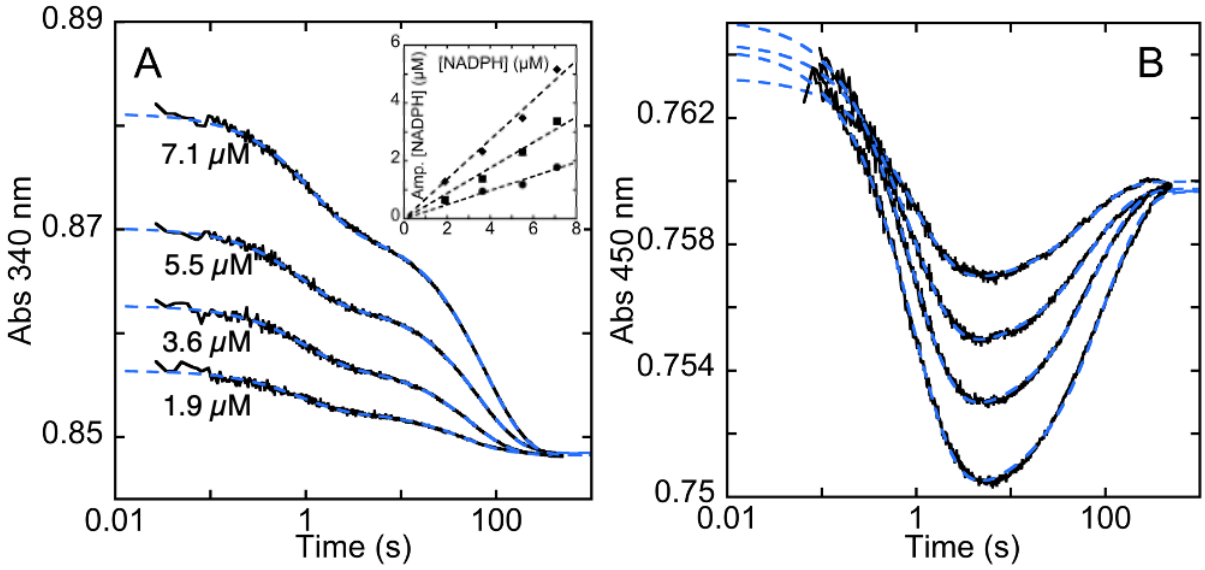

Figure 11. C671S variant DPD single turnover with varying NADPH concentration. A. DPD C671S variant (8.8 μM) with uracil (100 μM) titrating NADPH (as labeled) monitored at 340 nm. Traces were fit to a linear combination of 2 exponentials as described by Equation 4. Inset. Amplitudes of phases 1 (circles) and 2 (squares) and sum of both traces (diamond) from the fit of traces in plot A to Equation 4. B. Data from the same experiment collected at 450 nm, fit to Equation 4. For exposition of the data, both data sets were artificially adjusted to end at a common absorption value.

The data show two phases for each concentration of NADPH and were fit to Equation 4 to assess the relative amplitudes of each phase. The rate constants determined for each trace were ~1 s^{-1} and 0.015 s^{-1} in agreement with prior experiments (Figures 6 & 7, Table 1). That neither rate constant

titrates with NADPH concentration indicates that the data is not influenced by a prior equilibrium associated with binding and therefore that the affinity for this substrate is high. The ratio of the observed amplitudes is consistently 0.56 (Amp 1/Amp 2), suggesting either that the concentration of NADPH oxidized is different for each phase or that underlying absorption changes from the protein chromophores diminish or increase one or both of the observed amplitudes. Accordingly, when the sum of the amplitudes (in μM) is plotted against NADPH concentration the slope is 0.68, definitively indicating other concomitant processes decrease the overall amplitude observed by 30%. Evidence for concomitant spectrophotometric changes associated with the protein can be seen in Figure 11B for the same concentration series but observed at 450 nm, beyond the contribution of NADPH. These traces can be fit to the same rate constants derived from the fit in Figure 11A (~1 s^{-1} and 0.015 s^{-1}). This figure shows that the first phase observed in Figure 11A corresponds to a decrease at 450 nm that is also proportional in amplitude to the NADPH concentration and consistent with reduction of a flavin. The ensuing event observed at this wavelength is an increase in absorption, but the amplitude observed does not return the enzyme to the value observed at the initial state, added evidence that the chemistry of the first phase fundamentally changes the enzyme. Correlation with the data from Figure 10 indicates that this phase also includes ligand

binding perturbation differences between the uracil and dihydrouracil that arise during pyrimidine reduction (Figure 3).

In order to establish exact stoichiometries of NADPH consumption and pyrimidine reduction, acid quench experiments were conducted for single-turnover reactions of the C671S variant reacting with excess pyrimidines and limiting NADPH under anaerobic conditions. The reactions were quenched in trichloroacetic acid and returned to neutrality before HPLC analysis to quantify $NADP^+$ formed and pyrimidine consumed at specific times. In Figure 12 single-turnover traces collected at 340 nm for limiting NADPH reactions for both pyrimidine substrates are included for reference. These analyses show for both uracil and thymine that the ratio of NADPH:pyrimidine is 2:1. One half of the NADPH added is consumed in the first phase observed at 340 nm and reduction of pyrimidine occurs in the second phase during which time the remaining NADPH is oxidized. This convincingly shows that the first phase is a pre-activating reduction step that indicates, at a minimum, that the activated form of the enzyme is two-electron reduced on one subunit. Moreover, the data from Figure 10 indicate that electrons acquired during the first phase reside on a flavin cofactor and persist when the NADPH concentration is exhausted even in the presence of excess oxidant substrate.

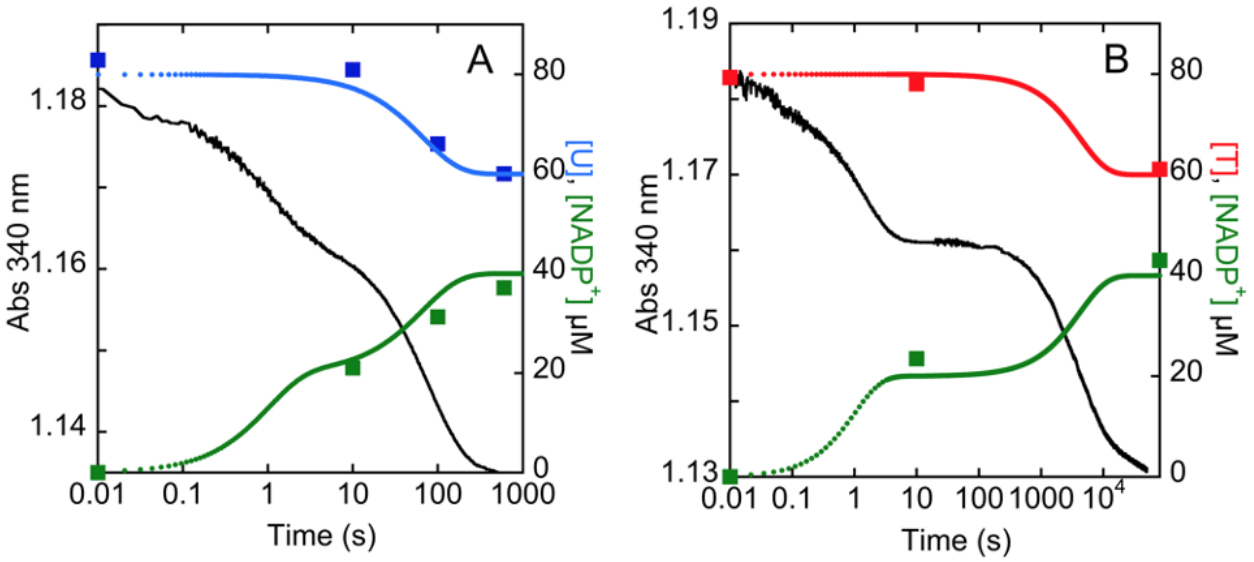

Figure 12. Acid quench HPLC analysis of C671S DPD single turnover reactions with uracil or thymine and limiting NADPH. A. DPD C671S variant (50 µM) was combined with saturating uracil (80 µM) and limiting NADPH (40 µM). B. DPD C671S variant (50 µM) was combined with saturating thymine (80 µM) and limiting NADPH (40 µM). Reactions were quenched in 1M TCA and 1 mM EDTA and neutralized. For each pyrimidine substrate the data from HPLC is overlayed with a single turnover reaction trace monitored at 340 nm with that substrate. These traces are added for correlation and are not derived from the same experiment. Theoretical curves for the accumulation of $NADP^+$ and the consumption of pyrimidine are added to plots A & B to illustrate the predicted data for the 2:1 NADPH:pyrimidine ratio proposed for activation and subsequent turnover. Concentrations of pyrimidine substrates and $NADP^+$ were determined at specific times. Points indicated at 0.01 seconds are from control samples quenched without the addition of enzyme and added as a reference representative of time zero.

Discussion

Dihydropyrimidine dehydrogenase catalyzes a relatively simple reaction involving two hydride transfers whose purpose is to reduce the pyrimidine bases uracil and thymine at the 5-6 vinylic bond to form dihydropyrimidine products (Figure 1). This activity is the initial step in the degradation of pyrimidine bases and is analogous to the reaction catalyzed by dihydroorotate dehydrogenases (DHOD) that install the 5-6 vinylic bond during pyrimidine biosynthesis. Moreover, class 1a DHODs have the same topology as domain IV of DPD[23, 27, 39]. The structure of DPD seemingly defies the simplicity of the chemistry catalyzed. Each protomer of the DPD head-to-

head homodimer has two substrate ligand binding sites each with a flavin cofactor and an apparent wire of four Fe_4S_4 centers that bridges the flavins (Figure 2). In nature, the type of chemistry catalyzed by DPD is more often achieved with a single flavin cofactor with sequential reductive and oxidative half-reactions (Figure 3), as is the case for class 1a DHODs. DPD has been studied extensively, but it should be asserted that a basis for its structural complexity has not yet been offered. In this study we use the chromophoric nature of DPD, its substrates, and products to observe WT and a variant form of the enzyme in order to formulate a model for the kinetic mechanism from single-turnover reactions.

Prior steady state analysis of mammalian DPDs have indicated both ping pong and random sequential mechanisms[5, 31]. In the case of DPD, these categories are not mutually exclusive as both substrates can and do add to the enzyme prior to catalysis and kinetic patterns consistent with a ping pong mechanism would be observed if an intervening reduced state of the enzyme were to accumulate. To some extent these prior studies highlight the extent to which traditional approaches fail to capture the complexity of two active sites linked by redox chemistry. As such, in this study we defined the chemistry and kinetic mechanism of DPD using almost exclusively transient state approaches under anaerobic conditions. These methods capture individual rate constants and stoichiometries and were employed to provide a more detailed account of the chemistry at work. Initially anaerobic

transient state experiments were used to define the energetics of the DPD reaction (Figure 8). Though the chemistry catalyzed by DPD has been consistently described as reversible[1, 2, 28, 32, 35], the degree of reversibility had hitherto not been measured. The data indicate that the reduction of pyrimidines is strongly favored to the degree that reversibility is not a significant factor in data analysis of the forward direction reaction, as depicted in Figure 1.

Despite having eight Fe_4S_4 centers per dimer, mammalian DPD enzymes can be purified in the presence of dioxygen to yield viable enzyme [29, 36]. This establishes that the iron-sulfur centers are sequestered and stable to external oxidants. Evidence for this can also be seen in oxygen consumption experiments where decoupling to dioxygen reduction occurs only in one of ~17 turnovers in a process that does not irreversibly inactivate the enzyme (Table 1). The fact that saturating pyrimidine can suppress dioxygen reduction by DPD to ~65% implies that electrons derived from NADPH either reside at or can only exit the enzyme via the FMN cofactor. In Table 1 we observe that mutation of the pyrimidine site candidate general acid, C671, to a serine slows the turnover of the enzyme by approximately 60-fold for uracil and 1,600-fold for thymine. The data presented do not provide an explanation for the 31-fold relative difference for the thymine versus uracil turnover numbers of the WT and C671S variant. That the measured turnover numbers correlate well with the second

phase observed in single-turnover reactions indicates that pyrimidine reduction is rate limiting in turnover (Figure 8). In the absence of pyrimidines and the presence of ~250 μM dioxygen, DPD reduces dioxygen at rates that are ~20-fold lower than the turnover number for uracil. This rate of turnover correlates directly to the apparent rate constant for reduction of DPD by NADPH in the absence of pyrimidine substrates (Table 1, Figure 7). This suggests that dioxygen reactivity is defined by the rate of reduction by NADPH. The data in Figure 7 were the initial indication that NADPH is oxidized by the enzyme at two rates. Characterization of these biphasic processes is the primary theme of the work presented.

The absolute requirement of the presence of the pyrimidine substrate for observation of catalytically relevant rates (Figure 7 vs Figure 8) meant that traditional approaches such as the observation of separate reductive and oxidative half reactions could not be pursued. We instead focused on the observation of single-turnover reactions with limiting substrate concentrations. In reactions where NADPH was limiting, two distinct phases are seen at 340 nm, a wavelength that captures, at a minimum, NADPH oxidation. The data shown in Figure 8 are included as justification for the predominant use of the C671S variant in this study. These data indicate that for both forms of the enzyme, the two phases are consistently observed. It also illustrates that the rate associated with the first phase is influenced by the form of the enzyme and the rate for the second phase is dependent both

on the pyrimidine substrate and the enzyme form. The rates of the two phases with the C671S variant enzyme provide a means for delineated observation of these two events. The amplitude of the second phase is proportional to the concentration of added pyrimidine indicating that the catalytic turnover of DPD is occurring in this phase (Figure 9). The preceding phase exhibits no dependence in terms of rate constant or amplitude on the concentration of the pyrimidine substrate, suggesting that this phase is a pre-activating reduction step (Figure 9). Time dependent spectra recorded in single turnover with limiting NADPH and analyzed by SVD, revealed the net absorption changes occurring in each phase observed. The difference spectrum for the first phase is consistent with both oxidation of NADPH and the reduction of a flavin at one protomer (Figure 10B). The difference spectrum for the second phase includes evidence of NADPH oxidation and spectral features associated with pyrimidine/dihydropyrimidine binding (Figure 10B vs Figure 3). Taken together, these spectra can be interpreted as phase one involving reduction of one of the two flavins of one subunit and phase two including further NADPH oxidation concomitant with reductive conversion of the pyrimidine substrate.

The net absorption changes at ~480 nm shown in Figure 10B are not consistent with reduction of one equivalent of a flavin in all DPD subunits. The change in extinction coefficient correlates only with the reduction of one flavin per DPD dimer (one half of ~7,600 $M^{-1}cm^{-1}$). Importantly, this change

in absorption at ~480 nm remains in the spectrum when the NADPH is exhausted and in the presence of excess oxidant substrate, which is strong evidence that the first phase is reductive activation. One possible explanation for the inability of pyrimidine substrates to fully oxidize the activated enzyme can be found in the available crystal structures of DPD. In the structures of the porcine enzyme in complex with 5-iodouracil, the position of cysteine 671 is apparently contingent on the occupancy of the NADPH binding site (Figure 13). In the presence of NADPH, this cysteine is equidistant at 3.9 Å from the C5 and C6 positions of the base. While in the absence of NADPH the cysteine is ~9 Å distant from the pyrimidine ring [7]. Taken together these data suggest a ligand gated conformational switch for C671 that accounts for the inability of pyrimidine to fully reoxidize activated DPD in the absence of NADPH in that the open complex does not complete the conduit for proton coupled electron transmission.

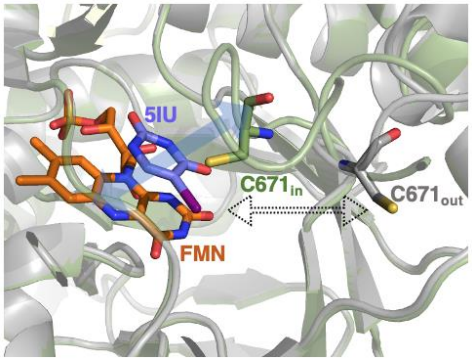

Figure 13. The observed positions of C671 in the presence of 5IU alone (PDB ID: 1GTE, grey) and 5IU with NADPH (PDB ID: 1GTH, green).

One of the most confounding features of the activation and ensuing pyrimidine reduction proposal is seen in Figure 11A. Limiting concentrations of NADPH with respect to the enzyme concentration yield biphasic traces at 340 nm. If the first phase were simply reductive activation as proposed, it stands to reason that all of the NADPH would be consumed in the activation phase. Biphasic kinetics suggests that the subunit harboring the flavin that is reduced with activation is then committed to reduction of pyrimidine in the second phase before the other subunit of the dimer is activated. It is therefore reasonable to assume that the activated subunit has considerably increased affinity for NADPH, such that it exclusively captures and utilizes the remaining NADPH. This evidence limited the number of possible models that would account for the product analysis of the C671S variant in single turnover (Figure 12). Analysis indicated that the stoichiometry of the two successive phases for NADPH and pyrimidine is 2:1 with respect to the subunit concentration. Figure 14 shows a model that accounts for the stoichiometry observed and a simulation of the biphasic data shown in Figure 11A based on this model. The model requires that after activation, unreacted NADPH would exchange with $NADP^+$ formed at the activated subunit before reduction of the pyrimidine occurs. This model was used to recapitulate the data from Figure 11A as proof of concept and is not offered as a definitive fit to the data. The simulation includes numerous ligand binding equilibria that were not defined in the current work. With the

exception of the binding of NADPH to the activated enzyme, undefined substrate binding equilibria were arbitrarily fixed to a K_d of 1 μM and undefined product binding equilibria were set to a K_d of 10 μM, with all association rate constants greater than 10^8 $M^{-1}s^{-1}$ and all dissociation rate constants fixed at 1000 s^{-1}. The rate constants for activation and pyrimidine reduction were set initially to the values determined from the analytical fits applied in Figure 11A (1.0 s^{-1} and 0.015 s^{-1}). As such convergence of the simulation and data is based only on variation of the binding constant for NADPH to the activated DPD•U•NADPH complex and the extinction coefficients associated with each phase. This simulation indicated that high affinity for NADPH in activated DPD•U•NADPH complex can account for the biphasic kinetics observed and predicts a sub-nanomolar dissociation constant for this ligand to this complex (annotated as *high affinity* in Figure 11).

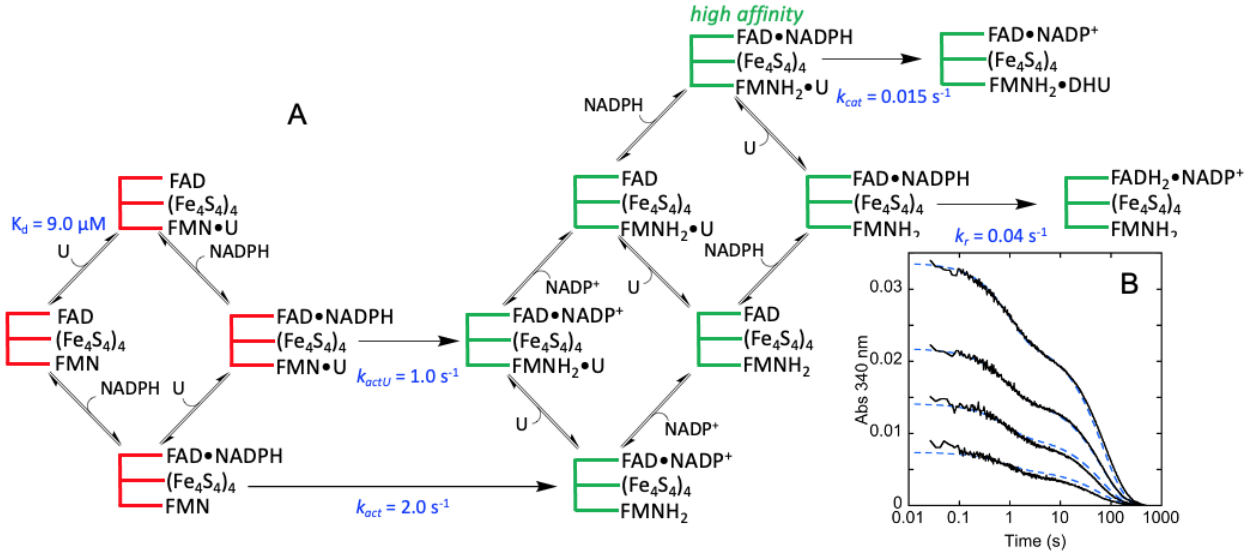

Figure 14. Kinetic model for DPD C671S accounting for 2:1 NADPH:pyrimidine stoichiometry observed in limiting NADPH single turnover experiments with uracil. A. The scheme depicts only activation and subsequent catalytic reduction of U by DPD C671S and is not inclusive of all ligand exchange equilibria. The activation and subsequent turnover of one subunit is shown using the notation of Gassner et al. (*Biochemistry* (1994) 33, 12184-12193). Activated forms of DPD are shown in green and inactive forms are shown in red. It is proposed that a parallel pathway for reductive activation of the enzyme exists in the absence of the pyrimidine substrate. Though the association of pyrimidine bridging the two pathways is depicted, no evidence for these equilibria is presented in this work. No reduced forms of Fe_4S_4 centers are shown, consistent with rapid electron transfer between active sites. B. Simulation of the biphasic kinetics shown in Figure 8A to the model shown in A. The data was modelled using enzyme and substrate concentrations shown shown for Figure 8A. With the exception of the dissociation constant for NADPH to the activated DPD•U•NADPH complex, undefined substrate binding equilibria were fixed to a K_d of 1 µM and undefined product binding equilibria were set to a K_d of 10 µM, with rapid ligand exchange rates (association rate constants > 10^8 $M^{-1}s^{-1}$ and dissociation rate constants fixed at 1000 s^{-1}). The rate constants for enzyme activation and pyrimidine reduction were fixed to the values determined from the analytical fits applied in Figure 8A (1.0 s^{-1} and 0.015 s^{-1}). The k_r step accounts for slow reduction of DPD in the absence of pyrimdine substrate, and is shown as reduction of the FAD, however, no evidence for the identity of the species reduced in this step is shown.

In the absence of other evidence, the model could imply a vestigial role for one of the two promoters in that only one is activated and subsequently reduces the pyrimidine, however, the second protomer presumably could be enlisted in subsequent turnovers and the single turnover approach used does not capture this process. The clearest evidence for this is that the turnover numbers in Table 1 correlate well with the rate constants measured for the second phase and were calculated by dividing by the DPD subunit concentration indicating both protomers are catalytic. Prior evidence indicative of alternating sites catalysis is available. In the structure

of the closed state shown in Figure 13 (PDB ID 1GTH) the catalytic state of the two subunits in this DPD dimer differs. In one subunit the 5-iodo-substituent of the pyrimidine has been eliminated suggesting completion of catalysis, while in the other subunit has the iodo-group in place [7]. Moreover, in 1998, Rosenbaum et al, observed biphasic reduction processes in the presence and absence of uracil under anaerobic conditions. In these experiments the amplitude of the initial phase at 340 nm that reports NADPH consumption, equated to approximately one half the enzyme concentration [30].

An alternative model posits cross dimer electron transfer and would require only reducing equivalents from pre-bound NADPH molecules. This model would rely on electron transfer to reduce the pyrimidine from the adjacent subunit's NADPH-FAD-iron-sulfur conduit and the closest approach for these centers is 24.5 Å, fully 15 Å further than the longest distance for proximal Fe_4S_4 centers that bridge the flavins in both subunits. It would therefore seem that the alternating subunit model is more likely.

Another consideration with regard to the design of the experiments depicted in Figures 5,7,8 & 9 is that limiting NADPH creates the possibility that the majority of the NADPH is bound. As such, the rate observed for the second phase in an alternating site model (reduction of the pyrimidine substrate) could be limited by the release rate constant for NADPH from the lagging subunit. However, the fact that the macroscopic rate constant, k_{cat},

for both enzyme forms reacting with both pyrimidine substrates agrees well with the rate constants measured for the second phase in transient state experiments (Table 1) and that these rates constants span four orders of magnitude, argues that the hydride transfer chemistry for the pyrimidine is predominantly rate limiting in catalysis.

Conclusive Remarks

The transient state single-turnover experiments shown here indicate that the reductive activation of DPD results in the reduction of one flavin per dimer consistent with alternating sites behavior. During the activation phase no evidence for reduced states of Fe_4S_4 centers is obtained. Similarly, during the ensuing turnover phase only oxidation of NADPH and absorption changes attributed to pyrimidine substrate/product binding are observed even when the turnover is as slow as 0.00024 s^{-1}. These both indicate that during pyrimidine reduction, electron transfer across the flavins and Fe_4S_4 centers is rapid relative to other process. If no intervening reduced state of the enzyme is observed, the net rate of transmission of electrons from NADPH to the pyrimidine (k_{cat}) must be determined exclusively by the rate of proton transfer from cysteine 671.

CHAPTER 2

THE INTERACTION OF PORCINE DIHYDROPYRIMIDINE DEHYDROGENASE WITH THE CHEMOTHERAPY SENSITIZER: 5-ETHYNYLURACIL

Introduction

Dihydropyrimidine dehydrogenase (DPD) catalyzes the first step in the catabolic pathway for the bases, thymine and uracil. The reaction catalyzed is two-electron reduction of the 5,6-vinylic bond of the pyrimidine substrate with electrons derived from NADPH. Such reactions are often catalyzed by flavoproteins that utilize a ping pong mechanism with an intervening reduced state of the flavin [26, 40, 41]. Indeed, Class 1 dihydroorotate dehydrogenases catalyze ostensibly the same chemistry using such a mechanism [24, 25, 42]. X-ray crystal structures of DPD reveal a seemingly unnecessarily complex architecture. DPD has two active sites each occupied by a flavin, one FAD and one FMN, that are separated by 52 Å and are bridged by a "wire" of four Fe_4S_4 centers. The FAD site interacts with NADP(H) molecules and the FMN site with pyrimidines (Figure 15). The two Fe_4S_4 centers proximal to the FMN cofactor are derived from the adjacent subunit in the obligate head-to-head oriented homodimer of 113 kDa protomers interlinked by a ~10,800 $Å^2$ interface [7, 27, 43].

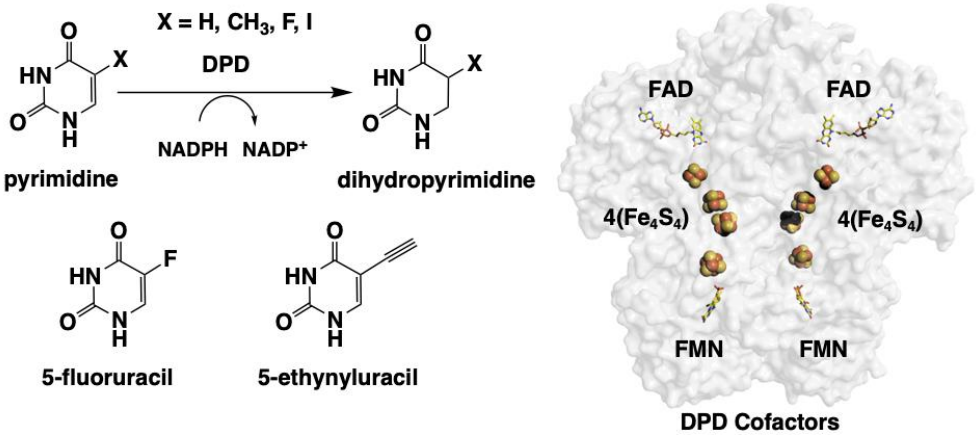

Figure 15. Chemistry catalyzed by DPD and cofactors employed by the functional DPD dimer

DPD has considerable clinical significance. The activity of DPD is the primary means of detoxification of 5-fluorouracil (5FU), one of the most highly prescribed chemotherapeutic agents that is used to treat a variety of cancers [15-17] (Figure 15). Some part of the cytotoxicity of 5FU is as a disruptor of nucleic acid metabolism via its incorporation into DNA and RNA. However, the majority of 5FU toxicity arises from being metabolized to 5-FdUMP, a potent inhibitor of thymidylate synthase (TS) [13]. Inhibition of TS reduces the cellular supply of thymidylate, thereby hindering DNA replication; 5FU is therefore particularly toxic to rapidly dividing cells. However, 5FU is a substrate for DPD, and is typically reduced and detoxified within 30 minutes of administration, undermining the efficacy arising from sustained toxicity [17]. The solution has been to administer 5FU over a period of several days via an ambulatory pump coupled to a central venous

catheter [44, 45]. Patient variability for net DPD activity also complicates dosing of 5FU. Patients exhibit a 30-fold variation in total DPD activity, dictating that dosing, as defined by the standard of care formula, results in a spectrum of responses ranging from very little toxicity and poorer outcomes, to efficacious toxicity or extremely high toxicity that can be fatal [46-48]. Inhibition of DPD has long been recognized as a means to eliminate dosing uncertainty. Moreover, the extended pharmacokinetic half-life would potentially allow the use of oral forms of 5FU, such as capecitabine, simplifying administration, lowering the financial burden and increasing compliance [49-53].

5-Ethynyluracil (5EU, eniluracil) is an analogue of uracil with an alkyne moiety substituent at the 5-carbon (Figure 15). The potential of 5EU to increase efficacy of 5FU by DPD inactivation was first realized in the early 1990's. It was shown that 5EU treatment of mice and rats could induce a linear 5FU dose to plasma concentration relationship by significantly prolonging the *in vivo* half-life of 5FU. This resulted in a 2- to 4-fold increase in the observed therapeutic index [20, 21]. Soon after, clinical trials and ensuing research articles examined 5EU as a potential adjunct chemotherapy agent [54, 55] along with consideration of the possibility of co-administration with oral 5FU-derivatives that have fewer complications in administration and higher rates of compliance [56-61]. In these studies, it was shown that in the presence of 5EU, 80% of the administered 5FU was excreted unchanged in the urine,

in contrast to the >80% detoxified by DPD in untreated patients [53]. These studies also quantified the return of DPD activity post 5EU treatment and observed an increase from 2-25% of baseline over a period of 20 days, though later studies indicated a return to baseline activity within 6 days [62]. For either case, these data indicated that 5EU produced a profound and lasting suppression of the net DPD activity that spans the period of target 5FU toxicity [58].

In clinical trials, 5EU has been shown to inhibit DPD activity and thereby sustain elevated 5FU concentrations *in vivo* [57-60]. Despite subsequent FDA approval with orphan drug status, 5EU has not yet been widely incorporated into the standard of care in clinical cancer facilities. The reason for this appears to be the lack of added benefit observed with the adopted administration strategies in conjunction with 5FU. Ten phase I and II clinical trials have evaluated the therapeutic value of 5EU. Summations of these findings suggest that the greatest benefit bestowed by 5EU co-administration is compliance in that orally available forms of 5FU are preferred by most patients [18, 51, 52, 63]. The lack of benefit designation was a stipulation of the FDA Oncologic Drugs Advisory Committee that roughly coincided with the discovery and adoption of alternative chemotherapies co-administered with 5FU such as irinotecan [64-67]. The reasons underlying why no added benefit was observed when 5EU is used in combination with 5FU continue to be analyzed and discussed [51, 68]. One possibility is that in the

majority of clinical trials the quantity of 5EU administered greatly exceeded what is required to inhibit DPD and may have encouraged off-target covalent interactions that complicated the therapy and/or diminished the efficacy of 5FU [68]. Suffice to conclude that 5EU based inhibition of DPD remains in development.

5EU was first synthesized in 1976 by Barr and coworkers with the intention that it be incorporated into nucleic acids *in vivo* in much the same manner as 5FU [69]. Schroeder et al. later recognized the capacity for thiol-specific alkylation of the ethynyl group at the 5-position of uracil [70]. However, it was Porter et al. that first identified 5EU as an inactivator of dihydropyrimidine dehydrogenase, identifying a conserved active site cysteine residue as the site of covalency in the bovine form of the enzyme [19]. When structures of porcine DPD later became available, the cysteine residue in question was observed to be the candidate general acid (C671 in porcine DPD) required to supply a proton to the 5-position during reduction of the pyrimidine at the FMN active site [7, 27, 43]. Collectively, these observations established that the mode of inhibition of DPD by 5EU was to bind in the site normally occupied by the pyrimidine substrate and cross-link with the active site cysteine general acid. This alteration potentially both occludes access to the pyrimidine binding site and severs the capacity to couple the movement of electrons and protons during catalysis.

The detailed kinetics and X-ray crystal structure of 5EU interacting with DPD have not been published. The 1992 Porter et al. study defined much of what is currently understood of 5EU's interaction with DPD [19]. This study measured a k_{inact} value and definitively identified the cysteine residue modified by 5EU during inactivation. Here we present the direct observation of the inhibition of DPD by 5EU. We have observed that 5EU inhibition occurs concomitantly with reduction of DPD by NADPH. Despite that thiol-yne covalent cross-linking does not require an external source of electrons, covalent linkage of 5EU to the active site catalytic cysteine is directly linked to the two-electron reduction of the enzyme. In a series of inhibition trials with 5EU and NADP analogues, complete inactivation of DPD was observed only in the presence of NADPH. The net changes in the absorption spectrum of DPD during crosslinking suggest that the electrons added from NADPH reside on one of the two flavin cofactors. Our data indicates that two-electron reductive activation of DPD is required for crosslinking as this process induces a conformational change that places the active site cysteine acid adjacent to the 5EU alkyne group. Three X-ray crystal structures were solved that together describe the sequence of steps required for inactivation, define the orientation of 5EU in the pyrimidine active site and establish the dominant position of crosslinking.

Materials and Methods

Materials and Quantitation

Uracil, thymine, dimethyl sulfoxide (DMSO, & D_6-DMSO), iron (II) sulfate ($FeSO_4$), disodium sulfate (Na_2SO_4), sodium dithionite ($Na_2S_2O_4$), glycerol, and isopropyl-β-D-1-thiogalactopyranoside (IPTG) were purchased from Acros Organics. Oxidized nicotinamide adenine dinucleotide phosphate ($NADP^+$) was obtained from Alfa Aesar while the reduced form (NADPH) was obtained from Amresco. Lysogeny Broth (LB) agar tablets were bought from Bio 101, Inc. Sodium chloride (NaCl), ethylenediaminetetraacetic acid (EDTA), ampicillin, diammonium sulfate ($(NH_4)_2SO_4$), sodium citrate dihydrate (NaCT), HEPES, and tri(hydroxymethyl)aminomethane (Tris) were purchased from Fischer Scientific. The plasmids used for expression of DPD wild type and variants were obtained from Genscript, and competent BL21(DE3) cells were obtained from New England BioLabs. Dibasic potassium phosphate (K_2HPO_4) and glucose oxidase were purchased from Millipore/Sigma Corp. The Miller formulation of lysogeny broth powder (LB), dithiothreitol (DTT), and flavin adenine dinucleotide (FAD) were obtained from Research Products International. Dextrose (D-glucose) was purchased from Spectrum Chemical. 5-Ethynyluracil and flavin mononucleotide (FMN) were obtained from TCI America. 6-Dihydro-NADP (6DHNADP) was prepared as previously described [71].

Concentrations of DPD substrates and products were determined spectrophotometrically using the following extinction coefficients (NADPH; ε_{340} = 6,220 $M^{-1}cm^{-1}$, $NADP^+$; ε_{260} = 17,800 $M^{-1}cm^{-1}$, uracil; ε_{260} = 8,200 $M^{-1}cm^{-1}$, thymine; ε_{264} = 7,860 $M^{-1}cm^{-1}$). The extinction coefficient used to quantify all forms of DPD was ε_{426} = 75,000 $M^{-1}cm^{-1}$ [36]. All concentrations indicated are post-mixing.

Expression and Purification of DPD Wild Type and Variants

Purification of porcine recombinant DPD and its variant forms was based on previous methods with alterations made to improve yield [29, 30, 36]. The DPD expression plasmid, pSsDPD, was transformed into BL21(DE3) *E. coli* and stored at -80 °C from early log phase LB cultures as 20% glycerol stocks. For expression, cell stocks were thawed and spread (100 µL/plate) onto LB agar with 100 µg/mL ampicillin selection and grown at 37 °C for 16 hours. Cell lawns were resuspended into sterile LB broth and added to bulk LB media with 100 µg/mL ampicillin and grown at 37 °C with shaking (220 rpm) to an optical density of ~0.5 at 600 nm. The temperature was then lowered to 30 °C for an hour before the introduction of 200 µM $FeSO_4$ and 1 mM Na_2SO_4 to the media. IPTG (100 µM final) was then added and the culture was incubated with shaking for an additional 20 hours. Cells were harvested and resuspended in 30 mM Tris buffer, 1 mM EDTA, and 2 mM DTT, pH 8.0 (equilibration buffer) with 50 µM of both FAD and FMN added.

Cells were sonicated on ice, and the cell debris was removed by centrifugation at 10,000 g for 45 min. The supernatant was then collected and brought to 35% $(NH_4)_2SO_4$ saturation before centrifuging at 10,000 g for 15 min. The resulting supernatant was then brought to 55% $(NH_4)_2SO_4$ saturation before centrifuging at 10,000 g for 15 min. The pellet was then resuspended in a quantity of equilibration buffer sufficient to bring the conductivity to <5 mS/cm before loading onto a preequilibrated Q-Sepharose anion exchange column connected to a Bio-Rad NGC FPLC system. A gradient to 300 mM NaCl in equilibration buffer was used to fractionate and elute bound proteins. Individual 5 mL fractions were assayed for activity before pooling the enzyme. The pooled enzyme was then concentrated to approximately ~2 mL and loaded onto a 26 x 1000 mm Sephacryl S-200 size exclusion column preequilibrated with 30 mM K_2HPO_4, 2 mM DTT, pH 7.4 (reaction buffer). The protein was eluted with reaction buffer and 5 mL fractions were collected. SDS-PAGE was used to assess purity and identify fractions to combine for storage. DPD samples were tested for activity and concentrated before storing at -80 $^{\circ}$C as ~100 µL aliquots.

Determination of 5EU Extinction Coefficient

The extinction coefficient for 5EU was determined by NMR using an internal standard of known concentration. Solutions of 5EU and thymine (~20 mM) were prepared separately in D_6-DMSO and the absorption

spectrum of each was collected using a Shimadzu UV-2600 spectrophotometer. The concentration of the thymine was determined using its known extinction coefficient (ε_{265} = 7,680 $M^{-1}cm^{-1}$). ^{1}H NMR spectra in D_6-DMSO were collected separately for the 5EU and thymine solutions. The 5EU and thymine samples were then combined in equal volume and the ^{1}H NMR spectrum of the mixture was recorded. The concentration of 5EU was then derived using thymine as the internal standard. The per-proton integration ratio for thymine in relation to that of 5EU was used to calculate the 5EU concentration and obtain its extinction coefficient spectrum.

Dissociation Constant for WT and Cys671Ser Variant DPD•pyrimidine Complexes

Binding isotherms for DPD•pyrimidine complexes were based on equilibrium perturbation of the absorption spectrum of DPD. Dissociation constant measurements were carried out at 20 °C in reaction buffer. DPD was titrated with ligand and an absorption spectrum (250 to 850 nm) was recorded for each addition of pyrimidine. Spectra were corrected for dilution and the fractional change in absorption at wavelengths where perturbation was largest were used as a measure of the DPD•pyrimidine complex ([DPD•Pyr]) concentration. The changes in absorption were fit to the quadratic form of the single site binding equation (Equation 5) in which [DPD] is the DPD concentration, [Pyr] is the pyrimidine concentration, and K_{Pyr} is the dissociation constant of the DPD•Pyr complex.

Equation 5. $$[\mathrm{DPD} \bullet \mathrm{Pyr}] = \frac{([\mathrm{Pyr}]+[\mathrm{DPD}]+ \mathrm{K_{Pyr}})-\sqrt{([\mathrm{Pyr}]+[\mathrm{DPD}]+ \mathrm{K_{Pyr}})^2-4([\mathrm{Pyr}]+[\mathrm{DPD}])}}{2}$$

DPD Activity Assay

Steady-state assays were used to determine the activity specific to DPD in crude and purified samples. DPD was added to a quartz cuvette containing reaction buffer with 200 μM NADPH. The reaction was monitored at 340 nm for ~100 seconds to assess the background rate of NADPH oxidation ($\Delta\varepsilon$= 6,220 M^{-1} cm^{-1}) that arises either from the activity of contaminant proteins and/or from the futile reduction of dioxygen [72]. After the period of background rate assessment, 100 μM uracil was added and the reaction was monitored for a further 100 seconds. The rate attributed to DPD was the difference of the two rates measured.

Michaelis-Menten analysis of the DPD Cys671Ser variant that reduces 5EU as a substrate was carried out in reaction buffer at 20 °C under anaerobic conditions using the double mixing mode of a Hi-Tech stopped-flow spectrophotometer (TgK Scientific). The enzyme was prepared anaerobically in a tonometer by exchanging argon for dissolved oxygen using a Schlenk line. The sample was subject to 30 alternating cycles of vacuum and argon gas with gentle agitation of the sample after each set of 3 cycles to promote exchange of dissolved gases. Once anaerobic, 2 U/mL glucose oxidase was added from the tonometer side arm. Substrate solutions were prepared in glass syringes. After the addition of 1 mM glucose

the solutions were depleted of oxygen by inverting and sparging with argon gas for 5 minutes. After sparging 2 U/mL of glucose oxidase was added and the sample was mounted onto the stopped-flow system [37]. For each assay the final concentrations were as follows, 1.96 μM DPD was mixed with varied concentrations of 5EU (0.24-128 μM) aged for 0.01 seconds, mixed with 250 μM NADPH and the reaction was monitored at 340 nm. Initial rates were determined from the first 50 seconds of turnover by fitting to a straight line. The observed reaction rates (v) were then plotted against the 5EU concentration and fit to the Michaelis-Menten equation (Equation 1).

Anaerobic Methods for Transient-State Observations

Transient-state inactivation measurements were made using a stopped-flow spectrophotometer. Experiments used either single mixing (1:1) or double mixing ((1:1):1) sequences. All transient-state observations were made under anaerobic conditions. The enzyme and substrate solutions were prepared anaerobically as described above. The sample chambers of the stopped-flow instrument were filled with an oxygen reactive solution for a minimum 3 hours prior to experiments. This solution, 30 mM KPi, 1 mM glucose pH 7.5, was added to the main chamber of the tonometer and was prepared anaerobically as described above. Once anaerobic, 2 U/mL glucose oxidase was added from the tonometer side arm and the solution was introduced to the instrument to remove any residual dioxygen.

Measurement of the Rate Constant for DPD Inactivation by 5EU

The rate constant associated with inactivation of DPD by 5EU was measured in 30 mM K_2HPO_4, pH 7.4. The reductant DTT was removed to avoid the potential for 5EU inactivation that was induced by adventitious reduction. The residual activity of DPD (2 μM) was measured after the enzyme was mixed either with 5EU (200 μM) or 5EU and NADPH (200 and 100 μM respectively) and aged prior to the addition of native substrates, uracil and NADPH. The enzyme and substrate solutions were prepared anaerobically as described above. Double mixing stopped-flow was used to initially age the reaction for a specified period and then mixed with saturating uracil (100 μM) and NADPH (100 μM) to observe residual activity based on the oxidation of NADPH at 340 nm. The steady-state rate data for individual age-times were fit to straight lines based on the initial rate of turnover measured from 5-10 seconds after the second mix (that introduced saturating concentrations of substrates). Initial uninhibited activity (100% activity) was based on an age-time of 0.01 seconds. The percent residual activity was plotted against the age-time and the data were fit to a single exponential according to Equation 6 to define the rate constant for inactivation. In this equation, k_{inact} is the rate constant, %Act. is the residual activity, Δ%Act. is percent inactivation, t is time, and C is the percent residual activity at infinite time.

Equation 6. $$\%Act. = \Delta\%Act.(e^{-k_{inact}t}) + C$$

The Influence of NADP Binding on 5EU Inactivation

The effect of NADP analogue binding at the FAD site on DPD inactivation by 5EU was tested by incubation of the enzyme with the inhibitor and an NADP analogue followed by assessment of residual activity. For each analogue, a sample of 50 μM DPD was divided in two and one of the samples was incubated with 2 mM 5EU and 1 mM of either NADPH, $NADP^+$ or 6DHNADP for ~5 min at 4°C. The untreated sample was kept as an activity control. After 5 minutes, ligands were removed by a ~40,000-fold buffer exchange using 15 mL Amicon centrifugal 10 kDa nominal molecular weight cutoff filters. The untreated control samples were subject to an equal number of buffer exchange cycles. The treated and untreated samples were then assayed for activity as described above with native substrates, NADPH and uracil. Control samples were also assayed before incubation to determine initial activity to correct for activity loss was a result of mechanical handling during buffer exchanges.

Transient-State Measurement of NADPH Oxidation Associated with 5EU Inactivation

The rate constant and approximate stoichiometry for 5EU-dependent oxidation of NADPH was measured by mixing DPD with 5EU and NADPH and observing the oxidation of NADPH at 340 nm under anaerobic conditions. Individual DPD samples were made anaerobic by adding concentrated (392 μM) aerobic enzyme to buffer pre-sparged with purified argon in the

presence of the glucose/glucose oxidase scrubbing system described above. DPD (2.5, 5, 10, 20 μM final) was mixed with 100 μM 5EU and 50 μM NADPH under anaerobic conditions. The data were fit to an exponential plus a straight line according to Equation 7 to obtain both an estimate of the NADPH oxidation rate constant and the amplitude of the exponential phase as a measure of the concentration of NADPH consumed. The straight-line term was included to account for an apparent non-catalytic NADPH oxidation/DPD reduction that occurs after the initial exponential process [72]. The terms in Equation 7 are: Abs_{340}; the absorbance at 340 nm, ΔAbs_{340}; the amplitude of the absorbance change at 340 nm, k_{obs}; the observed rate constant, m; the slope of the line for non-catalytic NADPH oxidation, t; time, and C; the absorbance value at infinite time for the exponential phase.

Equation 7. $$Abs_{340} = \Delta Abs_{340}(e^{-k_{obs}t}) + mt + C$$

The net absorption changes associated with the 5EU/NADPH-dependent inactivation of DPD were observed using a charge-coupled device (CCD) detector connected to the stopped-flow system in single-mixing mode. A tonometer containing 5.6 μM DPD was made anaerobic and mixed with 100 μM NADPH and 200 μM 5EU, and the resulting changes were monitored for 60 seconds. The net absorption change spectrum was obtained by subtracting the CCD spectra acquired at 50 seconds from that acquired at 1.0 second. Absorption traces at 340 and 463 nm were extracted from the CCD spectral data set and fit to Equation 8 that describes a single

exponential phase. In the general form of this equation, k_{obs} is the observed rate constant, Abs_X is the absorbance at wavelength X, ΔAbs_X change in absorption at wavelength X, t is time, and C is the absorbance value at infinite time.

Equation 8. $$Abs_X = \Delta Abs_X(e^{-k_{obs}t}) + C$$

Crystallization and Structure Determination of DPD•5EU Complexes

Structures representing the stages of DPD inactivation were captured using X-ray crystallography. In each case, DPD crystals were grown and harvested in the dark to prevent photo-degradation of the somewhat labile FMN cofactor[73].

The DPD•$5EU_{open}$ complex was obtained by co-crystallization using the hanging drop, vapor diffusion method. Drops were formed by a variation of the reported conditions of Dobritzsch et al., by mixing 3 µL of 39 µM of DPD, 1 mM 5EU, 1 mM NADPH in 25 mM HEPES, 10 mM DTT, 10% glycerol pH 7.5 with 3 µL of well solution (1 mL) containing 50-200 mM NaCl, 19% PEG 6000, 1 mM DTT pH 4.8 [27]. Rectangular hexahedron crystals grew in ~16-20 hours to a size of approximately 50 x 200 x 20 µm. Crystals were cryo-protected for data collection by mounting in a loop and soaking briefly in a solution containing 100 mM NaCl, 19% PEG 6000, 20% glycerol, 1 mM DTT pH 4.8. Mounted crystals were then frozen by plunging into liquid nitrogen. Monochromatic X-ray diffraction data were collected at the Life Science Collaborative Access Team LS-CAT beamline 21-ID-D at the Advanced

Photon Source at Argonne National Laboratory. Data were collected at a wavelength of 1.127 Å and a temperature of 100 K using a Dectris Eiger 9M detector. Data sets were processed and analyzed with Xia2 software[74, 75]. Data processing statistics are given in Table 1.

The DPD•5EU•NADP(H)$_{closed}$ and DPD-5EU•NADP(H)$_{covalent}$ complexes were obtained by soaking. In each case DPD was crystallized by the vapor diffusion, hanging drop method by mixing 3 µL of 39 µM DPD in 25 mM HEPES, 2 mM DTT, 10% glycerol, pH 7.5 with 3 µL of well solution containing 100 mM NaCl, 2 mM DTT, 18% PEG 6000, pH 4.7. Rectangular hexahedron crystals grew in ~16-20 hours to a size of approximately 50 x 200 x 20 µm. For the DPD•5EU•NADP(H)$_{closed}$ complex the crystals were soaked for 20 minutes in 25 mM HEPES, 100 mM NaCl, 2 mM DTT, 100 µM NADPH, 100 µM 5EU, 20% PEG 6000, 20% PEG 400, pH 7.5. Crystals were then frozen by plunging into liquid nitrogen. To obtain the DPD-5EU•NADP(H)$_{covalent}$ complex, the wells containing the crystals were made anaerobic by an addition of $Na_2S_2O_4$ to 10 mM and re-sealed with the cover slide before transfer to a Plas-Labs 830 series glove box housing a Motic binocular microscope coupled to a Accu-Scope Excelis 1080p camera projecting images to an 11.6 inch HD monitor. The glove box atmosphere was depleted of dioxygen by flushing with nitrogen gas. Total oxygen partial pressure inside the glove box was at most 0.4% during crystal handling. The crystals were soaked for 2 hours in 25 mM HEPES, 100 mM NaCl, 2 mM DTT,

100 μM NADPH, 100 μM 5EU, 20% PEG 6000, 20% PEG 400, pH 7.5 and then frozen in liquid nitrogen before being removed from the glove box. Diffraction data for the DPD•5EU•NADP(H)$_{closed}$ and DPD-5EU•NADP(H)$_{covalent}$ complexes were collected at 100 K at the Life Science Collaborative Access Team (LS-CAT) beamline 21-ID-D of the Advanced Photon Source at Argonne National Laboratory. The beamline was equipped with a Dectris Eiger 9M detector. The wavelength was fixed at 0.97856 Å. Data sets were processed and analyzed with Xia2 software, and data processing statistics are given in Table 1.

Model Building and Refinement

The DPD structure was solved by molecular replacement using PHASER in Phenix[76, 77]. The starting search model was the previously published structure of DPD (PDB code: 1H7X). The model building and refinement were accomplished in Coot[78] and Phenix, respectively, as an iterative process until the lowest possible R_{free}/R factor values were attained. Structural depiction figures were prepared from the model and omit density maps that were derived from removing 5EU, FMN, FAD, NADPH and Cys671 before being rendered in PyMol (Schrödinger Software).

Complex	**DPD•5EU$_{open}$**	**DPD•5EU•NADP(H)$_{closed}$**	**DPD-5EU•NADP(H)$_{covalent}$**
PDB code	7LJS	7LJT	7LJU
Space group	P 1 2_1 1	P 1 2_1 1	P 1 2_1 1
Unit Cell dimension			
α, β, γ (deg)	90, 95.95, 90	90, 95.71, 90	90, 96.03, 90
a, b, c (Å)	82.0, 160.0, 164.1	82.2, 158.9,162.1	82.1, 158.9, 163.2
Processed Resolution (Å)	2.00	1.98	1.87
R_{merge} [a] (%)	17.2 (86.9)	13.8 (81.5)	21.5 (106.6)
R_{pim} [c] (%)	12.1 (66.5)	7.4 (45.5)	11.7 (66.8)
I/σ (I)	5.6 (1.1)	7.6 (1.6)	6.30 (1.10)
CC ½ [d] (%)	99.2 (37.7)	98.9 (61.5)	98.9 (52.0)
Completeness (%)	90.2(66.0)	88.6 (77.0)	98.3 (92.4)
Multiplicity	2.9 (2.1)	4.2 (4.0)	4.1 (3.4)
No. Reflections	747583	1065501	1387185
No. Unique Reflections	255614	254113	336013
Refinement			
R_{work} [e]/R_{free} [f] (%)	17.21/22.86	18.30/21.90	17.19/21.09
No. of Atoms			
protein	30857	30847	30773
ligand	504	696	708
water	2171	3560	3389
Average B factors (Å^2)			
protein	30.16	20.39	26.33
RMSD [g]			
bond lengths (Å)	0.036	0.009	0.010
bond angles (deg)	2.32	1.10	1.22
Ramachandran plot (%)			
favored	94.84	95.44	96.25
allowed	4.34	4.02	3.35
outliers	0.82	0.54	0.40

[a]$R_{merge} = \Sigma|I_{obs} - I_{avg}|/\Sigma I_{avg}$, [b]The values for the highest-resolution bin are in parentheses, [c]Precision-indicating merging R, [d]Pearson correlation coefficient of two "half" data sets, [e]$R_{work} = \Sigma|F_{obs} - F_{calc}|/\Sigma F_{obs}$, [f]Five percent of the reflection data were selected at random as a test set, and only these data were used to calculate R_{free}, [g]Root-mean square deviation.

Table 2. Crystallographic data collection and model refinement statistics for the DPD•5EU complexes.

Results

Dissociation Constant for the DPD•5EU Complex

The concentration of 5EU was defined using the extinction coefficient ε_{285} = 4,340 $M^{-1}cm^{-1}$ that was measured by ^{1}H NMR integrations in the presence of an internal standard of known absorptivity (Figure 16A). In the absence of NADPH, 5EU associates with DPD to form an equilibrium concentration of the DPD•5EU complex. The association of 5EU perturbs the enzyme spectrum permitting sequential titration and determination of the binding equilibrium constant (Figure 16B). The changes in absorbance at the maximally perturbed transition (497 nm) were plotted against the 5EU concentration and fit to determine a dissociation constant of 9.5 ± 1.2 μM. Curvature in the isotherm is indicative of equilibrium binding and not stoichiometric covalent inactivation, indicating that 5EU alone is insufficient to inhibit the resting, non-activated form of DPD.

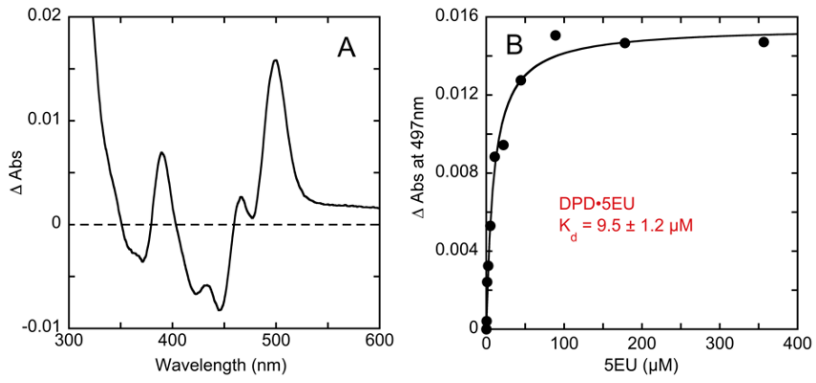

Figure 16. Determination of the DPD•5EU complex dissociation constant. A. The difference spectrum observed when 6.2 μM DPD was mixed with 100 μM 5EU. B. The ligand binding isotherm for 7.6 μM DPD titrated with 5EU (0.34-356 μM) fit to the quadratic form of the single site binding equation (Equation 5).

Measurement of the Rate Constant for DPD Inactivation by 5EU

The rate constant for bovine DPD inactivation by 5EU has been previously reported by Porter et al., as 0.30 ± 0.03 s^{-1} [19]. This measurement was made by 5EU titration in the presence of NADPH and absence of a substrate pyrimidine and so was a composite measurement that was influenced both by 5EU binding and the rate constant for inactivation. Though not stated, presumably these prior measurements were made by manual mixing, as the earliest measurement in these experiments corresponded to ~5 seconds. We measured the rate constant for inactivation by double mixing stopped-flow methods which provided both considerably higher time resolution and access to earlier incubation times. Porcine DPD was combined with saturating 5EU in the presence or absence of NADPH, aged for a specific time and then mixed with saturating concentrations of NADPH and uracil (Figure 17). The residual activity was measured by fitting the initial rate of the observed steady-state trace. This value was plotted against the age-time and the data obtained were fit to Equation 6. The data indicate that rapid inactivation of DPD by 5EU occurs only in the presence of NADPH with a rate constant of 0.22 ± 0.01 s^{-1}; in excellent agreement with the prior report. When incubated in the absence of NADPH, inactivation was not observed. From these data we can conclude that inactivation of DPD by 5EU is contingent on the inclusion of NADPH and that inactivation, at least in part, takes advantage of DPD activation catalysis (*see below*).

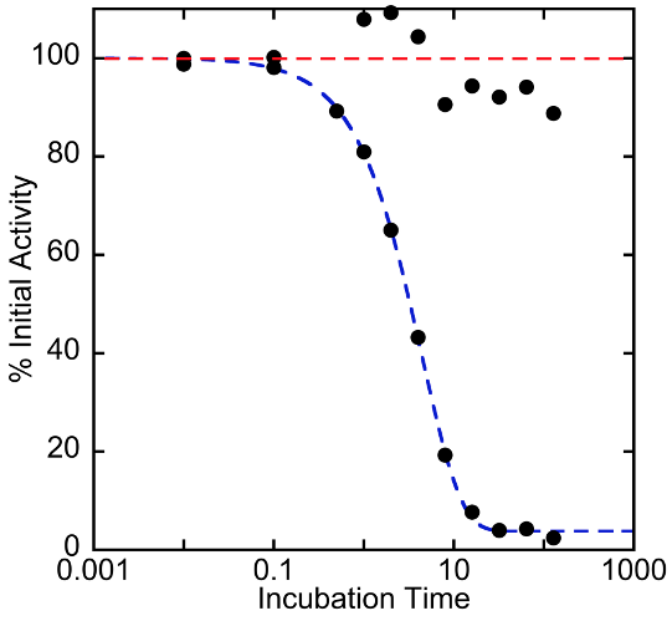

Figure 17. The rate and ligand dependence of inactivation of DPD. Circular graph markers depict the residual activity of 2 µM DPD when mixed with either 5EU (200 µM) (red dashed line) or NADPH (100 µM) and 5EU (200 µM) (blue dashed line). In each case the mixture was aged for a range of times and then mixed with 100 µM uracil and 100 µM NADPH (all concentrations post mixing) and percentage of residual activity was based on the rate of NADPH oxidation at 340 nm. The data obtained for incubation with 5EU and NADPH were fit to a single exponential according to Equation 6 to define a rate constant of 0.22 ± 0.01 s^{-1} and 96% inactivation. The data obtained for incubation with 5EU only were assumed to indicate scatter and were described by a line that is representative of the average activity for all aged times.

The Influence of NADP Binding on 5EU Inactivation

The chemistry of 5EU inactivation of DPD is presumed to be that of facile thiol-yne "click" chemistry that would not require an external source of electrons to bring about a covalent association of the 5EU ethynyl group and the thiol of DPD Cys671 [79]. To establish if DPD inactivation by 5EU involves hydride transfer from NADPH or is triggered solely by NADPH binding, DPD was incubated with 5EU in the presence and absence of NADPH and NADPH-analogues that are incapable of canonical hydride transfer. These samples were then buffer exchanged to remove the ligands and tested for residual activity relative to control samples manipulated in an identical manner (Figure 18). These data show that complete inactivation of DPD occurs only in the presence of both 5EU and NADPH. Incubation with either the product, $NADP^+$ or the NADPH isomer, 6DHNADP [71, 80] did not result in complete DPD

inactivation. However, both NADPH analogues induced fractional (~25%) inactivation compared to controls which suggests that 5EU inactivation includes a conformational component where occupancy of the NADP binding site proximal to the FAD cofactor induces partial inactivation by 5EU, 56 Å distant at the pyrimidine binding site proximal to the FMN cofactor.

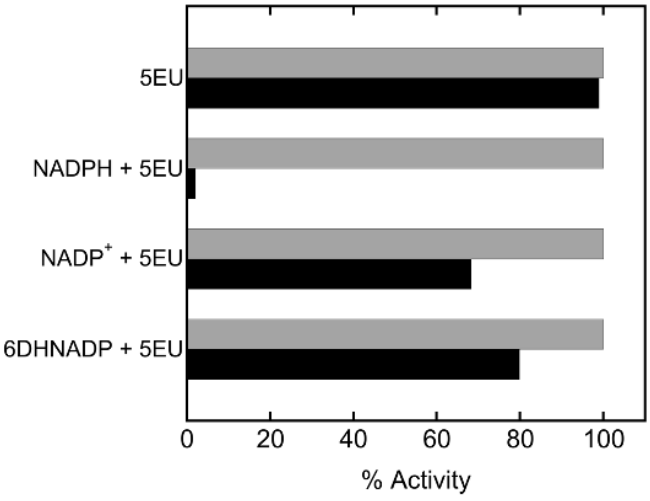

Figure 18. Ligand-Dependent Inactivation of DPD by 5EU. DPD, 50 µM was incubated with 1 mM 5EU and 1 mM of NADPH, $NADP^+$ or 6DHNADP for ~5 min at 4°C. Non-covalently bound ligands were then removed by a 40,000-fold buffer exchange. The samples were then assayed for activity with native substrates, NADPH and uracil. Control samples (grey) were treated in an equivalent manner (without added ligands) and were also assayed before incubation to determine initial activity to establish if activity loss was a result of mechanical handling during buffer exchanges. All data were normalized to the control samples to give percent activity for the 5EU treated samples (black).

Transient-State Measurements of NADPH Oxidation Associated with 5EU Inactivation

The data in Figure 19 suggest that the oxidation state of the NADP is a primary determining factor in 5EU inactivation of DPD. To establish whether NADPH oxidation is required for 5EU crosslinking, limiting concentrations of DPD were mixed with excess 5EU and NADPH using anaerobic stopped-flow methods and the change in absorbance at 340 nm observed (Figure 19). For each concentration of DPD for which the 5EU and NADPH concentrations were approximately pseudo-first order (2.5, 5.0, 10 µM DPD) the data could be adequately described by an exponential added to a straight line according

to Equation 7. This was interpreted as oxidation of NADPH that occurred with the average rate constant of 0.18 ± 0.02 s^{-1}, ostensibly coincident with the rate of 5EU crosslinking (*see above*). The ensuing linear decrease in absorption was assigned to slow uncoupled reduction of DPD by NADPH. The amplitudes obtained from the fit for the exponential phase were divided by the change in extinction coefficient for the oxidation of NADPH at 340 nm (6,220 $M^{-1}cm^{-1}$) and plotted against the DPD concentrations. The slope of the line obtained was 0.91 consistent with ~1:1 NADPH oxidation and DPD inactivation in the exponential phase (Figure 19 inset). In our prior studies of DPD we demonstrated that concentrations of NADPH lower than the enzyme concentration induce activity in only one of the two subunits of the DPD dimer. This was ascribed to very high affinity for NADPH of the activated subunit. In this instance the excess NADPH in these reactions permits activation of both subunits and brings the observed stoichiometry for NADPH-dependent activation and DPD crosslinking close to 1:1.

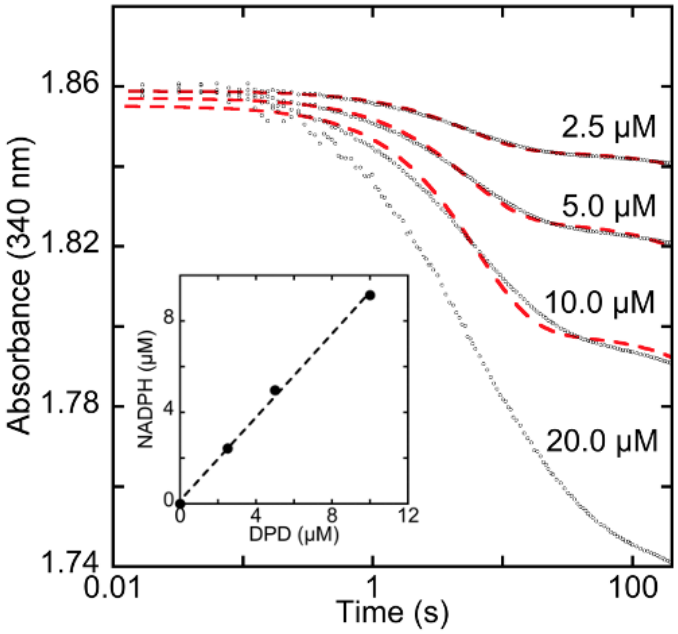

Figure 19. 5EU Dependent Oxidation of NADPH by DPD. Indicated concentrations of DPD were mixed with 50 μM 5EU and 50 μM NADPH under anaerobic conditions (all concentrations post mixing). The data for 2.5, 5.0, 10.0 μM DPD were fit (red dashed line) to an exponential plus a straight line according to Equation 7 to obtain an estimate of the NADPH oxidation rate constant and the amplitude of the exponential phase as a measure of the concentration of NADPH consumed. The data indicate a average rate constant for NADPH oxidation of 0.18 ± 0.02 s^{-1} and the concentration of NADPH consumed is approximately equal to the DPD concentration (Inset).

Given that crosslinking of the 5EU ethynyl group with the Cys671 thiol does not require redox chemistry, it is reasonable to conclude that electrons liberated from NADPH during DPD inactivation by 5EU must remain on the enzyme. To assess this possibility spectrophotometrically, DPD was mixed under anaerobic conditions using stopped-flow with saturating concentrations of 5EU and NADPH. Spectra were recorded from 250-800 nm using a charge coupled device (CCD) detector (Figure 20). The difference spectrum obtained for this process has the shape of the changes observed during reduction of a flavin added to that observed with oxidation of NADPH (Figure 20A inset). While quite qualitative, these data suggest that the two electrons consumed to bring about 5EU crosslinking reside on the isoalloxazine of one of the two flavins of DPD. Traces for 463 nm and 340 nm extracted from the CCD dataset show the time dependence of changes

that occur at these wavelengths (Figure 20B & C). These traces were fit to a single exponential expression (Equation 8) to define the rate constant and extinction coefficient changes associated with DPD inactivation. The fit of the trace for 463 nm returned a rate constant of 0.14 ± 0.01 s^{-1} and an extinction coefficient change of 6,800 $M^{-1}cm^{-1}$ when divided by the DPD concentration. The fit of the trace for 340 nm gave a rate constant of 0.17 ± 0.01 s^{-1} and an extinction coefficient change of 6,400 $M^{-1}cm^{-1}$ when divided by the DPD concentration. These rates are in good agreement with the inactivation rate constants measured in other experiments of this study and the changes in absorptivity are respectively consistent with reduction of a single flavin and oxidation of NADPH.

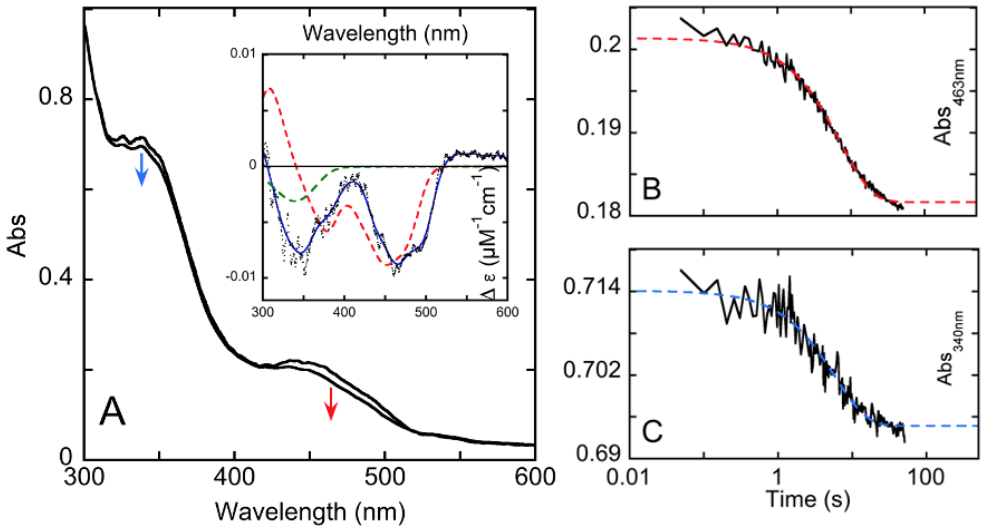

Figure 20. Spectrophotometric evidence that electrons taken up during 5EU-dependent inactivation of DPD from NADPH reside on a flavin cofactor. A. Shown at left are the spectra recorded at 1.0 and 50.6 seconds when 2.8 µM DPD was reacted with 200 µM 5EU and 100 µM NADPH under anaerobic conditions. Inset shows the difference of these two spectra fit to an interpolated line (blue line) and overlaid with the difference spectra for flavin reduction (red dashed line) and NADPH oxidation (green dashed line). B. The extracted trace for data collected at 340 nm fit to one exponential according to Equation 8 to yield a rate constant of 0.17 ± 0.01 s^{-1}. The observed amplitude at 340 nm is consistent with 2.8 µM NADPH consumption. C. The extracted trace at 463 nm was fit to Equation 8 to a rate constant of 0.14 ± 0.01 s^{-1} .

The Interaction of 5EU with the Cys671Ser Variant

As a proof of concept, 5EU was reacted with the Cys671Ser variant of DPD. The hydroxyl general acid available in this variant is inherently less reactive with the ethynyl group of 5EU and so is not crosslinked. As such 5EU is observed to be a substrate for this form of DPD and associates with a similar dissociation constant to that observed with the wild-type enzyme (Figure 16 ca. 17) The Cys671Ser variant has a turnover number 100-fold slower than that observed for the wild-type enzyme with uracil. Interestingly the rate of turnover of this variant with 5EU is similar to the rate observed with uracil and 35-fold more rapid than is observed with thymine [72]. These data indicate that volume of the pyrimidine 5-substituent has influence but is not the only determinant of the rate of turnover. Our prior studies have indicated that availability of the proton from cysteine (or serine) in the 671 position defines the rate of turnover and that this number is not correlated with the pKa difference for cysteine and serine residues [72]. This is in contrast to observations made with dihydroorotate dehydrogenase where substitution of the active site cysteine acid with serine resulted in a rate of hydride transfer that was 10^6-fold slower for the serine variant, roughly correlated with the difference in pKa's [24].

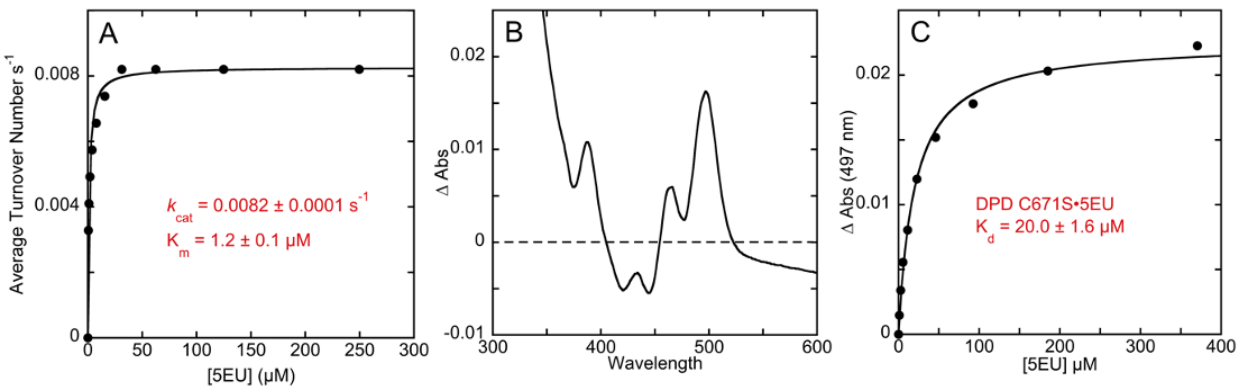

Figure 21. The interaction of 5EU with the C671S variant of DPD. A. Michaelis-Menten analysis of the C671S DPD variant. DPD, 1.96 μM, was mixed with varied (0.48-256 μM) 5EU in the presence of 250 μM NADPH and fit to the Michaelis-Menten equation (Equation 1). B. The difference spectrum observed when 4.7 μM DPD C671S was mixed with 370 μM 5EU. C. The ligand binding isotherm for 4.7 μM DPD C671S titrated with 5EU (0.36-370 μM) fit to the quadratic form of the single site binding equation (Equation 5).

Structures of DPD•5EU Complexes

For the three structures of DPD presented here, one asymmetric unit is comprised of four subunits that form two DPD dimers (AB-CD). Conformational changes relevant to 5EU inhibition are observed only in subunit C, potentially indicating a role for single-site asymmetry in the mechanism and/or the possibility of accessibility artifacts arising from dimer stacking in the crystal lattice. CD-dimer asymmetry arises as a consequence of conformational changes near the pyrimidine binding site for a single loop that contains the presumed catalytic general acid Cys671. The structure of the DPD•$5EU_{open}$ complex (PDB ID: 7LJS) was solved to a resolution of 2.00 Å and in terms of completeness is representative of the three structures presented (*see below*). This structure was obtained by soaking with both 5EU and NADPH, however, the soaking/cryo-condition used had a pH of 4.8 ensuring that all added NADPH was lost to cyclization [81]. As such the

resultant complex was captured with only 5EU in the FMN active site and the loop containing Cys671 in a conformation that placed the thiol 10.5 Å from the ethynyl group of 5EU (Figure 10A). In subunit A of this structure residues 675-681 (ERGMG) and 902-907 (AAFPPL) had no discernable density and were not modeled. Similarly, in subunit B residues 674-679 (GMGERG) and 902-907 (AAFPPL) were absent from the observed density. Subunit C is missing density only for residues 676-681 (RGMG). We have recently demonstrated that the active form of DPD is the two-electron reduced state that occurs when a hydride from NADPH is transferred to the enzyme in a process stimulated by the binding of pyrimidines[72]. The conformation observed in the DPD•5EU$_{open}$ complex therefore represents the resting, non-activated form of the enzyme in complex with the 5EU inhibitor.

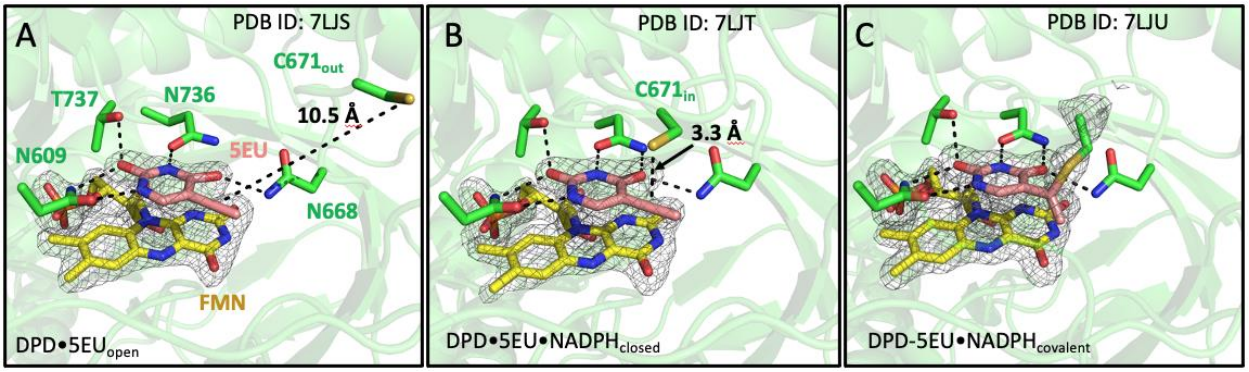

Figure 22. Structural analysis of DPD•5EU complexes. A. FMN active site of the DPD•5EU$_{open}$ complex. The Cys671-containing loop is observed in the open position in the absence of NADPH at the FAD site. B. FMN site of the ternary DPD•NADP(H)•5EU$_{closed}$ complex. C. The FMN site for the crosslinked structure of DPD-5EU•NADP(H)$_{covalent}$ complex. All structures display omit map density for flavin and 5EU contoured to 2.5 sigma and derived by omitting 5EU, FMN, NADPH (when applicable), FAD and Cys671 from the model.

In the subsequent 1.98 Å resolution structure for the DPD•5EU•NADP(H)$_{closed}$ complex (PDB ID:7LJT) the loop containing Cys671 of subunit C has a significantly changed conformation in that the thiol of

Cys671 is now 3.3 Å from the proximal carbon of the 5EU ethynyl group (Figure 10B). The RMSD compared to a single subunit of the DPD•$5EU_{open}$ complex structure for 7678 atoms was 1.567 Å, with the only significant conformational change occurring for this loop (669-684) (Appendix A). This complex formed *in crystallo* with a 20-minute soak in the presence of excess 5EU and NADPH. In this structure NADPH has been modelled into the observed density, though the oxidation state of this ligand was not known. The basis for modelling NADPH is that the activated form of the enzyme was previously shown to exhibit exceedingly high affinity for NADPH (supplied in excess with the soaking condition)[72]. It is observed that the dihydronicotinamide stacked with the isoalloxazine of the FAD cofactor such that the nicotinamide C4 is 2.8 Å from the flavin N5. In this position, the nicotinamide is localized in a region of apparent negative potential as a result of its proximity to the carboxyl groups of Asp342, Asp346, and Glu376 that are all within ~4 Å of the base (Appendix B). Selectivity for NADP(H) is evidently imparted by interactions of the substrate's 2'-phospho group with Arg364, Lys365, and Arg371. The binding of NADPH perturbs the positions of Arg364 that moves to form a charge association with NADP(H), and Asn487 that is displaced with the binding of this ligand but has no defined rotamer state when subunits are compared.

To capture the DPD-5EU•$NADP(H)_{covalent}$ crosslinked structure (PDB ID: 7LJU), DPD was soaked with excess 5EU and NADPH under diminished

oxygen atmosphere (0.1-0.4% O_2) for two hours. This structure was obtained at a resolution of 1.87 Å and exhibited similar gaps in density as defined above for the open complex. This structure clearly showed density linking the Cys671 thiol to the proximal carbon of what was the 5EU ethynyl group, consistent with Markovnikov regional selection (Figure 22C). In this structure the Cys671 loop (669-684) conformation is dramatically altered from that in the open complex (Appendix A).

These are the first DPD structures solved in complex with 5EU, an FDA approved 5FU chemotherapy sensitizer. Moreover, they represent a facsimile both the proposed normal sequence that occurs for reductive activation prior to catalysis [72], and of the sequence of events that occur in the inactivation of DPD by 5EU. Collectively they suggest that the 5EU molecule binds to DPD and stimulates reductive activation of the enzyme in a manner similar to that of substrate pyrimidines. Reductive activation induces a conformational change in the only significantly mobile part of the protein, the section of loop that includes the catalytic general acid Cys671. In catalysis this conformational shift places the Cys671 thiol adjacent to the pyrimidine for proton-coupled electron transfer from NADPH. However, for 5EU, this closed conformation promotes the thiol-yne reaction that results in indelible inactivation of the enzyme. As such 5EU is a mechanism-based inactivator that hijacks both the activation mechanism and the catalytic mechanism of DPD.

Discussion

The initial study of Porter et al. stands as the first biochemical investigation of DPD inactivation by 5EU [19]. Despite extensive investigation of the efficacy of co-administration of 5EU with 5FU, neither the detailed mechanism nor structural evidence of the interaction of 5EU with DPD has been presented. In this study we offer a comprehensive description for the events that occur during covalent modification of DPD by 5EU. The data indicate that 5EU is a mechanism based inactivator that utilizes the reductive activation mechanism of DPD to bring the alkyne and thiol moieties to within ~3 Å such that crosslinking may occur. The data show that specificity of 5EU for DPD is imparted as a consequence of 5EU inducing the reductive activation sequence in which two-electrons are acquired from NADPH in response to pyrimidine binding and that the reduced state of the enzyme exhibits a conformational bias that has the thiol of Cys671 proximal to the 5-position of the pyrimidine (Figure 23 & Figure 22).

The pyrimidine binding site has six apparent hydrogen bonding interactions with the base (Figure 22 & Appendix A). However, neither the 6 nor the 5 position is able to be engaged in such interactions, and no voluminous residues are observed that crowd this portion of the substrate [27]. In the absence of NADPH, 5EU is observed to bind reversibly to the DPD•5EU complex with high affinity that is only ~3-fold lower than that observed for uracil (Figure 16B). Prior studies have shown that DPD is somewhat

insensitive to the volume of the substituents at the 5-position of pyrimidine substrates, consistent with the dual specificity toward uracil and thymine [6, 7]. The added elongated volume of the 5EU methyne carbon compared to thymine does not impede binding significantly and no alterations in local structure are observed with association.

The observed rate of inactivation of DPD by 5EU is ~0.2 s^{-1} (Figure 17). This rate is correlated with the rate constants observed for 5EU induced NADPH oxidation and concomitant flavin reduction during activation (Figures 15 & 16). These data indicate that 5EU is sufficiently similar to native substrates to act as an effector, stimulating the enzyme to activate by taking up two electrons. That crosslinking, NADPH oxidation and flavin reduction are observed to occur concomitantly indicates that the actual rate of the thiol-yne reaction is rapid relative to the rate of hydride transfer from NADPH during activation. The observed rate of activation in the presence of 5EU is ~20-fold slower than the rate with uracil or thymine indicating that the identity of the pyrimidine associated at the FMN site influences the rate of hydride transfer from NADPH, 60 Å distant at the FAD site. This apparent capacity for the ligand in one active site to influence the fate of a ligand in another was observed for non-reducing NADPH analogues that were able to induce partial crosslinking by 5EU (Figure 17). In order to establish if the structural data presented in this study had evidence of conformational communication between FAD and FMN active sites, the DPD•$5EU_{open}$ and

DPD•NADP(H)•5EU$_{closed}$ complex structures were compared using the Structural Comparison facility in Phenix software. This analysis indicated no significant change in the position of either peptide backbone or residue side chain rotamers save for residues that comprise the mobile Cys671 loop as described.

The three structures presented in this study depict events in an apparent sequence that covalently modifies cysteine 671 of DPD rendering the enzyme inactive (Figure 22 & Figure 23).

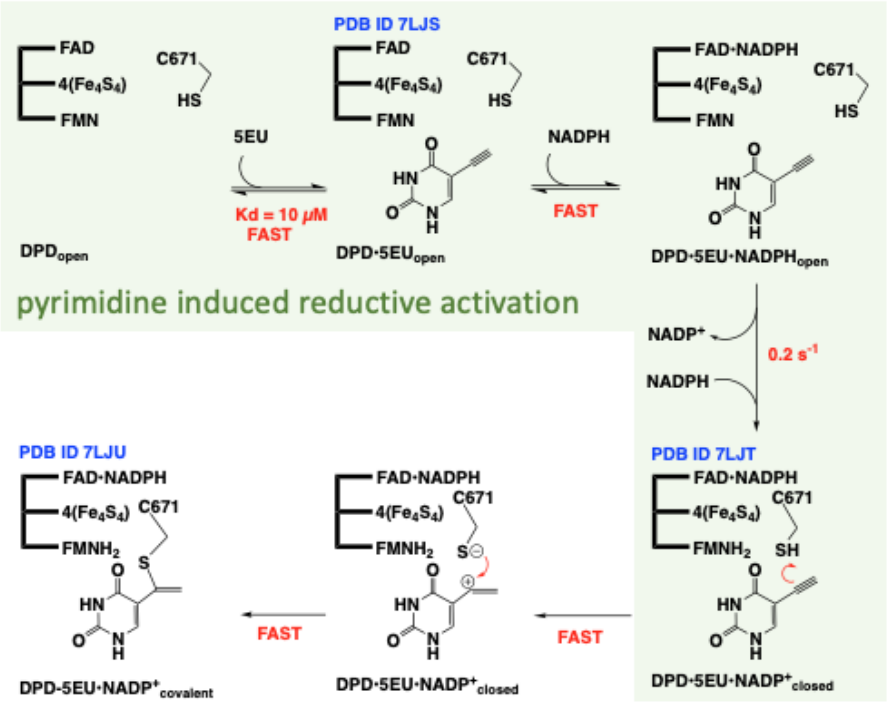

Figure 23. The proposed chemistry of 5EU DPD inhibition

The only significant structural movement observed among the three structures presented occurs for the loop that spans residues 669-684 and the two states of this loop toggle the position of the Cys671 general acid by

8 Å. In one state the thiol is 10.5 Å from the proximal ethyne carbon and in the other state it is 3.3 Å from this position. As was noted previously by Porter et al., in the absence of NADPH no crosslinking with 5EU is observed (Figure 18) [19]. These data correlated with the DPD•5EU$_{open}$ complex structure suggest that in the resting non-activated state of the enzyme, the dominant conformational state of the dynamic 669-684 loop is the open position, diminishing the opportunity for the 5EU crosslink reaction (Figure 22 & Appendix A). The structure of the DPD•5EU•NADP(H)$_{closed}$ complex is therefore a curiosity. In this structure the Cys671 thiol and 5EU ethynyl moiety clearly have not formed a bond and reside 3.3 Å apart. That these known reactive groups could be proximal without reacting is unexpected and suggests either that other local environmental factors influence the efficiency of the crosslinking reaction or that this reaction is impeded by the crystal lattice.

The inactivation of DPD by 5EU occurs coincident with reduction of a flavin cofactor (Figures 13, 15, 16). The DPD•5EU•NADP(H)$_{closed}$ structure was solved from a crystal subjected to a 20 min soak at near neutral pH in the presence of 5EU and NADPH under aerobic conditions. One possible explanation is that the oxidative inactivation of the enzyme by reduction of dioxygen changed the local electrostatic environment impeding the crosslinking reaction. However, that the loop is not observed to return to the open state in all subunits of the asymmetric unit suggests that this is not the

case. As such the preferred rationalization is that the crosslink forms more slowly *in crystallo*, which is supported by the fact that a two-hour soak yielded the crosslinked state.

The DPD-5EU•NADP(H)$_{covalent}$ complex was obtained by an extended soak with 5EU and NADPH in dinitrogen atmosphere with a low partial pressure of dioxygen. These conditions were chosen to retain the oxidation state of the activated and crosslinked enzyme. In this structure the oxidation state of the flavin cofactors could not be established by configurational shape as both FAD and FMN are flat within the model angle error of this 1.87 Å resolution structure. The flat shape of the FMN, however does not define the oxidation state as this cofactor is highly crowded and may not exhibit significant pleating when reduced[82].

The crosslink between 5EU and Cys671 is observed to form at the proximal carbon of the ethynyl group with respect to the pyrimidine ring defining the mode of action of the inhibitor. The events that induced this reaction are the events of activation where pyrimidine binding promotes hydride transfer from NADPH to form the two-electron reduced and activated state of the enzyme. In these *in vitro* experiments, the 5EU inhibitor is directed to react in the process of reductive activation. However, it is as likely that the inhibitor could crosslink with pre-activated enzyme that would be expected to predominate *in vivo*.

The formation of the crosslink eliminates the active site general acid and prevents turnover. However, this linkage does not appear to prevent the movement of the 669-684 loop as uracil can be observed to bind to the 5EU inactivated enzyme with a binding constant comparable (~3-fold) to that observed with the unmodified resting enzyme (Appendix C). It therefore must be concluded that crosslinking biases the loop position to reside more often in the closed state but does not prevent movement of this loop. Moreover, it must be asserted that the position of the dynamic loop is likely not fixed at any stage of catalysis or when inhibited as the exchange of substrate and product pyrimidines would be obstructed if the closed conformation were to persist and so we conclude that activation of the enzyme moves the equilibrium position of the loop to favor the closed state in order to sustain turnover.

Conclusive Remarks

DPD nullifies 5-fluorouracil toxicity by reduction forming 5-fluoro-5,6-dihydrouracil. 5-ethynyluracil enhances 5-fluorouracil chemotoxicity by covalent modification of the active site general acid cysteine of DPD. Inactivation of DPD by 5EU is dependent on the proximity of the ethynyl group of the inhibitor and the thiol of Cys671. The resting, as isolated, state of DPD is not subject to inhibition by 5EU. Inactivation occurs concomitantly with reductive activation of the enzyme by NADPH. This activation of the enzyme biases the average position of the only dynamic region of the

enzyme, the loop harboring Cys671, to a closed state that places the ethynyl and thiol groups within 3.3 Å. The thiol-yne reaction then occurs, forming a crosslink with the proximal ethynyl carbon, indelibly inactivating the enzyme.

CHAPTER 3

PERTURBING THE MOVEMENTS OF HYDROGENS TO DELINEATE AND ASSIGN EVENTS IN THE REDUCTIVE ACTIVATION AND TURNOVER OF PORCINE DIHYDROPYRIMIDINE DEHYDROGENASE

Introduction

Dihydropyrimidine dehydrogenase (DPD) catalyzes the reduction of the 5,6-vinylic bond of the pyrimidines, thymine and uracil with electrons derived from NADPH [1, 2, 5] (Figure 24).

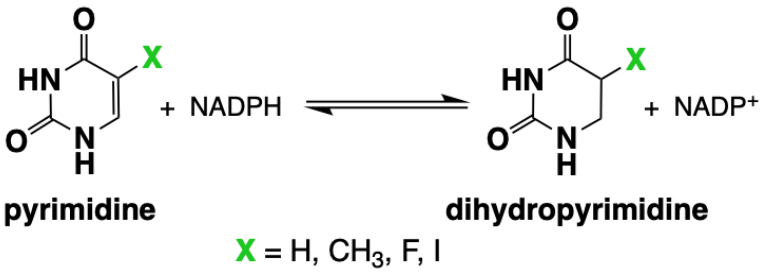

Figure 24. The chemistry catalyzed by DPD

DPD has considerable medical relevance as it rapidly detoxifies ($t_{1/2}$ ~20 min) the antineoplastic agent, 5-fluorouracil (5FU) [11-18]. Net DPD activity varies between individuals (30-fold)[16, 83] and is therefore both a therapeutic complication in dosing and a primary determinant of 5FU toxicity/efficacy [15, 17-22]. Inhibition of DPD has long been recognized as a means to improve outcomes of chemotherapeutic regiments for numerous cancers[20, 21]. The chemistry catalyzed by DPD is typical of numerous flavin-dependent

dehydrogenases[24, 42, 84, 85] but its architecture is atypical. DPD exists as a homo-dimer of 113 kDa protomers that each contain six redox cofactors; an FAD, an FMN and four Fe_4S_4 clusters (Figure 25). The DPD dimer interlocks with a head to head orientation, positioning the four Fe_4S_4 clusters (two provided from each protomer) to form an apparent electron conduit, linking the FAD and FMN that are separated by 56 Å [7, 27]. Crystal structures of DPD-ligand complexes have revealed that NADPH binds adjacent to the FAD cofactor and that the pyrimidine substrates associate within the cavity containing FMN. Additionally, the FMN active site general acid C671 is observed to be proximal to the bound pyrimidine to facilitate proton-coupled electron transfer from NADPH [7].

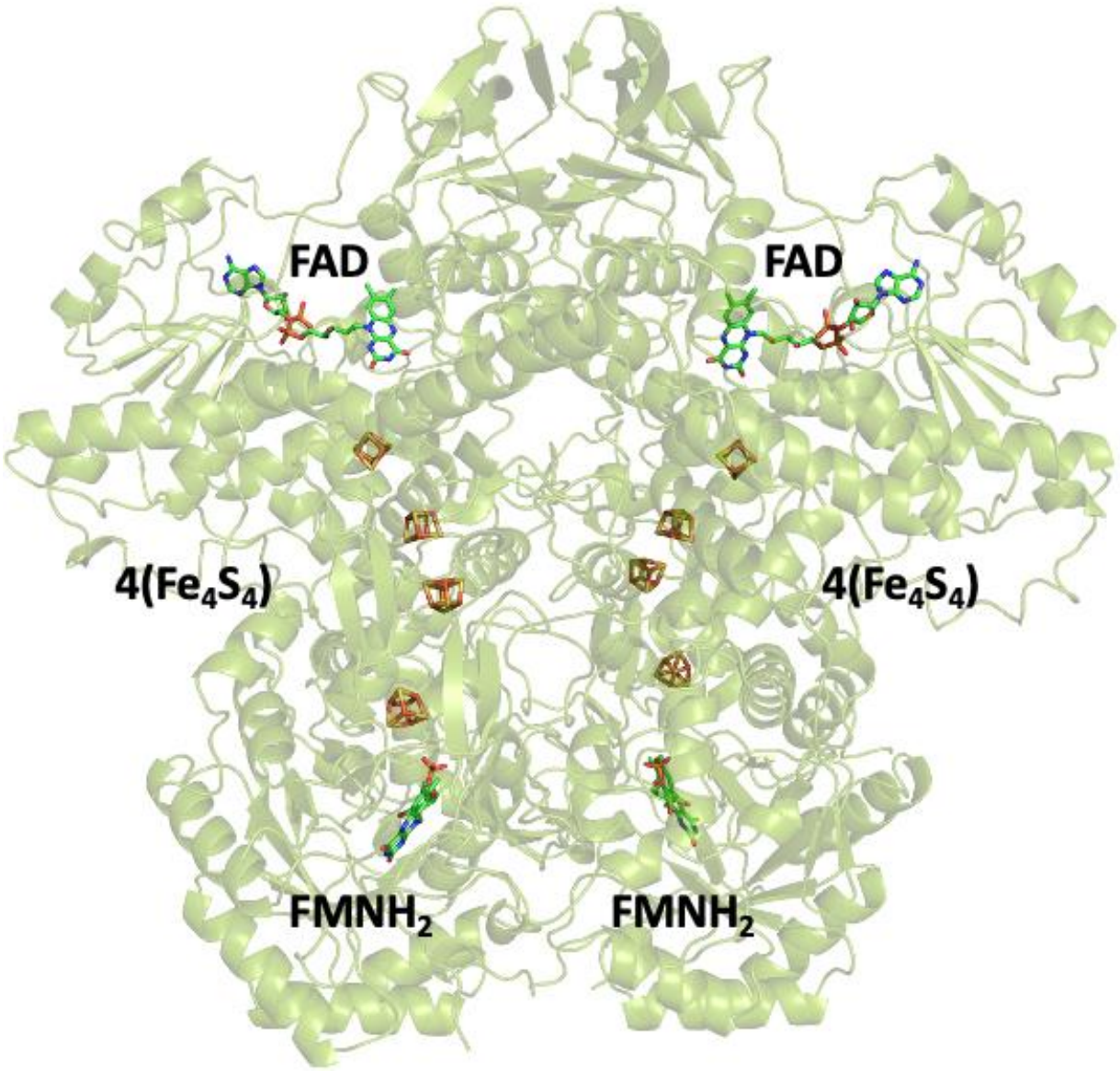

Figure 25. The structure of porcine dihydropyrimidine dehydrogenase

For nearly three decades DPD has largely defied attempts to describe its behavior. Early reports on the kinetic mechanism of DPD used almost exclusively aerobic steady-state methods and failed to capture primary mechanistic details [1, 2, 4, 5, 28-31]. Similarly, initial transient state data collected under anaerobic conditions concluded that the presence of uracil

stimulated the rate of the electron transfer from NADPH by two orders of magnitude but did not reconcile these observations with any discrete mechanistic conclusions [30]. The limited scope of conclusions drawn in prior DPD investigations was in part a result of a paucity of pure active enzyme either from native or heterologous sources [1, 4, 29, 32]. Recent improvements in the recombinant production of DPD have to some extent overcome yield barriers and allowed for more detailed reassessment of the mechanism [36]. Single turnover reactions have revealed biphasic first-order kinetics [72]. The delineation of the two phases was markedly enhanced in the C671S variant that significantly slows the rate of reduction of the pyrimidine. These data indicate that the initial phase is two electron activation that likely results in the reduction of the FMN cofactor. It was concluded that the proposed activated form of DPD (FAD, $4(Fe_4S_4)^{2+}$, $FMNH_2$) has high affinity for NADPH and so sequesters the co-substrate to bring about turnover as the second phase observed. The overall stoichiometry of these two processes was confirmed by acid-quench and HPLC product analysis. Furthermore, it was shown that the activated form of DPD persists when NADPH is exhausted in the presence of saturating oxidant pyrimidine substrate. This indicates that the electrons acquired for activation are retained and are not available to reduce pyrimidine substrates. On this basis, it was established that catalysis is preceded by a reductive activation step [72].

The data presented in this study further supports a kinetic model for DPD turnover that requires an initial NADPH dependent reduction step that occurs most efficiently in the presence of substrate pyrimidines. Using variant forms of DPD that slow or halt the turnover reaction of the enzyme, structures of the presumed activated form of the enzyme were obtained. These structures capture the proposed activated form where the FMN is two-electron reduced. Additionally, we investigate deuterium solvent and kinetic isotope effects on the activation and turnover reactions. Combined with prior observations, the data support a mechanism in which DPD behaves as a Newton's cradle for electrons where incoming reducing equivalents from NADPH rapidly displace electrons onto the pyrimidine substrate but at rate that is governed by movement of the loop that carries the active site general acid C671 required for proton coupled electron transfer.

Materials and Methods

Materials, Quantitation and Reaction Conditions

Competent BL21 (DE3) cells were obtained from New England Biolabs. Tris(hydroxymethyl)aminomethane (Tris) buffer, dipotassium hydrogen phosphate (KPi), ethylenediaminetetraacetic acid (EDTA), nicotinamide adenine dinucleotide phosphate ($NADP^+$), ammonium sulfate, 2-[4-(2-hydroxyethyl)piperazin-1-yl]ethanesulfonic acid (HEPES) buffer, 2-(N-morpholino)ethanesulfonic acid (MES) buffer, 1D-glucose, acetic acid, and the Miller formulation of lysogeny broth (LB) powder were purchased from

Fisher Scientific. Dithiothreitol (DTT) and reduced nicotinamide adenine dinucleotide phosphate (NADPH) were purchased from RPI Research Products. The sodium salt of ampicillin and dextrose powder were obtained from Spectrum Chemical. Uracil, ATP, and glucose oxidase were acquired from Sigma-Millipore. Glucose-6-phosphate dehydrogenase (G6PD) and hexokinase were from Alfa Aesar. Deuterium oxide and deuterium chloride were from Acros Organics.

All concentrations of DPD substrates and products were determined spectrophotometrically using known extinction coefficients (NADPH; ε_{340} = 6,220 $M^{-1}cm^{-1}$, $NADP^+$; ε_{260} = 17,800 $M^{-1}cm^{-1}$, uracil; ε_{260} = 8,200 $M^{-1}cm^{-1}$, thymine; ε_{264} = 7,860 $M^{-1}cm^{-1}$). The extinction coefficient used to quantify DPD was ε_{426} = 75,000 $M^{-1}cm^{-1}$ [36]. All concentrations indicated in this text are post-mixing.

Preparation of DPD and Experimental Protocols

Recombinant DPDs were expressed and purified and stored as described previously [36]. Prior to experiments DPD was thawed and diluted or exchanged into the required buffer. Exchanges were carried out using repeated steps of centrifugal concentration using 10 kDa nominal molecular weight cut-off filters (Amicon) and subsequent dilution to the target concentration. All preparative steps were performed at 4 °C.

To ensure a constant osmotic pressure for experiments that required a range of pH values, a mixture of 50 mM MES, 50 mM acetic acid, 100 mM Tris, 2 mM DTT (MAT buffer) was used to buffer for pHs 5.2 - 8.5 [86]. Deuterium oxide buffers and substrate solutions were prepared by dissolving reagents in D_2O and adjusting to the target pH with concentrated DCl with correction for the response of the pH electrode in D_2O solvent[87].

Enzyme samples were made anaerobic in glass tonometers using a modified Schlenk line and alternating cycles of vacuum and pure argon according to published protocols[37]. The samples were further protected from residual and infiltrating dioxygen contamination by the inclusion of 1 mM glucose and the addition of 1 U/mL glucose oxidase that was added from a side arm once the exchange cycles were completed. The tonometer was then mounted onto a HiTech stopped-flow spectrophotometer (TgK Scientific). Solutions that included substrates and products were made anaerobic in buffer containing 1 mM glucose by sparging for 5 minutes with argon prior to the addition of 1 U/mL glucose oxidase and mounting onto the stopped-flow spectrophotometer.

Steady-State Observations of DPD Catalysis

The influence of pH, viscosity and solvent derived deuterium on the turnover of DPD were each assessed in the steady state. Previous studies had indicated that reduction of the pyrimidine is fully rate limiting in turnover[72]. Turnover number (TN) is defined as the rate measured in the

presence of saturating substrates standardized to the enzyme subunit concentration and is taken to be synonymous with the term, k_{cat}. The influence of hydrogen ions on the TN of the wild type and the C671S variant of DPD was assessed using stopped-flow, pH-jump methods. A tonometer containing 1 μM DPD (WT or C671S) was prepared anaerobically in buffer containing 5 mM potassium phosphate, 2 mM DTT and 1 mM glucose, pH 7.5. Substrate solutions contained 100 μM NADPH and 100 μM uracil and were prepared in MAT buffer adjusted to the target pH using acetic acid and then sparged with argon prior to mounting onto the instrument. Reactions were monitored for 50 seconds at 340 nm and 20 °C, and the rate was assessed from the slope of the trace from 2-20 seconds. The influence of pH on the TN could be described by a single ionization expression (Equation 9)[88]. The K_a values determined from titratable phenomena X, (in this case apparent TN, TN_{app}) were determined by plotting the pH against TN_{app}; where X_{AH} and X_{A-} represent the respective fully protonated and unprotonated arms of the titration.

Equation 9. $$X = \frac{(X_{AH}[H^+] + K_a X_{A-})}{[H^+] + K_a}$$

The influence of solvent derived deuterium atoms was evaluated under anaerobic conditions in the steady-state. The time required for deuterium exchange equilibrium was evaluated by monitoring the consumption of NADPH ($\Delta\varepsilon$=6220 $M^{-1}cm^{-1}$) at 340 nm for varied incubation times (0, 60,

100, 120, 180, 210 sec). Wild type DPD (570 nM) in MAT buffer containing 1 mM glucose was prepared in either H_2O or D_2O at pH 8.5 or pD 8.09 respectively. Tonometers were made anaerobic as described and mounted onto the stopped-flow spectrophotometer. Reactions were initiated by mixing with 150 μM NADPH and 150 μM uracil and monitored for 40 seconds. The linear portion (1 - 10 sec) of the data traces was fit to a straight line to determine the rate.

To account for viscosity changes resulting from the introduction of D_2O (η_{rel} = 1.25), the effect of solvent viscosity on the TN of DPD was assessed for viscosities 1-1.75 using added glycerol[89]. DPD C671S (4 μM) was prepared as above in 1/20 MAT buffer, 1 mM glucose, pH 7.5. Glycerol (0-31.8% v/v) was dissolved in 2/1 MAT buffer, 1 mM glucose, 150 μM NADPH, 150 μM uracil, pH 8.5 and sparged with argon for 5 mins and glucose oxidase 1 U/mL was then added prior to mounting to the stopped flow instrument. DPD activity was observed at 340 nm for 50 seconds and the rate of turnover was assessed by fitting a straight line to the data for 2-20 seconds. These data were then plotted against relative viscosity (η_{rel}) and fit to a straight line.

The number of protons in flight during turnover of DPD with uracil under anaerobic conditions was estimated using the proton inventory method [90]. The influence of the deuterium fraction of the solvent was assessed by reacting DPD with uracil in the presence of varied fraction of

solvent deuterium. The fraction of solvent deuterium was controlled by preparing MAT buffer containing 1 mM glucose in both H_2O and D_2O and adjusted to corresponding pL values. These were then combined to obtain a specific deuterium fraction ratio (0, 10, 25, 50, 70, 90 and 100%) and added to 5 mL glass syringes. Substrate solutions were made anaerobic by sparging with argon for 5 minutes prior to the addition of 150 μM of both uracil and NADPH. Glucose oxidase (1 U/mL) was added prior to mounting onto a stopped-flow spectrophotometer. Anaerobic enzyme solutions were prepared by sparging the buffer of desired deuterium fraction for 5 minutes. After sparging 10 μL of concentrated DPD was added to obtain a final concentration of 1 μM prior to the addition of 1 U/mL of glucose oxidase. The syringe was then mounted onto the stopped-flow spectrophotometer. Reactions were monitored at 340 nm for 50 sec at 20 °C. The linear portion of the trace (5 - 10 sec) was fit to a straight line and the rate determined. The ratio of rate constants (k_n/k_0), where 0 represents 100% H_2O and n is the fraction of D_2O, was plotted against the deuterium fraction, n of the buffer. To evaluate the inventory for the number of protons in flight, data were fit to variations of the Kresge-Gross-Butler equation, Equation 10, 11, 12 respectively[91, 92]. Equation 10 describes a medium effect whereby greater than two protons contribute to the observed effect. In Equation 11 describes the case for one (v = 1) or two-proton (v = 2) in flight in the transition state when reactant fractionation factors approximate unity. In this equation, the

inverse of the transition state fractionation factor, $1/\varphi^T$, is equal to the kinetic isotope effect when there is a single proton contributing to the effect, or $v = 1$. The fit for this equation had the ordinate intercept, i, as a variable. Equation 12 accounts for fractionation factors less than one that contribute to the effect from the reactant and transition state. The fit to this equation provides φ^R/φ^T; the value of solvent kinetic isotope effect.

Equation 10. $$k_n/k_0 = (\frac{k_H}{k_D})^{-n}$$

Equation 11. $$k_n/k_0 = (i - n + n\varphi^T)^v$$

Equation 12. $$k_n/k_0 = (1 - n + n\varphi^T)/(1 - n + n\varphi^R)$$

Transient-State Observations

The pH dependence of the DPD C671S reductive activation reaction was assessed under transient state conditions. C671S variant DPD (10 μM) was prepared in 5 mM potassium phosphate, 2 mM DTT and 1 mM glucose, pH 7.5. This DPD solution was then made anaerobic in a tonometer as described above and mounted onto the stopped-flow spectrophotometer. Substrate solutions of NADPH (50 μM final) and thymine (100 μM final) were prepared 2/1 MAT buffer titrated with HCl to the desired pH, placed in glass syringes and sparged with argon for 5 minutes before the addition of 1 U/mL glucose oxidase. The substrate and DPD solutions were mixed and monitored for 50 seconds at 340 nm and 20 °C to observe only the reductive activation reaction. Data were fit to a linear combination of two exponentials and a

linear component that accounted for the facile breakdown of NADPH at lower pH values (Equation 13). From this equation, the absorbance amplitudes (A_n) and associated rate constants (k_n) were determined. The term m is the slope of the rate accounting for NADPH degradation at low pHs and C is the final absorbance at 340 nm for the exponential phases. The effect of pH on rate constants or absorption changes was described by a single ionization expression (Equation 9). The K_a values were determined from the titratable phenomena, X (in this case k_{2obs}).

Equation 13. $$A_{340nm} = A_1(e^{-k_1 t}) + A_2(e^{-k_2 t}) + mt + C$$

The pH dependence of the activation of DPD C671S indicated that increased kinetic resolution for the reductive activation of the enzyme was observed at lower pH values. Similarly, the activation reaction of the C671A variant was similarly delineated in this way but at pH 7.5. To ascertain what processes were contributing in each of the phases observed for activation, transient state reactions were conducted for each variant that captured the net spectrophotometric changes that occur during reductive activation only. DPD C671S (14 μM) was prepared anaerobically in 1/20 MAT buffer, 1 mM glucose, pH 7.5, in a tonometer as described above and mixed with NADPH (50 μM) and thymine (100 μM) in 2/1 MAT buffer, 1 mM glucose pH 5.75 that was made anaerobic by sparging as described above. In this case thymine is a slow substrate inducing a TN of 0.00024 s^{-1} such that the reductive activation reaction can be observed largely separate from ensuing

turnover events. DPD C671A (15 μM) was prepared anaerobically in MAT buffer, 1 mM glucose, pH 7.5, in a tonometer as described above and mixed with NADPH (13 μM) and thymine (100 μM) in MAT buffer, 1 mM glucose pH 7.5 that was made anaerobic by sparging as described above.

For each variant, absorption changes were observed at 340 and 590 nm using photomultiplier detection and at all wavelengths spanning 300-850 nm using charged coupled device (CCD) detection. The single wavelength data were fit to a linear combination of two exponentials according to Equation 14. In this equation the absorbance changes at X wavelength were fit to obtain amplitudes (A_n) and associated rate constants (k_n).

Equation 14. $$A_{Xnm} = A_1(e^{-k_1 t}) + A_2(e^{-k_2 t}) + C$$

The CCD data were collected for two time-frames for each variant (C671S; 0-2.5 & 0-25 seconds, C671A 0-2.5 & 0-12.5 seconds) and spliced together at 2.5 seconds to form datasets that had time resolution sufficient for processes with substantially different rate constants. The datasets were fit to a two-step irreversible model using the Spectrafit singular value decomposition routine available in KinTek Explorer software (KinTek Corp.). The spectra returned were then subtracted to reveal the net absorption changes in each phase.

Transient-state kinetic isotope effects for DPD C671S were determined by comparing single turnover reactions in the presence of NADPH or Pro-S NADPD. The C671S variant of DPD was used in these experiments as this

form has delineated the activation and turnover processes[72]. DPD C671S was prepared anaerobically in MAT buffer pH 7.5 as described above and mounted to the stopped-flow spectrophotometer. Kinetic isotope effects were assessed by monitoring the reaction of DPD C671S (15 μM) at 340 nm in the presence of uracil (100 μM) and NADPH/D (9 μM) under anaerobic conditions at 20 °C. NADPH and Pro-S NADPD were prepared enzymatically immediately prior to experimentation. In each case a solution of 200 μM $NADP^+$, 200 μM ATP, 10 mM Mg^{2+} and 1 mM of either glucose or 1D-glucose was prepared for the production of NADPH and NADPD respectively. This was then mixed with 1 U of glucose-6-phosphate dehydrogenase and 1 U of hexokinase in MAT buffer pH 7.5. Reaction progress was monitored at 340 nm until complete (~ 200 sec) at which time the enzymes were removed by centrifugation using 10 kDa nominal molecular weight cutoff filters. The concentration of NADPH and NADPD were determined by absorption and diluted with MAT buffer to the desired reaction concentration.

The Crystal Structures of the Activated C671S and C671A Variants

Diffraction quality crystals of DPD variants, C671S and C671A with elongated morphology were obtained by the hanging-drop vapor diffusion method. Crystallization conditions were adopted from Dobritzsch et al., 2001 [27]; ~4.5 mg/mL (~40 μM) of DPD variants, C671S or C671A in 25 mM HEPES, 2 mM DTT, 10% glycerol at pH 7.5 were prepared and mixed 1:1 with well solution containing 100 mM sodium citrate, 2 mM DTT, 15% PEG

6000 at pH 4.5 to 4.9 to give a 6 µL drop. Crystallization was carried out in the dark to eliminate photo-degradation of the quasi-labile FMN cofactor[93]. Crystals appeared after 16 hours as both single elongated rectangular hexahedron forms (200 x 50 x 50 µM) or urchin-like clusters. Only crystals from the single crystal form were harvested and placed in a Plas-Labs 830 series glove box in which a Motic binocular microscope coupled to an Accuscope 1080p high definition camera was placed. Before being placed in the glove box, the well solutions of the selected crystals were made anaerobic with the addition of 10 mM dithionite and resealed with the cover slide. The glove box was then made anaerobic by flushing with pure nitrogen gas for approximately 10 minutes at which time the fractional dioxygen was 0.1 %, as indicated by a Forensics Detectors oxygen meter. Atmospheric dioxygen was measured throughout the soaking procedure and was held below 1%. C671A and C671S DPD crystals were soaked for a minimum of 20 minutes in 25 mM HEPES, 100 mM sodium citrate, 2 mM DTT, 100 µM NADPH, 100 µM uracil (C671A) or thymine (C671S), 20% PEG 6000, 20% PEG 400, pH 7.5 prior to submersion in liquid nitrogen. Frozen crystals were then removed from the anaerobic environment and stored in liquid nitrogen.

Diffraction data were collected at 100 K at the beamline 21-ID-D of the Advanced Photon Source at Argonne National Laboratory. The beamline was equipped with a Dectris Eiger 9M detector. Data were collected using an oscillation angle of 0.5° over a range of 240° and an exposure time of 1

second per frame. The wavelength was fixed at 1.127 Å. Diffraction images were processed using xia2. Data processing statistics are given in Table 1. Phasing was conducted via molecular replacement using the program phaser. A model of Porcine DPD (PDB ID 1H7W) was used as a starting search model. The model building and refinement was undertaken in Coot [41] and Phenix [42] respectively in a repeated manner until the lowest R_{free} was achieved. The coordinates and structure factors have been deposited in the Protein Data Bank with accession codes 7M32 and 7M31 (Table 1). Structural analysis and figures are made using PyMOL Version 2.0 (Schrödinger, LLC.).

Table 3. Crystallographic data collection and model refinement statistics for the DPD variant complexes

Complex	**DPD C671A**	**DPD C671S**
PDB code	7M32	7M31
Space group	P 1 2_1 1	P 1 2_1 1
Unit Cell dimension		
α, β, γ (deg)	90.0, 95.9, 90.0	90.0, 95.7, 90.0
a, b, c (Å)	81.9, 158.7, 162.7	82.0, 159.6, 162.9
Processed Resolution (Å)	1.82	1.69
R_{merge} [a] (%)	14.7 (194.6)	19.0 (185.1)
R_{pim} [c] (%)	7.4 (96.9)	9.6 (94.4)
I/σ (I)	7.4 (0.9)	6.0 (0.9)
CC ½ [d] (%)	99.6 (34.1)	99.2 (35.0)
Completeness (%)	96.5(96.2)	99.0 (99.8)
Multiplicity	4.8 (4.9)	4.7 (4.8)
No. Reflections	1705022	2169918
No. Unique Reflections	354924	459508
Refinement		
R_{work} [e]/R_{free} [f] (%)	16.81/20.09	17.65/19.99
No. of Atoms		
protein	30714	30857
ligand	496	684
water	2630	4306
Average B factors (Å^2)		
protein	34.39	25.74
RMSD [g]		
bond lengths (Å)	0.006	0.005
bond angles (deg)	1.00	1.02
Ramachandran plot (%)		
favored	96.33	96.15
allowed	3.35	3.50
outliers	0.32	0.35

[a]$R_{merge} = \Sigma|I_{obs} - I_{avg}|/\Sigma I_{avg}$, [b]The values for the highest-resolution bin are in parentheses, [c]Precision-indicating merging R, [d]Pearson correlation coefficient of two "half" data sets, [e]$R_{work} = \Sigma|F_{obs} - F_{calc}|/\Sigma F_{obs}$, [f]Five percent of the reflection data were selected at random as a test set, and only these data were used to calculate R_{free}, [g]Root-mean square deviation.

Results

Recently we have shown that DPD undergoes reductive activation whereby the initial two electrons to enter the protein from NADPH reside on one of the two flavin cofactors and it is this form of the enzyme that is competent in catalysis [72]. Our earlier data suggested that these electrons enter at the FAD site but reside on the FMN. In this article we explore rate limiting processes in both the activation and turnover of DPD and present structural evidence for the activated state of the enzyme. These data suggest that the rates of activation and turnover are respectively influenced by the protonation state of groups that are near or part of the FAD and the FMN cofactors.

Steady-State Rate Dependence on pH and Solvent Deuterium Fraction

Available crystal structures and observation of variant forms of DPD indicate that C671 is the active site general acid that delivers a proton to the pyrimidine substrate concomitant with hydride transfer from the reduced FMN cofactor[7, 27, 72, 94]. If the pKa of C671 controlled the rate of catalysis it would be reasonable to conclude that a pH profile for the TN would show a maximum rate at lower pH values. Figure 26A depicts the pH dependence of the apparent TN of DPD WT and C671S variant as a function of pH. MAT buffer was chosen as a suitable buffer system as it maintains a constant osmotic pressure across all pH values used[86]. These data indicate that the

apparent TN increases ~fourfold from low to high pH values for both the WT and C671S variants. Similar observations were made by Podschun et al. 1993[2].

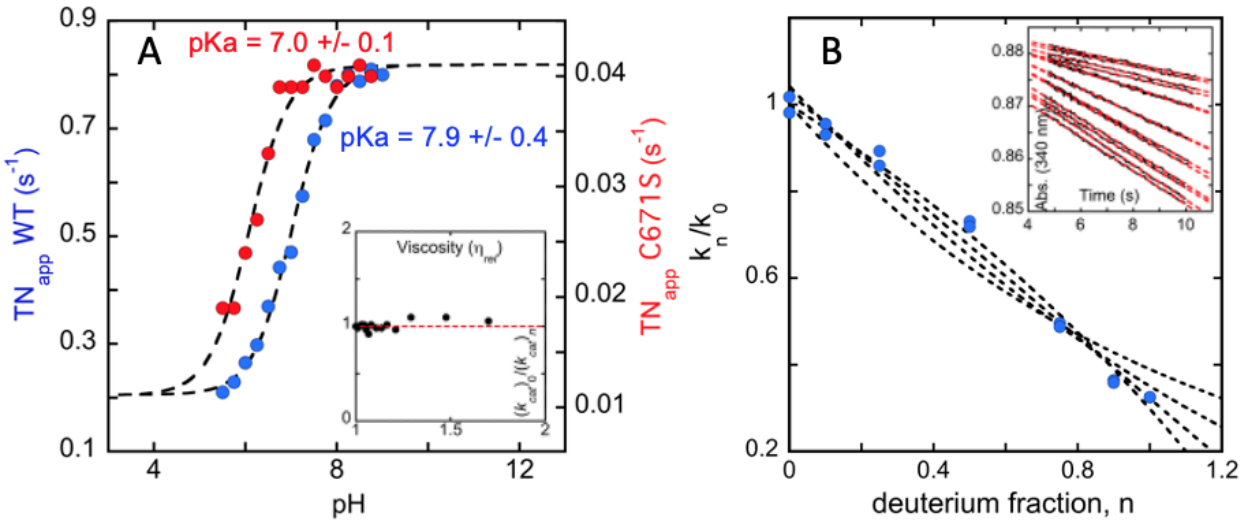

Figure 26. pH dependence for DPD WT and C671S and steady-state solvent isotope effects for DPD WT. A. Determination of the macroscopic pKa for the apparent turnover number of DPD WT (blue) and DPD C671S (red). A solution containing 1 µM of enzyme prepared in dilute MAT buffer (1/100) was mixed with 150 µM NADPH and 150 µM uracil prepared in MAT buffer adjusted to the desired pH between 5.5 and 8.5. The apparent turnover (TN_{app}) number was determined by observing the reaction at 340 nm for 50 seconds and fitting the initial data from 2-20 seconds to a straight line. The pH-dependence of the TN value was fit to Equation 9. Inset depicts the viscosity effect control for the C671S variant as a proxy for both enzymes. For this control 2.5 µM DPD C671S in dilute MAT buffer (1/100) pH 7.5 was combined with 150 µM NADPH and 150 µM uracil in MAT buffer pH 8.5 with various fractions of glycerol and observed at 340 nm. Rates were determined from the linear portion of the trace (2 - 20 sec). B. Proton inventory for DPD WT. The number or protons in flight in the pyrimidine reduction transition state was assessed by reacting 1 µM DPD WT in dilute MAT buffer (1/100) pH 7.5 with 150 µM NADPH and 150 µM uracil in MAT buffer pH 8.5. Inset shows traces of reactions monitored at 340 nm for 50 sec at 20 °C in buffer containing the desired deuterium fraction. Rates were determined from the linear portion of the trace (5 - 10 sec). The data were fit to Equation 10 (most concave), Equation 11 (for the two- (concave) and one-proton (linear) cases) and Equation 12 (convex).

Our data indicate single pKas of 7.92 ± 0.41 and 7.02 ± 0.04 for WT DPD and the C671S variant respectively (Figure 26). While the pK_a value for the former could be ascribed to the native C671 residue, the latter cannot be correlated with a serine residue in this position. Moreover, similar to previous reports the TN increased to a limit with increasing pH, which is counter to the expectation if the protonation of the residue at 671 was a

requirement for turnover. These data suggest that the titration of a group other than the thiol of C671 is influencing the rate of pyrimidine reduction. The pKa of free $FMNH_2$ is derived from titration of the N1 proton to give the neutral or anionic forms and has been shown to be 6.7; qualitatively similar to the pKa's observed [95].

The effect of the deuterium fraction of solvent on the observed TN was assessed and used to obtain a proton inventory for WT DPD. Reactions were carried out in MAT buffer for reasons discussed above. A pL of 8.5 was selected as it is a pL independent region of the activity curve (Figure 26A). As a control, the TN was also assessed over a range of glycerol concentrations to account for viscosity changes with the introduction of D_2O (η_{rel},1.25). These data indicate no dependence of the observed rate of turnover on solvent viscosity, consistent with rate limiting chemistry (Figure 26A)[96]. The results of the reaction of DPD with saturating uracil and NADPH clearly show that the steady-state rate of turnover is influenced by the concentration of solvent deuterium. The proton inventory data sets were fit to one and two-protons in flight and solvent medium effect equations (Equations 10 and 11, respectively) that each assume fractionation factors of one. The data were also fit to Equation 12 that accounts for fractionation factors for the hydron donating species in the reactant and transition states as would be expected for the involvement of a thiol acid. The shape of the dependence was observed to be convex and best fit to Equation 12 that

assumes the movement of a single proton that exhibits fractional deuterium substitution. The fits returned a solvent kinetic isotope effect (SKIE), defined here by φ^R/φ^T, of 3.35 ± 0.50. It is conceivable that the curve could also be described by the movement of two protons, however the data presented does not have the precision to effectively discriminate between these cases. Two exchangeable hydrogens are transmitted to the pyrimidine during reduction of the base; one proton from the active site acid C671, and one as a hydride from the reduced FMN N5 position. It is surmised that the transfer of these hydrogens is simultaneous and contingent on the availability of the C671 proton as the C671A variant is not catalytic and the C671S variant has a markedly slower rate of turnover[72]. Together the pH profile and the SKIE data suggest, that one or more hydrogens are displaced in the transition state for pyrimidine reduction and that one of these is likely derived from the C671 thiol and that the deprotonation of a group at or near the reduced FMN promotes the rate of pyrimidine reduction by fourfold.

Transient-State pH Effects on the Reductive Activation of the DPD C671S Variant

As stated, the C671S variant of DPD exhibits pronounced delineation in terms of observed rate constants for the reductive activation and ensuing turnover events[72]. The effect of pH on the reductive activation reaction of the C671S variant with saturating thymine was assessed under single-turnover conditions with limiting NADPH. The traces obtained at 340 nm

revealed further resolution of the activation phase at low pH values (Figure 27A) and were fit to a combination of 2 exponentials and a linear phase (Equation 12).

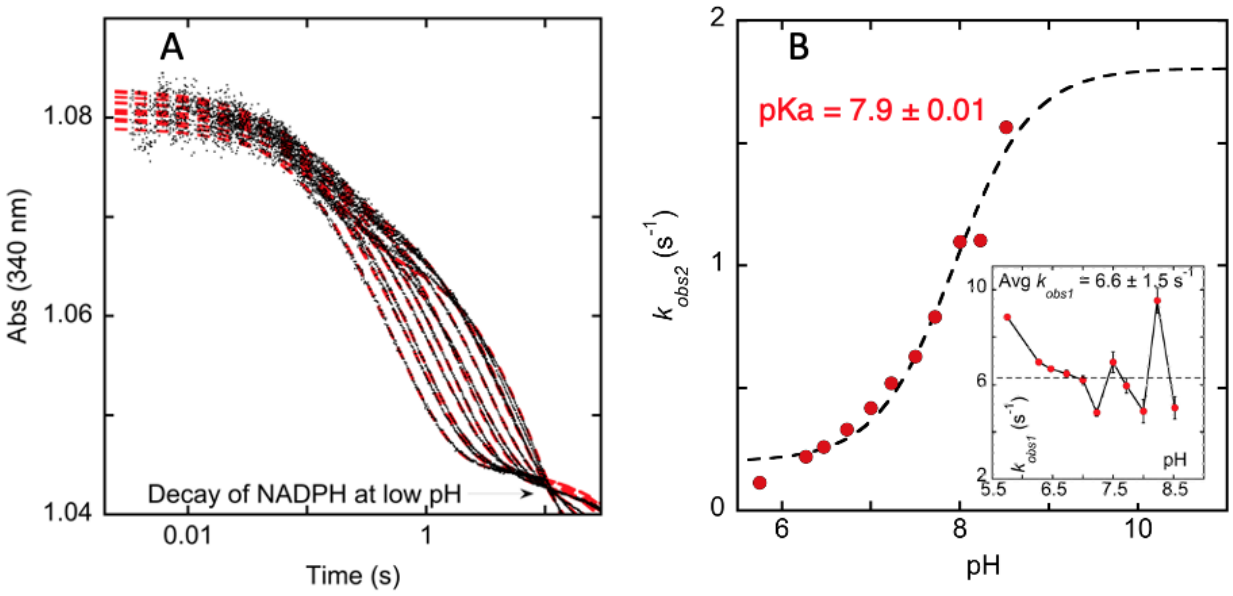

Figure 27. The effect of pH on the activation phase of C671S DPD. A. The effect of pH was assessed by mixing 10 µM of DPD C671S with 50 µM NADPH and 100 µM thymine at varying pH values (5.75, 6.0, 6.3, 6.5, 6.7, 7.0., 7.2, 7.5, 7.72, 8.0, 8.23, 8.52) under anaerobic conditions. The reaction was monitored at 340 nm for 10 seconds at 20 °C. B. The dependence of the rate for the second phase (k_{obs2}) on pH when the rate of k_{obs1} is fixed to the mean value of 6.6 s^{-1} that was determined from rates returned from fitting to a combination of exponentials (Equation 13). Data were fit to Equation 9.

The two initial exponential phases (k_{obs1} and k_{obs2}) report the steps of reductive activation that consumes two electrons from NADPH[72]. A linear phase was added to qualitatively account for denaturation of NADPH at low pHs. The value for k_{obs1} derived from the fit scattered for different pH values about a mean of 6.6 ± 1.5 s^{-1} but did not titrate predictably with pH. The value returned for k_{obs2} (when k_{obs1} is fixed to its mean) was plotted against the pH of the reaction. The data in Figure 27B was fit to Equation 9 and

returned a pK_a of 7.9 ± 0.01 where k_{obs2} had a positive dependence on the concentration of hydroxyl ions. Previous experiments at pH 7.5 were largely monophasic for activation as was observed in the data presented here. Lower pH values appear to slow the hydride transfer for activation and separate the data into two phases. The pH dependent phase in prior work was shown to report the oxidation of NADPH and the concomitant reduction of a flavin cofactor[72]. Our data suggest that these electrons cross the protein and reside on the FMN yielding the active form of DPD. The observed pKa of 7.9 for the activation step differs from the value observed for the pH dependence of turnover with this variant (pKa - 7.0, Figure 26A). As such we tentatively ascribe the pK_a observed as arising from a deprotonation within the region of hydride transfer at the FAD and suggest that the protonation state of this group(s) influences the rate of reductive activation. Prior to activation both flavins are oxidized and would exhibit pKa values at the extremes of the pH range and markedly distant from 7.9. It is therefore reasonable to conclude that the pKa observed is for groups proximal to one or both of the flavin cofactors that when protonated impede the propensity of the isoalloxazine(s) to receive electrons.

Spectrophotometric Deconvolution of DPD Reductive Activation

The delineation of the activation process into two phases (Figure 27) provided an opportunity to identify and assign more of the chemistry involved. For both the C671S and C671A variants the activation process was

observed by CCD spectrophotometric detection and the three-dimensional datasets obtained were deconvoluted by singular value decomposition to give the pure spectra of the participating states (Figure 28).

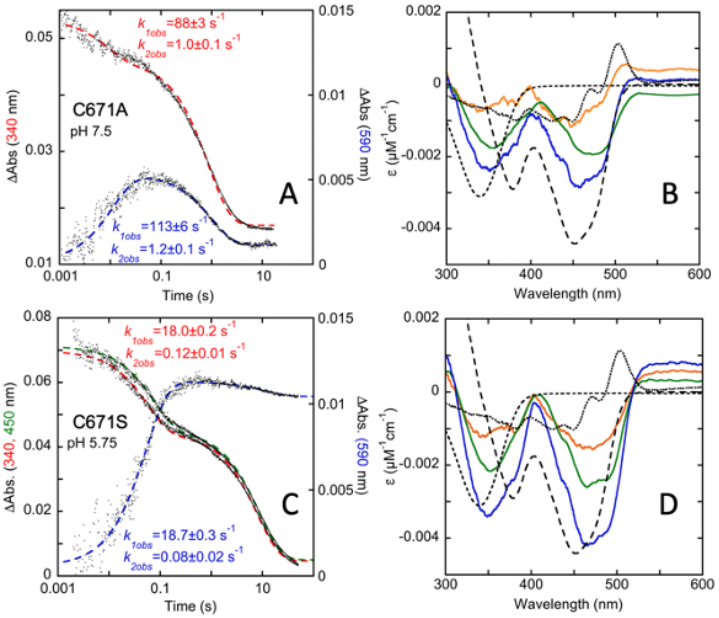

Figure 28. Deconvolution of DPD C671S and C671A activation events. Top. DPD C671A (15 μM) was mixed with NADPH (13 μM) in the presence of thymine (100 μM). A. Absorbance changes observed at 340 nm (red) and 580 nm (blue) for the reductive activation of DPD C671S. The data were fit to a linear combination of two exponentials according to Equation 14 which returned rate constants as shown. B. Difference spectra derived from component spectra derived from singular value decomposition of the absorption changes observed during activation of DPD C671A. Orange, difference spectrum for phase 1. Green, difference spectrum for phase 2, Blue net difference spectrum for both phases. Overlaid are reference difference spectra for reduction of a flavin/2 (large dashes), oxidation of NADPH/2 (small dashes), binding of $NADP^+$ at pH 7.5 (dotted). Bottom. DPD C671S (14 μM) was mixed with NADPH (50 μM) in the presence of thymine (100 μM). C. Absorbance changes observed at 340 nm (red), 450 nm (green) and 580 nm (blue) for the reductive activation of DPD C671S. The data were fit to a linear combination of two exponentials according to Equation 14 which returned rate constants as shown. D. Difference spectra derived from component spectra from singular value decomposition of the absorption changes observed during activation of DPD C671S. Orange, difference spectrum for phase 1. Green, difference spectrum for phase 2, Blue net difference spectrum for both phases. Overlaid are reference difference spectra for the reduction of a flavin/2 (large dashes), oxidation of NADPH/2 (small dashes), binding of $NADP^+$ at pH 5.75 (dotted).

Subtraction of successive spectra then yielded the net absorption changes in the intervening step. The NADPH concentrations used for each variant differed and so each dataset revealed unique aspects of the activation process.

DPD C671A variant eliminates the proton coupled electron transfer required to reduce pyrimidine substrates. However, the variant is observed to take up electrons from NADPH and activate in the presence of substrate pyrimidines. This variant exhibited delineation of the activation steps at pH 7.5 (Figure 28A). The data indicate that charge transfer absorption centered around 590 nm accumulates at ~100 s^{-1}, concomitant with the first phase of

activation. This charge transfer then decays at ~1.1 s^{-1}. The decay corresponds to the net hydride transfer that reduces one of the two flavins of the protomer. Consistent with these conclusions, spectrophotometric deconvolution revealed that the first phase does not include oxidation of NADPH or reduction of a flavin (Figure 28B, orange spectrum). The difference spectrum for the species that accumulates in the first phase instead is qualitatively similar to difference spectrum for binding of $NADP^+$ (Figure 28B, dotted spectrum) added to the charge transfer feature centered around 580 nm. Together these data report the association of NADPH in the first phase observed[97]. In the methods used DPD C671A variant was combined with both NADPH and thymine simultaneously. That no evidence of the distinctive pyrimidine binding difference spectrum[72] was captured indicates that pyrimidine binding is rapid relative to NADPH association. The difference spectrum for the ensuing step indicates oxidation of NADPH added to the absorption changes for reduction of a flavin (Figure 28B, green spectrum) denoting that the second phase is the two-electron activation step. Aspects of these data deviate from expectation. It is unclear why the sum of the difference spectra for both phases does not equal to the absorption changes expected for reduction of one flavin per dimer. Moreover, if only a fraction of the C671A sample is stimulated to activate as the net changes would indicate, it is not apparent why the charge transfer band would not persist in the presence of the residual unreacted NADPH.

These inconsistencies suggest that the C671A variant sample was partially non-functional.

The C671S variant exhibits both delineation of reductive activation into two phases at low pH values and exceptionally slow turnover with thymine (0.00024 s^{-1}) [72]. This variant therefore can be induced to behave similarly to the C671A variant and ostensibly isolate the observation of reductive activation events from subsequent reduction of pyrimidine. In these experiments the concentration of NADPH was fourfold that of the variant (Figure 28C). The purpose of the excess reductant was to demonstrate where the electrons acquired during activation reside within the catalytically active enzyme. If the origin of charge transfer is NADPH•FAD complex, exchange of the $NADP^+$ formed during activation with exogenous NADPH will reinstate/maintain the charge transfer absorption indicating that reduced FAD does not accumulate in the reductive activation reaction. Accordingly, it was observed that excess NADPH promoted sustained charge transfer indicating that the FAD is oxidized in the activated state of the enzyme. The rate of accumulation of this absorption is again coincident with a decrease at all wavelengths between 300 and 500 nm that occurred with a rate constant of ~18 s^{-1} (Figure 28C). This absorption then diminished slightly as the enzyme was reduced with a rate constant of 0.08 s^{-1}. However, for this variant, the difference spectrum associated with the first phase does not have character indicative of NADPH binding and would appear to be

dominated by partial flavin reduction that presumably occurred with excess NADPH. The subsequent reductive phase is tenfold slower than observed with the C671A variant as was expected at pH 5.75, but in this case the net extinction coefficient changes are consistent with the reduction of ~one flavin per dimer.

Structural Evidence for the Activated State of DPD

Kinetic evidence presented herein and in prior studies indicate that the active form of DPD is two-electron reduced. The evidence obtained has implied that electrons from NADPH transiently reduce the FAD but rapidly traverse the protein and reside on the FMN cofactor. The prior evidence for this conclusion was principally that DPD dioxygen reactivity was suppressed by the addition of pyrimidine.[72] Herein, we have presented additional kinetic evidence that the electrons acquired in activation reside on the FMN cofactor. To obtain structural evidence for activation, crystals of DPD variants C671S and C671A were soaked in NADPH and pyrimidine substrates under low oxygen partial pressure in attempt to capture the activated form of the enzyme. As stated, the C671S variant has extraordinarily slow rate of turnover with thymine as a substrate; completing a single turnover in approximately 50,000 seconds[72]. This form of the enzyme therefore has an extended period after activation before significant turnover has occurred, during which the activated state of the enzyme could be captured in the crystal and structurally resolved. Similarly, the C671A variant is incapable of

completing turnover with pyrimidine substrates but retains the reductive activation process. As such, crystals of both forms of the enzyme were soaked in NADPH and pyrimidine for 20 minutes (largely in the absence of dioxygen) and then frozen in liquid nitrogen.

The C671S variant structure was solved to 1.69 Å resolution and is the most complete structure of DPD yet reported, missing density only for residues 675-678 (MGER). The asymmetric unit includes two dimers (AB-CD) and the A subunit is representative of the four protomers. Importantly, the relative high resolution of this structure permitted the discrimination of configurational differences for the flavin cofactors. These data are consistent with the proposed activated state of the enzyme that has the FMN cofactor reduced.

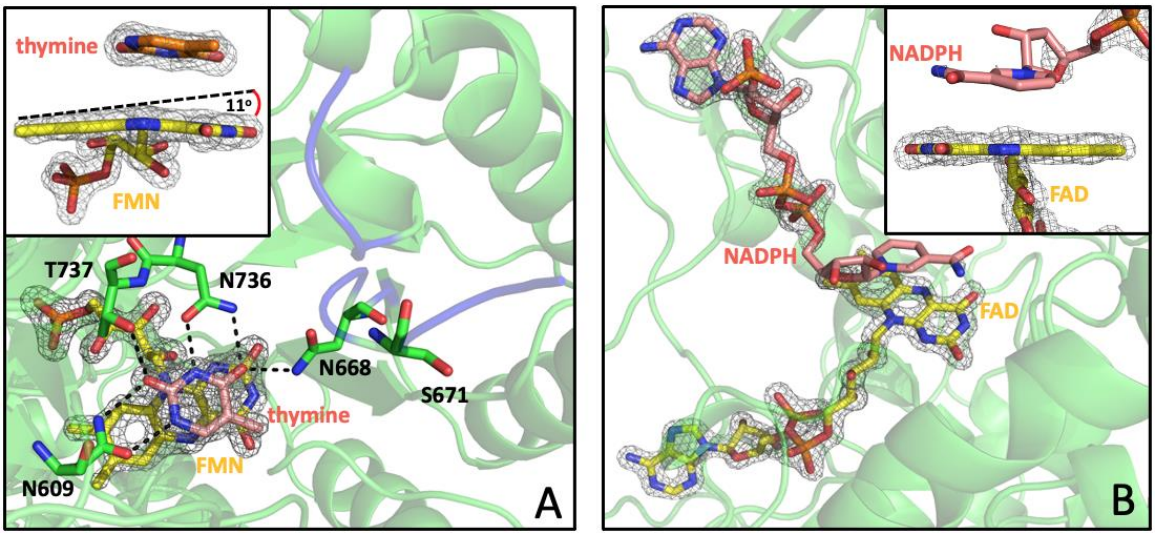

Figure 29. Crystal structure of the activated (DPD-FMNH$^-$) form of the DPD C671S variant in the presence of thymine and NADPH (PDB ID: 7M31). Density is for the omit map was contoured at 2.0σ and was generated by excluding, FAD, FMN, NADPH, thymine and S671 for the model. A. Pyrimidine active site with bound thymine (pink) and FMN (yellow). All residues within hydrogen bonding distance of thymine are shown as green sticks and the mobile loop is shown in blue. B. NADPH binding site with bound NADP(H) (pink) and FAD (yellow). Insets, close-up of active site ligands. The angle (pucker) of the flavin isoalloxazine is indicative of the oxidation state of the flavin; pucker indicates a reduced flavin.

This cofactor while confined by the pyrimidine substrate and residues that stack closely on the *re* and *si*-faces of the isoalloxazine, exhibits an 11° pleat at the N1 and N5 axis, suggesting that the destination of the initial two electrons from NADPH that activate the enzyme (Figure 29A inset). In addition, the density for the FAD isoalloxazine ring is flat within angle error for this structure and was modeled in the oxidized state consistent with the predicted net oxidation state for the activated form of DPD (Figure 29B inset). Importantly, all prior published structures of DPD, some of which were solved to higher resolution, have density for the FMN that indicates the isoalloxazine is planar[7, 27, 98]. While the source of the electrons cannot be definitively known for method that utilizes ionizing radiation, it can reasonably be claimed that this is the first DPD structure to exhibit a reduced cofactor. Regardless of the source of the electrons, this structure was solved in the presence of excess NADPH and is representative of the proposed state of the activated enzyme charge-transfer complex observed in Figure 28C & D.

In the C671S structure, the thymine substrate is positioned over the $FMNH_2$ cofactor with the 6-methyne carbon 3.3 Å from the flavin N5. The variant serine residue is 11.1 Å from the thymine 5-position that would ultimately receive the proton from this side chain. As such this structure captures a state of the enzyme that precedes reduction of the pyrimidine in which the active site general acid, located on the only mobile structural

element within the protein, is distant from this substrate. Conformational mobility for residues 669-684 has been observed in multiple structures of DPD and the presumed function of this movement is to gate ingress and egress of pyrimidines and potentially shelter the reaction from solvent[7, 27]. That this loop was captured in a conformation that places the 671 general acid distant from the site of protonation suggests that catalytic turnover in the crystal lattice is impeded in addition to the pronounced slow turnover exhibited by this variant with thymine as a substrate[72].

The C671A variant structure that was generated from crystals soaked in a similar manner to those of C671S did not reveal definitive evidence of the reduction state of either flavin cofactor. The reason for this was presumably the slightly lower resolution obtained for this structure (1.82 Å). This structure is presented only to illustrate the contrast for what was ascertained at each level of resolution (Appendix D). Nonetheless, $FMNH_2$ was the cofactor oxidation state that best fit the density observed.

Transient-State Kinetic Isotope Effects

Transient-state kinetic isotope effects (KIE) were assessed by observing the successive activation and turnover phases of DPD C671S at 340 nm in the presence of either NADPH or Pro-S NADPD[27]. For both substrates $NADP^+$ was enzymatically reduced using the same methods to avoid observing changes in rates derived from contaminants specific to the preparatory protocol. When observed at 340 nm, the Pro-S NADPD substrate

resulted in a kinetic isotope effect of 1.90 ± 0.03 on the activation phase of DPD and the ensuing turnover phase was unaffected by the nicotinamide-derived deuterium (Figure 30).

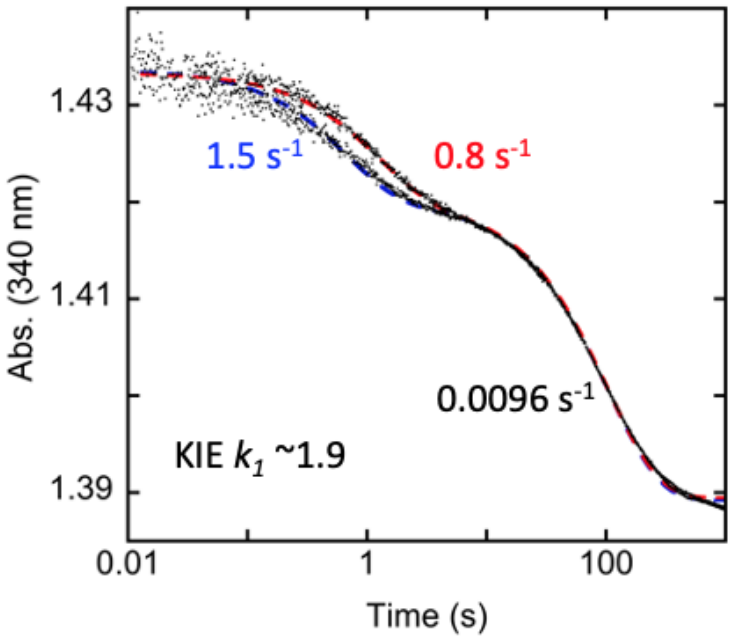

Figure 30. Transient state kinetic isotope effects on C671S DPD. C671S variant (15 µM) in MAT buffer prepared anaerobically mixed with saturating uracil (100 µM) and either NADPH (blue) or NADPD (red) (both 9 µM). Traces were collected under single turnover conditions monitored and at 340 nm for 1000 seconds at 20 °C. Data was fit to a combination of exponentials (Equation 13).

This indicates that hydride transfer from NADPH to the FAD isoalloxazine is rate limiting in activation. Assuming that the oxidation of $FADH_2$ is rapid, the deuteride that is transferred to the FAD N5 slows the observed rate of reduction of the FMN. In this manner the FMN is acting as an electron sink, drawing electrons across the assumed barrier-less/low resistance of the FAD, iron-sulfur center conduit. Reductive activation in this manner requires protonation of the FMN N5 via an active site general acid. The only residue observed to be proximal to this position is Lysine 574 (3.1 Å) which has a conformation that places the amine in line with the plane of the

isoalloxazine, an appropriate position to both protonate the sp^2-hybridized N5 of the oxidized form of this cofactor.

Discussion

The fundamental curiosity of DPD is the complexity of the enzyme relative to the chemistry catalyzed (Figure 25, Figure 24). Flavoproteins that catalyze dehydrogenation reactions typically have ping-pong mechanisms that have an intervening reduced state of the flavin that exchanges oxidized substrates. These enzymes can be studied comprehensively using transient-state methods as reductive and oxidative half-reactions by omitting substrates required for the preceding or ensuing half-reaction. Our recent publications have shown that DPD cannot be studied using transient-state half-reactions. The reason for this is that once the enzyme has undergone reductive activation no further reduced form of any of the cofactors is observed during catalysis. The overarching conclusion is that the internal electron transfer rate is rapid relative to the low rate of turnover (WT DPD 0.9 s^{-1}) which is defined by a slow process on which electron transfer is contingent.

We recently published two transient-state and structural investigations of DPD that revealed the active state of DPD is two-electron reduced and that these electrons come from NADPH and reside on one of the two flavins within the enzyme[72, 94]. In this study we consolidate these observations with further investigation of the observable steps of reductive activation and

turnover reactions. Reductive activation of the enzyme is an initial process prior to catalytic turnover that is observed as a consequence of the enzyme being isolated under aerobic conditions ensuring that all cofactors are oxidized. In single turnover reactions of the WT enzyme, the reductive activation step is not kinetically distinct from the subsequent turnover phase. As such, in most instances we have employed the C671S variant of DPD that alters the pyrimidine active site general acid and slows the rate of catalytic turnover to a greater extent than the rate of reductive activation. This kinetic delineation of functionally separate processes has permitted a more focused investigation of what occurs in each[72].

The pH-dependence of the apparent rate of turnover indicated that deprotonation of a group or groups with a net pKa of ~8 increases the rate of catalysis by fourfold (Figure 26A). This is opposite for what is expected for the titration of an active site acid residue. Moreover, this pKa is changed to 7 in the C671S variant indicating that the rate is not defined by the pKa of the residue in the 671 position. We tentatively conclude that the pKa reports the protonation state of the adjacent $FMNH_2$ cofactor that has more capacity to delocalize electrons when the N1-position is deprotonated and thus is more competent to reduce the pyrimidine. However, we do not attribute the protonation state of the FMN as defining the rate of turnover, but rather that the anionic form of this cofactor increases the probability that pyrimidine reduction will occur (see below).

The convex shape of the proton inventory data for the rate of pyrimidine reduction reveals that DPD has a hydrogen in flight in the transition state for the step that reduces the pyrimidine substrate that has fractional deuterium occupancy in D_2O solvent (Figure 26B). These data, however, do not definitively distinguish between one and two hydrogens in flight and so do not unambiguously resolve the mechanism of pyrimidine reduction. The data are however consistent with the donation of the C671 proton in the rate limiting step. The hydrogen bonded to the N5 position of $FMNH^-$ is also subject to exchange with solvent and the transfer of this hydride must occur in the same step unless the transient formation of a pyrimidine anion is proposed. However, the formation of such a species can be discounted by the fact that the C671A variant is incapable of pyrimidine reduction.

The N5 hydrogens of both $FADH_2$ and $FMNH^-$ are displaced during turnover; however, the hydride that was donated to the FAD N5 from NADPH is displaced as a hydrogen when in D_2O solvent only if the rate of electron transmittance from this cofactor greatly exceeds the rate of solvent exchange. That the rate of turnover is unaffected when Pro-S NADPD is used as a substrate (Figure 24) indicates that the required displacement of the N5-deuterium from the reduced FAD is rapid, validating the proposal that electrons are, in both activation and turnover, rapidly transmitted forward from $FADH_2$. That activation of the C671S variant can be further resolved

into two phases at low pH, that binding of NADPH is the first process observed and that reduction of the FMN is the second (Figure 28A & B), indicates that the rate of activation is limited by the rate of hydride transfer from NADPH to FAD and not the rate of oxidation of $FADH_2$ (Figure 27A). This conclusion is supported by the fact that the pKa of ~8 observed for the limiting rate of activation differs from the pKa observed for the turnover phase for this variant (Figure 26, pKa of 7), suggesting that the pKas arise from the titration of separate groups. These are tentatively ascribed to a deprotonation event near the FAD that increases the rate of hydride transfer from NADPH in reductive activation and deprotonation of another group at or near the reduced FMN that increases the rate of pyrimidine reduction in turnover.

Evidence that transmittance of electrons across the protein is facile and rapid relative to the rate of turnover is based in the observation that the absorption of the enzyme's cofactors is largely unchanging in turnover[72]. Other than small perturbations of both flavin spectra in response to substrate/product association, no further reduced state of the enzyme is observed. This is interpreted as the substrate and cofactor set utilizing a Newton's cradle mechanism in which two-electrons enter the system from NADPH as two electrons are displaced onto the pyrimidine, without the accumulation of an intervening reduced state for any cofactor[72]. This is not a perfect analogy as exchange of electrons between adjacent cofactors in the

conduit would occur in a single-electron and stepwise manner, but the speed of these exchanges means that observationally electrons enter the system with the same rate at which they exit. The requirement for single electron steps is supported by the data of Lohkamp et al., who established that non-activated DPD is EPR silent indicating that the Fe_4S_4 centers are in the 2+ state and populated only with Fe(II) ions[34], in this state the clusters can conventionally only accept one electron. Moreover, stoichiometry measurements for NADPH consumption and the structural data presented here indicate that these centers do not change oxidation state with reductive activation[72]. One illustrative implication of this for the activated form of the enzyme is that the two electrons provided by NADPH are used only to reinstate the oxidation state of the $FMNH_2$ cofactor and thus reduce the pyrimidine substrate that is acquired with the subsequent turnover. Further evidence for rapid electron transfer is found in the activation step that establishes the functional oxidation state of the FMN (Figure 28). The accumulation of NADPH•FAD charge transfer is observed without observation of reduced FAD, indicating that electrons from NADPH rapidly traverse the protein.

Figure 31 summarizes the observed and inferred processes of the C671S DPD activation and turnover reactions. While not comprehensive for all possible random binding and release steps, the scheme does illustrate a mechanism consistent with the observations made here and in our prior

publications[72, 98]. This scheme indicates that the observed rate of turnover of DPD is slow despite proposed rapid electron transmittance[72]. As such, we must conclude that some other factor limits the rate of turnover.

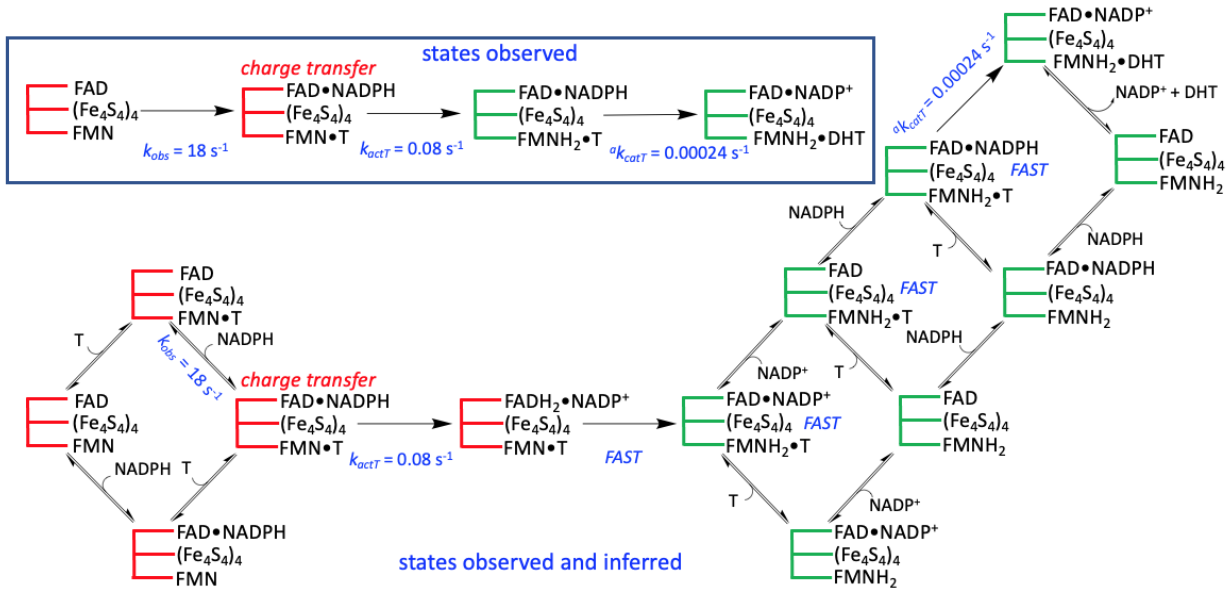

Figure 31. Observed and inferred steps in DPD C671S activation and turnover with thymine. Non-activated enzyme is shown with a red cofactor scaffold and active with a green scaffold. The primary scheme depicts all steps observed and inferred while the boxed reaction sequence depicts only what is observable. *a* – taken from Beaupre et al., 2020 Biochemistry, 59 pp 2419-2431.

We propose that for the activated enzyme the input of electrons from NADPH at the FAD site is controlled by the positioning of the distant 671 residue (C or S) that when proximal to the pyrimidine substrate completes the proton-coupled electron-transfer conduit. We and others have observed that the loop bearing the 671 residue is the only structural feature to exhibit multiple conformations in X-ray crystal structures[22, 48]; and this loop is observed to be dynamic even when the C671 residue is covalently tethered to a reactive substrate analog [7, 27, 98]. While the donation of the proton supplied by this residue is assumed to be facile, the relative scarcity of the proton arising

from movement of the 669-684 loop is suggested to be the primary governing factor in the rate of catalysis.

CHAPTER 4

MAMMALIAN DIHYDROPYRIMIDINE DEHYDROGENASE

Introduction

Dihydropyrimidine dehydrogenase (DPD) catalyzes the first step of pyrimidine catabolism by promoting the reduction of the 5,6-vinylic bond of thymine or uracil with electrons acquired from NADPH (Figure 32).

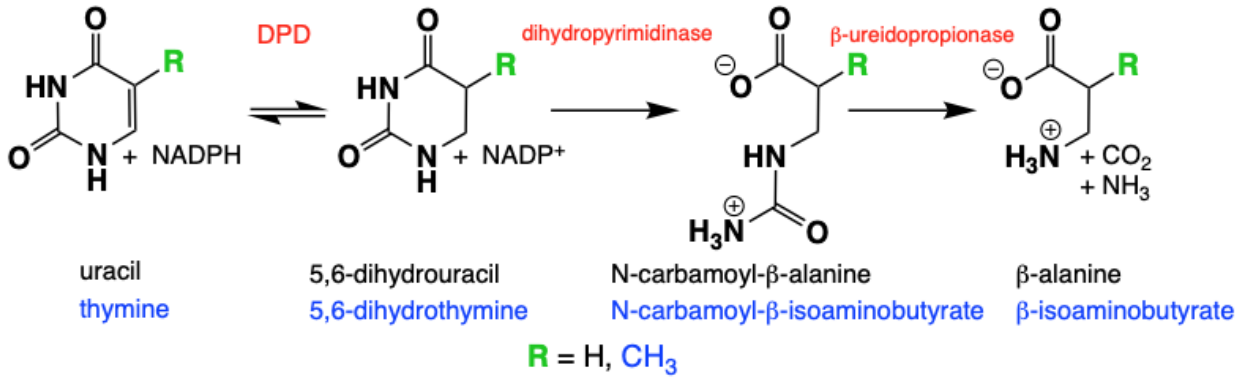

Figure 32. Pyrimidine catabolism

DPD has considerable clinical significance as it accepts the pervasive chemotherapeutic 5-fluorouracil as a substrate, severely shortening its pharmacological half-life and dictating the use of elaborate compensatory administration protocols to achieve efficacious toxicity [16, 47]. The pyrimidine reduction reaction catalyzed by DPD is similar to the reaction catalyzed by dihydroorotate dehydrogenase (DHOD), an enzyme that oxidizes the 5,6-bond of dihydroorotate to orotate as part of pyrimidine biosynthesis. Despite

the simple net hydride transfer chemistry, DPD uses an elaborate cofactor set to facilitate pyrimidine reduction. Mammalian DPD is a functional homodimer, and each subunit contains an FAD, an FMN and four Fe_4S_4 centers with two Fe_4S_4 centers from each subunit forming an electron transfer conduit that link the flavins within each subunit. The catalysis of DPD has been studied for five decades, but its unconventional architecture and catalytic behavior has largely impeded detailed assessment of its catalytic mechanism. Recent observations have revealed unexpected sequences of redox cycling and hydrogen transfers that have narrowed the mechanistic possibilities. The purpose of this review is to describe these advances in the context of prior mechanistic and clinical observations that have been reported for this enzyme.

Clinical Significance

5-Fluorouracil (5FU) and 5FU prodrugs are among the most-commonly prescribed cytotoxic agents used in the treatment of cancer. In the United States approximately 570,000 courses of treatment are prescribed each year. 5FU was synthesized and offered as a potential inhibitor of tumor cells when it was discovered that liver tumor cells sequestered uracil at a rate above that of normal liver cells[8, 9]. 5FU has since proven to be one of the more versatile and durable cancer therapeutics and remains as the central component of the standard of care for colorectal, specific types of breast, aerodigestive, ovarian, head and neck, and skin cancers. With near

equivalent shape to that of uracil, 5FU is incorporated into RNA and DNA via the nucleotide 5FUMP (Figure 33).

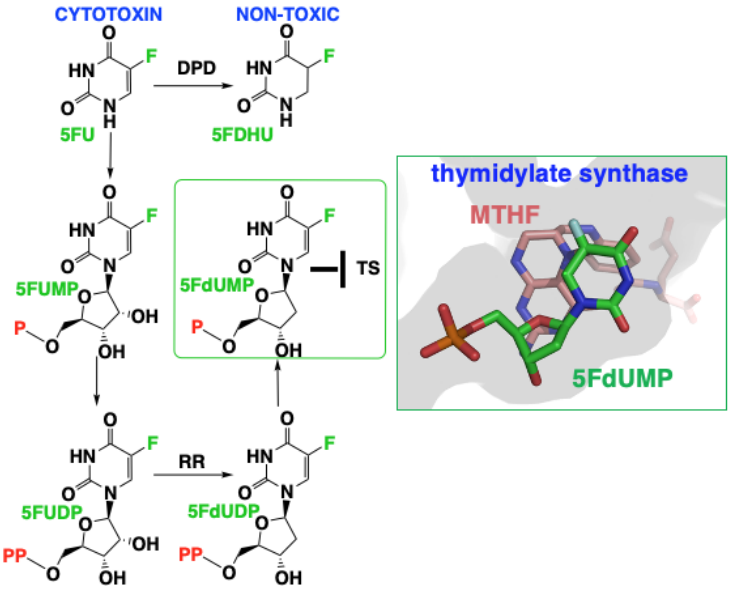

Figure 33. Metabolism of 5-fluorouracil. 5FU is initially incorporated into RNA nucleotides. Ribonucleotide reductase (RR) accepts 5FUDP as a substrate leading to the production of 5FdUMP. 5FdUMP forms an inhibitory ternary complex with methylenetetrahydrofolate (MTHF) and thymidylate synthase (TS), limiting the production of thymidylate

RNA and DNA biosynthesis are linked via the activity of ribonucleotide reductase (RR) that will convert 5FUDP to 5FdUDP, which when dephosphorylated to form 5FdUMP becomes a potent inhibitor of thymidylate synthase (TS)[13]. 5FU is therefore able to stall *de novo* synthesis of thymine nucleotides, halting cell division and inducing apoptosis[99, 100]. While toxic to all cells, 5FU is particularly toxic to cells undergoing rapid growth and division. However, 5FU is rapidly detoxified ($t_{1/2}$~8-14 mins) by DPD[11-18]. The efficiency with which DPD detoxifies 5FU has meant that patients are typically administered a bolus followed by ~48 hours of continuous infusion using an ambulatory pump coupled to a central venous catheter. Infusion via the pump can provide sustained 5FU levels but incurs complications of infection, thrombosis and reduced compliance. Moreover, the 30-fold

variability of net DPD activity in individual patients means that dosing for optimal tolerance and efficacy is difficult[16, 47, 48, 83, 101-103]. Inhibition of DPD activity has been extensively offered as the means to reliably attain and sustain patient specific optimal dosing[18, 21, 57, 104]. 5FU can also be administered orally as the prodrug, capecitabine, but as a consequence of DPD activity the cellular 5FU concentrations achieved are dramatically lower than by infusion[105]. Inhibition of DPD would therefore also potentially provide a path to an improved therapeutic index for capecitabine-based 5FU administration[49, 106] that would in turn increase both compliance and neoplastic toxicity while also reducing infection rates and cardio-thrombic complications associated with indwelling central venous catheters. Inhibition of DPD has consequently been a prominent component of research of the enzyme. Inhibitors of DPD have universally been pyrimidine analogs with modifications to the substituent at the C5 of the pyrimidine ring. Two such molecules are 5-ethynyluracil (5EU) and 5-iodouracil (5IU) (Figure 34). 5EU inhibits DPD by thiol-yne click chemistry with the thiol of the pyrimidine active site general acid cysteine [19, 94] (see below) irreversibly inactivating the enzyme.

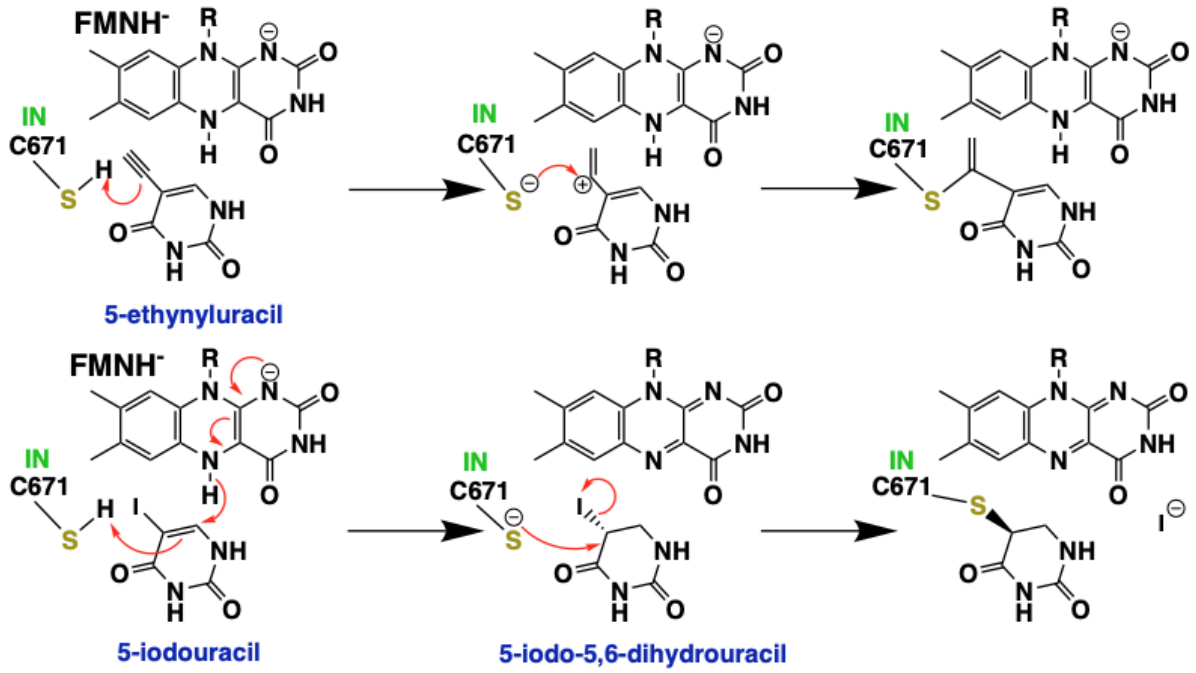

Figure 34. Proposed mechanisms for inactivation of DPD by 5-ethynyluracil and 5-iodouracil

5IU also has been shown to inhibit DPD through covalent modification of the same residue but has not been studied extensively. It is thought that 5IU is a substrate for DPD and the product, 5-iodo-5,6-dihydrouracil, is the inhibiting form of the ligand that induces nucleophilic attack by the active site cysteine acid with displacement of the iodo-group[6]. Mechanistic aspects of DPD inhibition by 5EU will be discussed below in the context of structural changes that occur during catalysis.

Structure of DPD

Dobritzsch et al. were first to report X-ray crystal structures of porcine DPD and so can be credited with much of our current structural

understanding of the enzyme[7, 27]. Consequently, throughout this review residue numbering will reference the primary structure of the porcine enzyme. The initial structural analyses were later comprehensively compiled in a review article by Schnackerz et al[23] and will be summarized briefly here. Each 1025 amino acid subunit of DPD has five domains (Figure 35). Domain I (residues 27-173) is comprised solely of α-helices and contains two Fe_4S_4 centers near the N-terminus that are proximal to the FAD and NADPH binding site. The Fe_4S_4 center most proximal to the FAD has a unique ligand arrangement with three cysteines and one glutamine coordinating the iron ions of the cluster[107]. Domain II (residues 174-286, 442-524) consists of a parallel β-sheet stacked with α-helices and houses the FAD binding site. Domain III (residues 287-441) consists of antiparallel and parallel β-sheet, the latter of which is stacked with α-helices to form the NADPH substrate binding site.

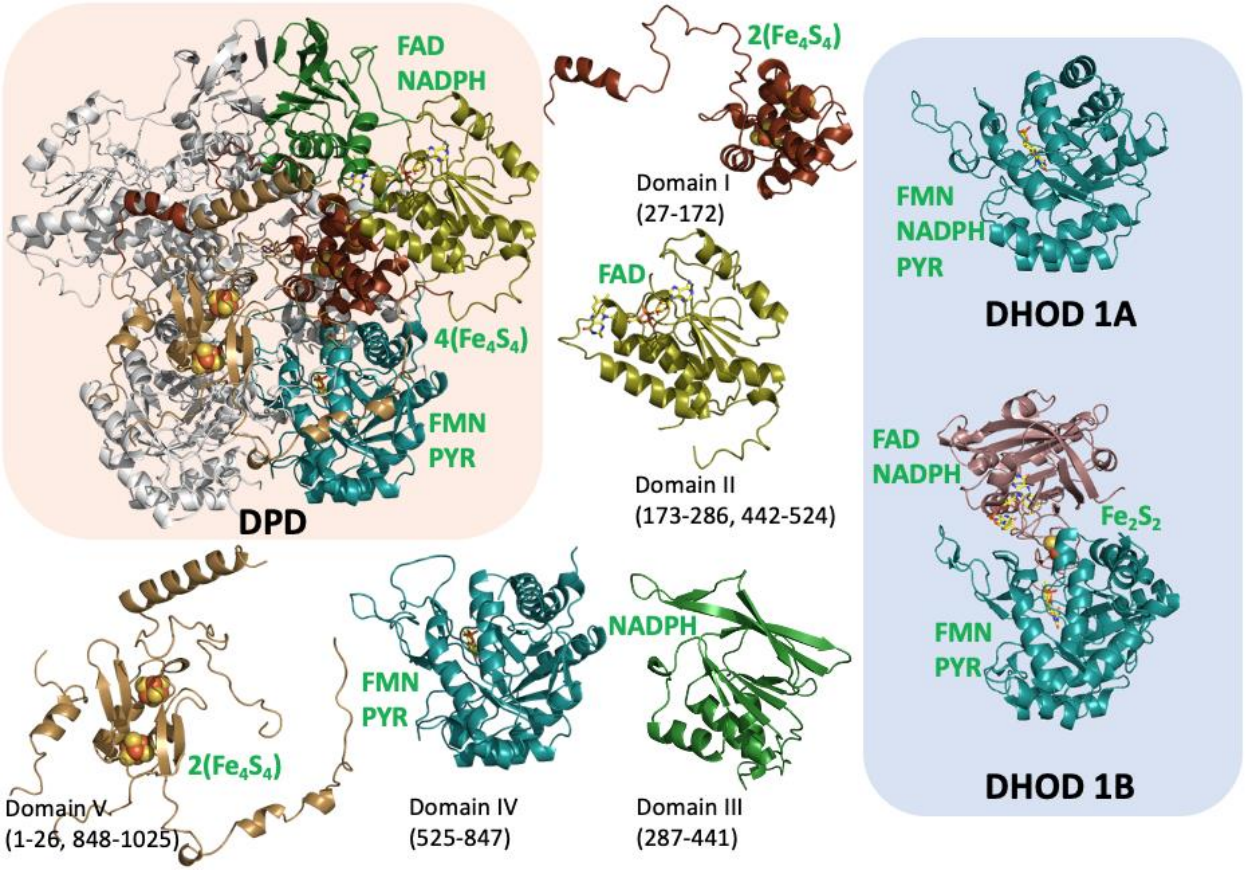

Figure 35. The domains of DPD.

The combined topology of domains II and III are highly similar to adrenodoxin reductase [108, 109] and when added to domain I form a structural module whose topology can been identified in other multi-flavin-dependent enzymes that each use intervening iron-sulfur clusters to deliver electrons between flavins (Figure 36)[110].

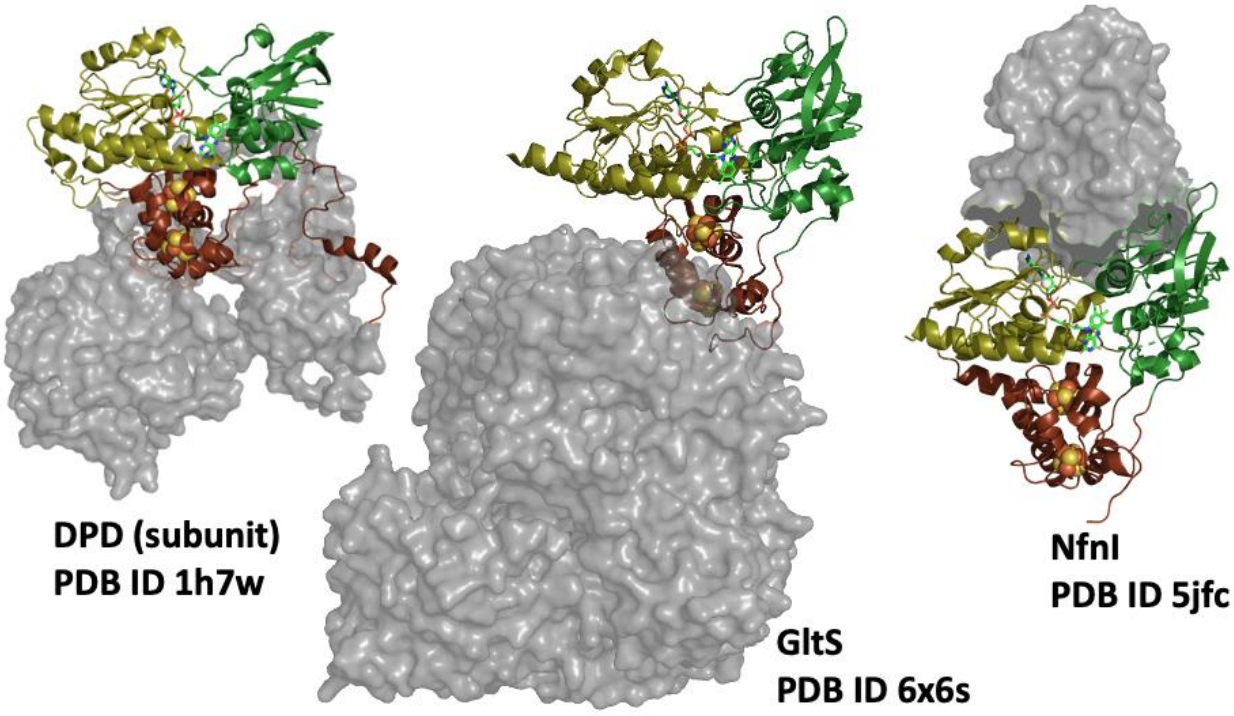

Figure 36. The conserved electron insertion module. Domains I, II and III of DPD comprise $2Fe_4S_4$, FAD and NADPH binding domains and form a conserved structural feature that is also observed in bacterial glutamate synthase (GltS) and NADH-dependent ferredoxin:NADP oxidoreductase (NfnI).

Domain IV (residues 525-847) is an $\alpha_8\beta_8$ TIM barrel fold[111] that forms the binding site for the FMN cofactor and substrate pyrimidines that are localized ~60 Å distant from the NADPH active site formed by domains II and III. A catalytically critical residue, C671, resides in Domain IV proximal to the pyrimidine binding site. This residue has been shown to donate its sulfhydryl proton to complete pyrimidine reduction[23, 27, 30, 34, 72, 94, 112]. Domain V (residues 1-26, 848-1025) contains the two C-terminal Fe_4S_4 centers that lie adjacent to the pyrimidine active site of the partner subunit.

Domain IV resembles the structure of *Lactococcus lactis* class 1A dihydroorotate dehydrogenase (DHOD), an enzyme that catalyzes a similar

reaction oxidizing 5,6-dihydroorotate to orotate as the fourth step of *de novo* pyrimidine biosynthesis[39, 113]. Domain IV also resembles the N-terminal domain of the class 1B DHODs establishing that the machinery for redox chemistry in the catabolism and synthesis of pyrimidine bases is largely conserved (Figure 35). Furthermore, class 1B DHODs have FAD and FMN cofactors each bound at separate sites that are bridged by a single Fe_2S_2 center. These sites interact with $NADP^+$ and 5,6-dihydroorotate respectively, and so the cofactors are arranged similarly to those observed in DPD[42].

All five domains have contact with the adjacent subunit and collectively form a subunit-subunit interface of ~10,800 Å^2 [27]. DPD has been shown to be rigid in its tertiary and quaternary structures. When comparing the structures of holoenzyme and ternary complex of wild type DPD, the only significant deviation in the structure is the conformation of the 669-684 loop, an apparently mobile protein segment that contains the general acid residue, C671. The ligand-free DPD as well as pyrimidine binary complexes were shown to have the mobile loop in an open position with C671 positioned ~10 Å from the site occupied by the C5 of the pyrimidine. The closed form of DPD is observed only in the NADP(H) and pyrimidine ternary complex. In this position C671 is ~3.3 Å from the pyrimidine C5, a position clearly more conducive to proton transfer[7, 27, 94].

The DPD architecture suggests that the FAD, FMN, NADPH, pyrimidines and two Fe_4S_4 centers from each subunit form a linear electron conduit that

shunts electrons from NADPH to pyrimidine substrates (Figure 37). Two Fe_4S_4 centers and the FAD cofactor are coordinated by domain I and II of the same subunit. The Fe_4S_4 centers nearest the FMN cofactor are from the domain V of the adjacent subunit. As such electrons traverse a path that includes parts of both subunits of the DPD dimer. This ~60 Å transmission of electrons is formally only inferred from the structure as no observation has yet recorded a reduced state of the Fe_4S_4 centers during catalysis[30, 34, 94, 112, 114]. The available structures however do plainly imply that catalysis begins with transfer of a hydride from NADPH to the isoalloxazine of FAD and that these electrons then transmitted through the Fe_4S_4 centers to the FMN and on to the pyrimidine.

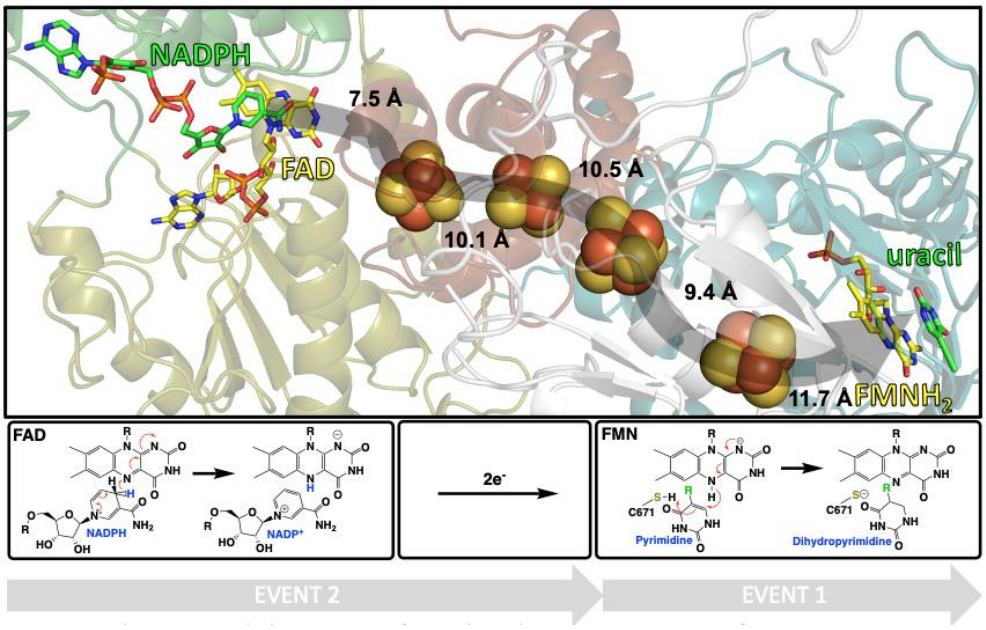

Figure 37. The proposed electron transfer path and reaction sequence of DPD. Distances indicate the proximities of cofactors.

It can be assumed that electrons travel sequentially through the obligate one-electron acceptor/donor Fe_4S_4 centers [107]. It is therefore expected that the flavins will cycle between oxidized, hydroquinone and semiquinone states during catalysis to receive and transmit electrons through the chain of Fe_4S_4 centers. A hydride equivalent is transferred to the FMN and then to the C6 of the pyrimidine and this is reliant on proton addition from the thiol of C671 to the pyrimidine C5 [23, 33]. The precise sequence of events that bring about pyrimidine reduction are not known, though recent advances have confined the mechanistic possibilities considerably (see below).

The Interactions of Substrates within the Active Sites

In Figure 30 and 31 the ligand interactions of NADPH and pyrimidine are depicted. In Figure 38 NADPH is observed to bind with its dihydronicotinamide ring localized conventionally with respect to the FAD[115].

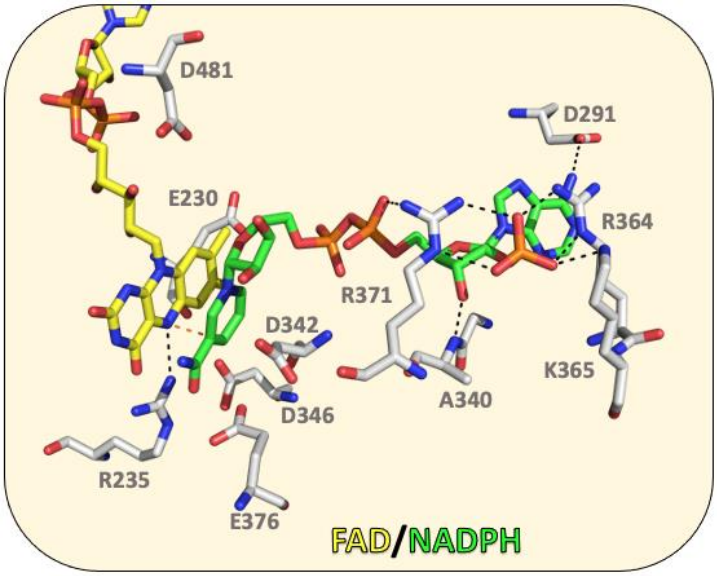

Figure 38. The FAD/NADPH active site ligand interactions of DPD.

The nicotinamide ring is stacked parallel to the FAD isoalloxazine with its C4 2.9 Å from the flavin N5 (gap depicted in orange). DPD has non-covalent interactions primarily with the AMP nucleotide of NADPH where a clustering of positively charged residues form ion pairing interactions with the 3'-phospho-group of the AMP ribose and the pyrophosphate moiety. Single hydrogen bonding interactions are also observed for the adenine and ribose moieties of AMP. Curiously, no hydrogen bonds are observed for the nicotinamide riboside. This single charge pairing interaction for the pyrophosphate added to five negative and one positively charged residue near the stacked dihydronicotinamide•isoalloxazine complex may function to lower the reduction potential of the FAD and thereby facilitate electron transfer to the iron sulfur center conduit.

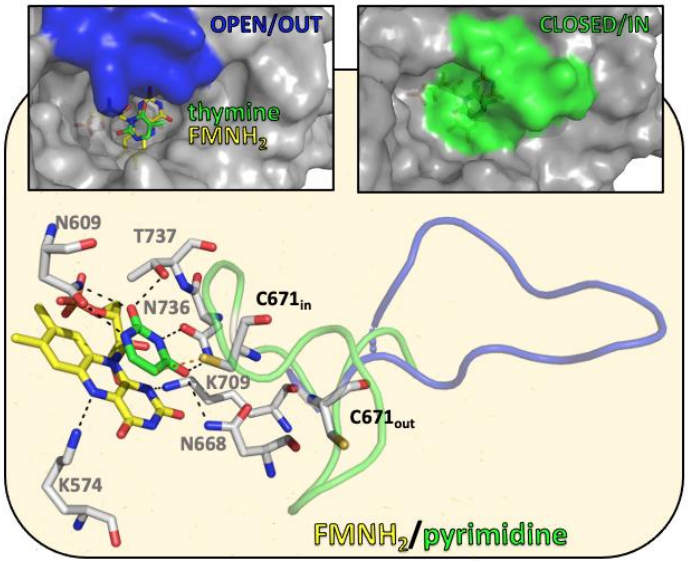

Figure 39. The $FMNH_2$/pyrimidine active site ligand interactions of DPD. A. The complex of NADP(H) with the FAD active site. B. The complex of uracil with the FMN active site. The two positions of the dynamic loop (669-684) are show in green and blue. Insets depict the surface rendering of the active site cavity proximal to the $FMNH_2$ active site. Left inset has the loop residues 669-684 colored in blue and the right inset has these residues colored green.

Figure 39 shows the FMN/pyrimidine active site ligand interactions and the observed conformational states of the 669-684 loop. Pyrimidine substrates are localized adjacent and parallel to the FMN isoalloxazine by six apparent hydrogen bonding interactions; five of which are from the amide residues, N609, N668 and N736 and one from T737. This binding pose places the pyrimidine C6 3.6 Å from the N5 of the FMN isoalloxazine, a position favorable for hydride transfer. The movement of the 669-684 loop toggles the position of the active site acid, C671 by 7.7 Å such that in the *in* position (depicted in green) the thiol sulfur is 3.3 Å from the C5 of the pyrimidine (distance shown in orange). There are no interactions within 4 Å of the pyrimidine C5 position, consistent with the acceptance of uracil, thymine and other 5-substituted uracils as substrates [1, 6, 16]. Two lysine residues first recognized by Dobritzsch et al., K574 and K709, are within hydrogen bond distance to the FMN N5 and N1 of the isoalloxazine respectively[27]. The function of these residues has not been investigated, however there exists requirements to accept (N5) and donate (N1) protons as the FMN is reduced in successive one-electron steps and then oxidized with hydride transfer. These lysine residues are oriented to participate in such acid/base chemistry. Furthermore, the positive potential of these basic residues may raise the redox potential of the FMN such that it can act as the electron sink in the conduit of electron transfer from NADPH.

Mechanistic Studies of DPD

The steps of pyrimidine catabolism were mapped throughout the 1950's and onward [116, 117] and the record of enzymatic research of DPD commences around 1970 [118]. The majority of early studies describe purification from endogenous sources and basic steady-state analyses [1-3, 5, 28, 31]. This advanced through the 1990's and 2000's to pre-steady state kinetics, kinetic isotope effects, spectroscopic studies and investigations of the wild type relative to variant forms of DPD [30, 33, 34, 114]. As stated, the first structures of DPD were reported in the early 2000's[7, 27, 43] and given its unexpected and elaborate cofactor set, it is fair to surmise that the lack of structural data during the prior three decades confounded efforts to comprehend how the enzyme functions[30, 114]. Evidence for this is apparent in the chronology of reports for cofactor content. DPD has been purified from human, murine, ovine, and porcine tissues [1, 28, 29, 32] and the porcine enzyme has been expressed heterologously in *E. coli* [30, 36] and the analytical accounts for cofactor content for these preparations vary considerably.

Despite the lack of structural data for DPD, collaborative studies between the Cook and Schnackerz laboratories developed much of the foundational mechanistic understanding of the enzyme [2, 5, 23, 28]. In particular, the notion of physically separate enzymatic half-reactions was established by these authors. In 1990 Podschun et al. published a study of the steady-state kinetic mechanism of DPD[5]. At low concentrations

competitive inhibition by NADPH versus uracil was observed and uncompetitive inhibition by uracil for NADPH. Product inhibition and dead-end inhibition using ATP-ribose and 2,6-dihydroxypyridine was suggestive of an unconventional two-site ping pong mechanism in which $NADP^+$ dissociation constituted the requisite irreversible step under initial velocity conditions[5].

Three years later Podschun and coworkers published a very detailed pH and solvent kinetic isotope effect study of DPD using steady state approaches [2]. In this study a $^{D}k_{cat}/K_m$NADPH kinetic isotope effect (KIE) of ~1.1 was observed that suggested hydride transfer to FAD is not significantly rate limiting in this half reaction. Solvent kinetic isotope effects (SKIE) for k_{cat}/K_mNADPH of ~2 and for k_{cat} of ~3 were interpreted as derived from the movement of protons at the FAD having significant contribution to the turnover number. From pH dependencies, pKas of 5.8 and 8.2 were observed for k_{cat}/K_mNADPH and were said to be derived from proton movements associated with conformational changes with NADPH binding. Later in a review article published after the first DPD structures were reported, D342 was implicated as the source of the 5.8 value and R235 proposed to be the base abstracting a proton from the FAD N5 with reduction (Figure 38). These researchers also noted that no groups with dissociable protons were located adjacent to N1 of the FAD, suggesting transient formation of the anionic FAD hydroquinone is favored [23].

In the 1993 study by Podschun et al, steady state data that report chemistry at the FMN/pyrimidine active site were SKIEs on k_{cat}/K_mUracil of ~0.7 consistent with ionization of a thiol residue in the events of the half reaction at this site. A SKIE on k_{cat} of ~3.3 is consistent with the transfer of a solvent derived proton in the rate limiting step and was confirmed in later transient state SKIE measured for pyrimidine reduction [112]. pKas of 5.6 and 9.1 observed for k_{cat}/K_mUracil were later proposed to arise from titration of C671 and K709 respectively. As mentioned, the two lysine residues K574 and K709 are proposed to be the general acid/base residues that abstract and supply protons to N5 and N1 respectively during redox cycling of the FMN cofactor (Figure 39) [23].

Characterization of DPD from bovine liver was conducted using steady state and pre-steady state kinetics[31]. The data obtained suggested the enzyme has a random rapid-equilibrium mechanism with independent dissociation constants for uracil and NADPH. DPD was shown to readily catalyze the exchange of tritium from Pro-S NADPT for solvent protons; this exchange rate was maintained even when using 5EU-inactivated DPD. This supported a separate active site model because, as stated, 5EU covalently links itself near the pyrimidine active site while having no influence on NADPH binding. The first order rate constant of deuterium exchange for bound Pro-S NADPD with solvent protons was 5.4 s^{-1}, more rapid than the reported k_{cat} of 1.6 s^{-1}, further validating the proposed rapid-equilibrium

mechanism. These data were similar to those of Podschun et al. 1990 who showed exchange of radio-label between NADPH/$NADP^+$ and uracil/dihydrouracil pairs[5] indicating reversible hydride transfer at both flavins independent of catalytic turnover.

Rosenbaum et al. published secondary tritium isotope effects for 5-^{3}H-uracil in H_2O and D_2O. The only modestly more inverse KIE in deuterium solvent (0.9 vs 0.85) suggested that the hydride transfer and protonation required to reduce pyrimidines were not concerted. These authors argued for a stepwise transfer of the hydride from $FMNH_2$ and a proton from an active site acid. In a separate study published in the same year Rosenbaum et al. reported the first anaerobic transient state data for recombinant porcine DPD. This study measured ligand binding equilibria and included enzyme monitored turnover data that report spectrophotometric changes of the enzyme in the presence of excess substrates [30, 119]. This investigation documented a number of observations that interlock with recent findings (see below). Specifically, ligand binding data indicated low micromolar dissociation constants for uracil and NADPH, which create near first-order conditions in transient state experiments at low substrate concentrations. When DPD was mixed with NADPH with or without pyrimidine under anaerobic conditions, multiphasic fractional reduction involving one flavin per dimer without evidence of reduction of the Fe_4S_4 centers was observed. In the absence of pyrimidine, reduction occurred with a rate many-fold slower

than catalysis (0.02 s^{-1}). Anaerobic reduction of WT DPD by NADPH alone has also been studied by Podschun et al. who showed that incubation of NADPH with DPD in D_2O brought about the incorporation of deuterium into the Pro-S position of the C4 of NADPH [2]. Later Beaupre et al. observed the kinetics of reduction of DPD by NADPH in the absence of pyrimidines under anaerobic conditions. Titration of NADPH showed a corresponding absorption change at 440 nm with first-order reaction behavior for saturating concentrations. Similar to the observations of Rosenbaum et al., the kinetic traces were fit to two exponentials with rate constants of ~2 and ~0.04 s^{-1}; the latter of which was approximately 10 to 20-fold lower than the steady state turnover number for WT DPD in the presence of uracil and thymine respectively and was therefore assigned as not catalytically relevant[72]. The total extinction coefficient change observed for both phases was ~6500 M^{-1} cm^{-1}, approximately equal to the reduction of one flavin per subunit [72]. Together, these data show slow reversible reduction of the enzyme by NADPH in the absence of pyrimidine substrates.

In the presence of uracil, the initial rate of reduction was approximately two orders of magnitude more rapid, resulting in the conclusion that bound pyrimidine promotes hydride transfer from NADPH and establishing an effector role for the pyrimidine substrate[30, 72]. For the enzymatic reaction under anaerobic conditions, it was proposed that the $NADP^+$ formed in the reaction was inhibitory and prevented the complete

reduction of the equivalent of one flavin per subunit. In recent studies the reported fractional reduction observed is accounted for by pyrimidine induced two-electron reductive activation of the enzyme prior to catalytic reduction of the pyrimidine (see below)[72].

Recent Findings that Reframe the Catalytic Mechanism of DPD

The first structures of mammalian DPD settled numerous questions for the chemistry involved[7, 27, 43]. These data made it plain that two hydride transfer events bookend transmission of two electrons across a 56 Å span via four Fe_4S_4 centers that act as a wire (Figure 37). This architecture creates mechanistic constraints that require the flavins mediate the two-electron, hydride transfers that occur from and to the NADPH and pyrimidine substrates and the one-electron chemistry that occurs at the Fe_4S_4 centers. Hagen et al., showed that the resting form of DPD is EPR silent and so all Fe_4S_4 centers are assumed to be in the 2^+ state[107, 114]. It is therefore surmised that in order to sequentially transmit electrons through the chain of Fe_4S_4 centers during catalytic turnover the FAD and FMN will cycle

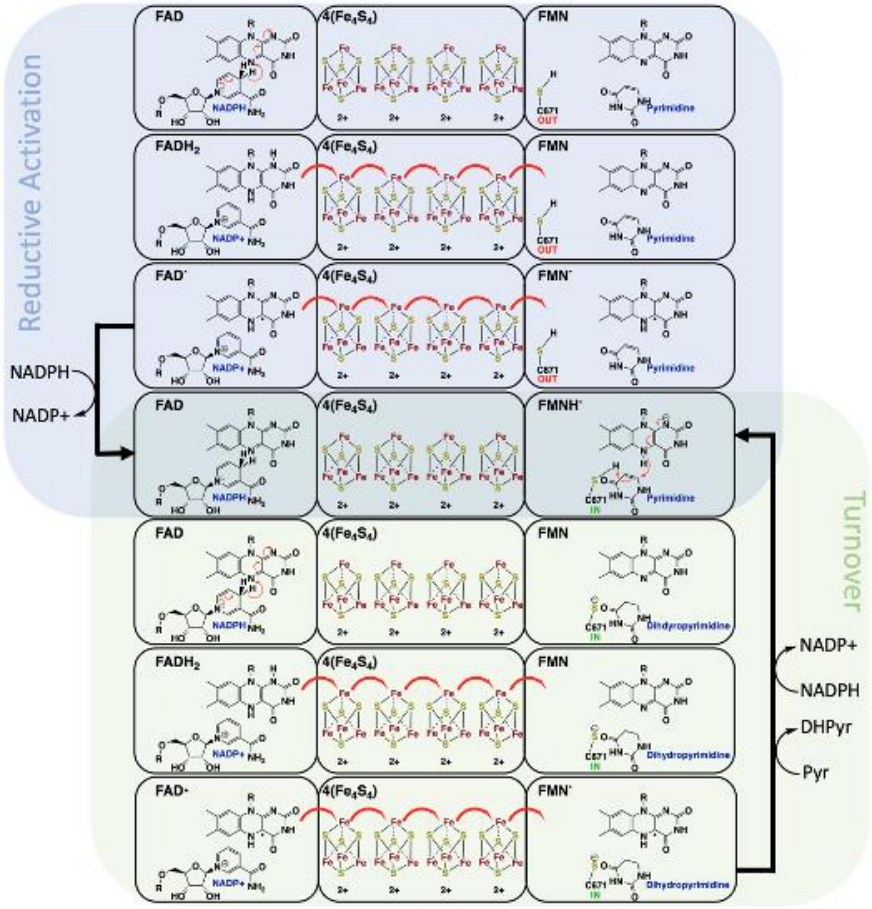

Figure 40. The proposed steps in reductive activation and turnover of DPD between oxidized to hydroquinone to semiquinone states. These constraints, however, do not define the order of events that result in pyrimidine reduction and recent data have revealed rather unexpected sequences for electron transfers within DPD, that arise from the requirement for two-electron reductive activation before pyrimidine reduction can occur. In this section we will describe what has recently been deduced from a combination of steady-state and transient-state reactions of wild type and variant DPD's studied under anaerobic conditions[36, 72, 112]. The experiments described

reveal the net chemistry that occurs in each step observed and Figure 40 summarizes the conclusions that were drawn from these data.

As stated, the residue C671 is the necessary proton donor for pyrimidine reduction. Substituting the cysteine with a serine or alanine has shown a respective slowing or abolishment of DPD activity[30, 72, 112]. The movement of the loop on which C671 resides (Figure 39)[7, 27, 94, 112] limits the availability of the thiol proton and would appear to dictate the rate of turnover. Importantly, the C671S variant delineated successive events in single turnover, permitting an account to be made of electrons entering the protein based on spectrophotometric deconvolution and quantitative product analyses that together expanded the understanding of DPD's electron transfer processes[72, 112].

Reductive Activation

Anaerobic transient-state spectrophotometric analyses of the DPD C671S variant established that when DPD is combined with limiting NADPH and excess pyrimidine, the reaction exhibits two phases when observed at 340 nm[72]. The rate of the first phase was shown to be dependent on the enzyme form (WT or C671S) while the second rate was tied to both the enzyme form and pyrimidine substrate (uracil or thymine) and the amplitude of the second phase was proportional to the concentration of available pyrimidine. The first phase was shown to consist of a reduction of a flavin within enzyme with oxidation of NADPH and that this process was rapid only

in the presence of pyrimidine substrate. In this phase NADPH equal to one half the enzyme concentration (as defined by subunit concentration) is oxidized with concomitant reduction of one of the two flavins of one subunit. This apparent half-reaction stoichiometry was surmised to be a result of the reductively activated subunit having high affinity for NADPH and therefore sequestering the residual NADPH, out-competing NADPH binding and activation at the second subunit. This supposition was qualitatively confirmed by simulation of the observed phases using a comprehensive kinetic model in which the dissociation constant for NADPH for the reductively activated subunit was three orders of magnitude smaller than for the non-activated enzyme.

At low pH values the reductive activation phase was delineated further, revealing an additional early phase[112]. This phase was assigned as resulting from the binding of NADPH adjacent to the FAD cofactor. The difference spectrum for this phase indicated that NADPH binding perturbs the DPD spectrum in the visible region and induces broad long-wavelength charge transfer (CT) transitions. In the presence of limiting NADPH the CT transitions decay with the subsequent phase in which the enzyme is reductively activated indicating that the FAD is restored to the oxidized state and implicating the FMN as the recipient of the two electrons that activate the enzyme. Conversely, in the presence of excess NADPH the CT transitions are sustained indicating that the FAD•NADPH complex is reformed by NADP

ligand exchange, consistent with the activated enzyme exhibiting high affinity for NADPH. The deconvoluted difference spectra for each of the two early reductive activation phases show only evidence of NADPH binding in the first event followed by flavin reduction and NADPH oxidation in the second, demonstrating that hydride transfer from NADPH to FAD is rate limiting in activation and that electron transmission from $FADH_2$ to FMN is relatively rapid such that $FADH_2$ is not observed to accumulate. This was verified by transient-state kinetic isotope effect (KIE) single-turnover experiments with the C671S variant using excess pyrimidine and limiting NADPH or Pro-S NADPD. The experiment returned a KIE of ~1.9 for the reductive activation phase confirming that the hydride transfer from NADPH to the FAD isoalloxazine is rate limiting for enzyme activation[112]. The reduction of the FMN cofactor during reductive activation was demonstrated directly by soaking NADPH to crystals of the DPD•thymine complex under near anaerobic conditions. The resulting 1.69 Å resolution structure clearly indicated pleating of the FMN cofactor along the N10-N5 axis of the isoalloxazine consistent with the expected sp^3 geometry of reduced flavin[112].

The pH dependence of the observed rate constants for the two phases of reductive activation showed that the rate of binding of NADPH was largely independent of pH and that the reduction of FMN, via the cofactors of the electron transfer conduit, was highly dependent on pH. The reduction of FMN increased in observed rate constant with increasing pH with a pK_a of 7.9 [112].

This pK_a was tentatively assigned to a group on or near the FAD cofactor that when deprotonated enhances electron transfer from NADPH to FAD and on to the FMN. This assignment was in part based on the assumption that electrons rapidly depart the $FADH_2$ state due to the lowering of the reduction potential of the FAD by a clustering of proximal negative charges (Figure 38). The active state of DPD was thus shown to have the cofactor set of FAD-4(Fe_4S_4)-$FMNH_2$ and this two-electron reduced state of the enzyme was shown to remain even in the presence of saturating oxidant pyrimidine[72]. The FMN cofactor thus is behaving as an electron sink, receiving electrons from across the assumed low resistance conduit formed by the $FADH_2$ and iron-sulfur centers[112].

Structural data for DPD solved in the presence of substrates under near anaerobic conditions reveal that the mobile loop that carries the FMN active site general acid, C671, moves from an open to a closed state with reductive activation. This conformational change both positions the cysteine thiol adjacent to the pyrimidine substrate and occludes the active site from solvent (Figure 39). Interestingly, only in the presence of NADPH does pyrimidine reduction take place, indicating that the two active sites have contingent processes that communicate substrate occupancy.

5EU is FDA approved and has been clinically studied as an adjunct chemotherapy sensitizer to enhance the toxicity of 5FU [49, 51, 56-59, 120, 121]. Though not yet adopted into standard of care protocols, it is established in

rodents that 5FU levels are sustained by its co-administration[21]. The *in vitro* interaction of 5EU with DPD has been investigated in two studies and has proven instructive for the mechanism of reductive activation. In the first study, Porter et al. demonstrated reversible binding to the resting enzyme with a K_d of 1.6 μM and showed that irreversible inactivation could be measured only in the presence of NADPH and that it occurred with rate constant of 0.3 s^{-1}. These researchers also identified covalent attachment of 5EU to an active site cysteine residue[19]. More recently Forouzesh et al. studied kinetic and structural aspects of covalent inactivation of DPD by 5EU. In this study the inactivation rate constant was found to be in good agreement with the Porter et al. study (0.2 s^{-1}). It was also shown that NADPH was oxidized during inactivation and via a combination of anaerobic transient state methods and spectral deconvolution it was shown that one flavin is reduced per subunit concomitant with inactivation of the enzyme. This 1:1 NADPH:(flavin/subunit) stoichiometry for reductive activation differs from the 0.5:0.5 ratio observed for reductive activation with native substrates. These data indicate that 5EU is an effector molecule much the same as native pyrimidines that stimulates DPD reductive activation by NADPH and that this chemistry is required for crosslinking to occur. This structural basis for this was also reported. Three X-ray crystal structures were solved that capture the sequence of events in the 5EU inactivation reaction. These structures show that in the absence of NADPH the target

cysteine is 10.5 Å from the ethynyl group of 5EU and that binding and oxidation of NADPH brings this cysteine within 3.3 Å promoting crosslinking and indelible inactivation.

Pyrimidine Reduction

The substrate stoichiometries for the transient state phases of the DPD reaction were obtained using single-turnover reactions of C671S DPD with excess pyrimidine and limiting NADPH that were acid quenched and subject to HPLC product analysis[72]. Comparing the formation of $NADP^+$ with the reduction of pyrimidine throughout the reaction determined the ratio of NADPH consumption and pyrimidine reduction to be 2:1. NADPH is oxidized both in the reductive activation phase and in the subsequent phase concomitant with reduction of an equivalent of pyrimidine. This demonstrated that the first phase of DPD single turnover is a reductive activation and the second is pyrimidine reduction[72].

The difference spectrum for the pyrimidine turnover phase of DPD in single turnover with saturating uracil and limiting NADPH showed characteristics of substrate binding around 500 nm added to the absorbance change for oxidation of NADPH at 340 nm[72]. The difference spectra showed NADPH oxidation comparable to the reductive activation phase, indicating pyrimidine reduction occurs with NADPH oxidation and is distinct from the reductive activation process. An additional aspect of the difference spectrum for pyrimidine reduction is the absence of a reciprocal change at ~480 nm

when compared to the activation difference spectrum. The lack of an observed flavin oxidation event during pyrimidine reduction even in the presence of excess uracil indicates the enzyme's activated redox state (FAD-4(Fe_4S_4)-$FMNH_2$) persists[72, 112]. This therefore suggests the oxidation of NADPH observed in the pyrimidine reduction phase is used to reinstate the $FMNH_2$ *after* electrons are transferred to the pyrimidine[112].

pH profiles for the rate of WT and C671S DPD turnover were undertaken to ascertain if the pK_a of the active site general acid C671 controlled the rate of catalysis. For both forms of DPD the turnover number reports the rate of pyrimidine reduction[72]. This rate was shown to increase ~4-fold from low to high pH, opposite to the trend for titration of a cysteine thiol. Calculated pK_as were 7.9 and 7.0 for WT and C671S respectively. While the pK_a for the WT could be attributed to the active site cysteine residue, the number for the variant form cannot reasonably be assigned to a serine residue. These data collectively suggest that a different group from the C671 thiol is titrated with pH and that the protonation state influences the rate of pyrimidine reduction. The N1 proton of the $FMNH_2$ was hypothesized as a potential candidate having a pK_a of 6.7 in solution[112]. It was proposed that the observed pK_a's report the protonation state of the $FMNH_2$, attributing the increased rate of pyrimidine reduction to the anionic form of the reduced cofactor that is more prone to delocalize electrons to reduce the pyrimidine[112].

The effect of solvent deuterium for WT DPD was assessed in the presence of excess NADPH and uracil. The proton inventory data were fit best to a solvent kinetic isotope effect (SKIE) of 3.4 that includes significant fractionation factors indicative of the movement of a thiol-derived proton establishing that proton transfer from C671 is occurring in the rate limiting step. The SKIE data could have also been attributed to two exchangeable protons, but the data did not permit definitive discrimination of the two possibilities. Two exchangeable hydrogens are in-flight in the pyrimidine reduction transition state. One as a hydride from the reduced FMN N5 and the second from the thiol of C671. These transfers are inferred to be concerted as the C671A variant can only reductively activate and does not turnover with pyrimidines. As such pyrimidine reduction is dependent on the conformational availability of the C671 and the SKIE value is likely multiplicative for concerted movement of both deuterons.

The indication of rapid transferal of electrons across the protein is based on the absence of observed intervening reduced states of the enzyme during catalysis. With the exception of small perturbations to the flavin spectra from ligand association, no spectrophotometric evidence for the accumulation of a reduced state beyond FAD-4(Fe_4S_4)-$FMNH_2$ has been detected. This has been interpreted as the enzyme operating observationally analogous to a Newton’s cradle; two electrons enter the transfer conduit from NADPH as two more exit with the dihydropyrimidine. The actual order

of events may undermine the value of this analogy as pyrimidine reduction is likely to be the instigating step in catalysis followed by NADPH oxidation to reinstate the active enzyme[34]. Despite apparent rapid electron transmittance, DPD turnover is relatively slow (0.8 s^{-1}). It has been proposed that mobility of the 669-684 loop, and with it the C671 residue, limits opportunity for concerted hydride-proton transfer; a limitation that governs the overall rate of catalysis [112].

Conclusive Remarks

DPD has been a curiosity for enzymologists for more than fifty years. The unexpectedly complex cofactor arrangement seems unnecessarily elaborate in that highly similar chemistry is accomplished by numerous smaller single-domain enzymes that carry only a single flavin cofactor. Nonetheless, the linear path formed by the Fe_4S_4 centers to transmit electrons between the NADPH and pyrimidine, each bound in active sites separated by ~60 Å, would appear to define mechanistic possibilities. From inspection of the enzyme's structure one can appropriately deduce that two obligate two-electron reactions bookend multiple obligate one-electron transfers and that these steps are mediated by the oxidoreductive versatility of the flavins that occupy each active site. Recent advances in the study of DPD have shown that the above deductions are likely correct, but also that the functional state of the enzyme is two-electron reduced at the FMN and that this oxidation state directs an unexpected order of events to bring about

pyrimidine reduction and reinstatement of the active enzyme. Figure 40 depicts a hypothetical mechanism that accounts for much of the recent data assembled for DPD. In this figure it is assumed that a primary function of DPD is the reduction of the FMN cofactor via the FAD-4(Fe_4S_4) conduit with electrons from NADPH. The FMN is assumed to have a relative high reduction potential such that electrons cascade in energy from the NADPH/FAD to the FMN. This process is observed as a reductive activation phase when non-activated, oxidized DPD is combined with pyrimidine and NADPH and as a back-filling reaction after the $FMNH_2$ cofactor passes a hydride to the pyrimidine. In such a mechanism, reduction of the pyrimidine is the instigating and rate-limiting step in catalysis. Reductive reactivation then follows and occurs with a rate more rapid than pyrimidine reduction accounting for the fact that no other reduced state of the enzyme is observed in turnover. Pyrimidine reduction occurs slowly as it is contingent on the proximity of the active site cysteine general acid that resides on a mobile loop that is constantly moving between two conformational states that open and close access the FMN/pyrimidine active site.

In some respects, it is a cyclical argument to define pyrimidine reduction from $FMNH_2$ as the instigating step in the reaction given that the NADPH is oxidized to reduce the FMN cofactor. However, the fact that the FAD-4(Fe_4S_4)-$FMNH_2$ state persists in the presence of excess pyrimidine substrate and the absence of NADPH indicates that the two-electron reduced

form is the resting active state of the enzyme. Moreover, for the reductive (re)activation of DPD to occur at a catalytically relevant rate pyrimidine must be bound in the FMN/pyrimidine active site. This requirement specifies that the two active sites can relay ligand complexation information and will only reduce pyrimidine when NADPH is bound. Though it has not been demonstrated what mechanism links the two active sites, one possibility for the FAD-4(Fe_4S_4)-$FMNH_2$ state is that the average position of the 669-684 loop is biased toward the closed state in the presence of NADPH and the pyrimidine substrate. Only in this conformation is C671 positioned for reduction of the pyrimidine. With the transfer of a hydride and proton to the pyrimidine, oxidation of NADPH backfills the reduced state of the FMN cofactor completing the catalytic cycle.

Targeting the active site general acid cysteine for covalent modification using 5-substituted pyrimidines that mimic the native substrates or products is an effective approach for DPD inhibition [6, 19]. These molecules act as effectors and induce reductive activation and closure of the active site loop in which the general acid cysteine resides, placing it proximal to the reactive 5-substituent. From a clinical standpoint, the problem of inhibition of DPD has in large part been solved. 5EU provides targeted and complete mechanism-based covalent inhibition of DPD and is well tolerated by patients[122]. Why 5EU inhibition of DPD during 5FU chemotherapy hasn't yet resulted in a clear advantage compared to other adjunct therapies is a

question that has been explored extensively by Spector and others[49, 57, 68, 120, 122]. It is possible that excessive 5EU dosing in clinical trials undermined efficacy by causing accumulation of uracil that then competes with 5FU for incorporation into ribonucleotides and thereby diminishes toxicity via 5FdUMP (Figure 33). In a rat model Spector and Cao were able to show complete tumor regression in 88% of rats tested at 1 mg/Kg 5EU and that this rate decreased to 25% at 5 mg/Kg[68].

APPENDIX A

COMPARISON OF THE MOBILE LOOP POSITIONS IN THE DPD•5EU$_{OPEN}$ AND DPD•5EU•NADP(H)$_{CLOSED}$ COMPLEXES

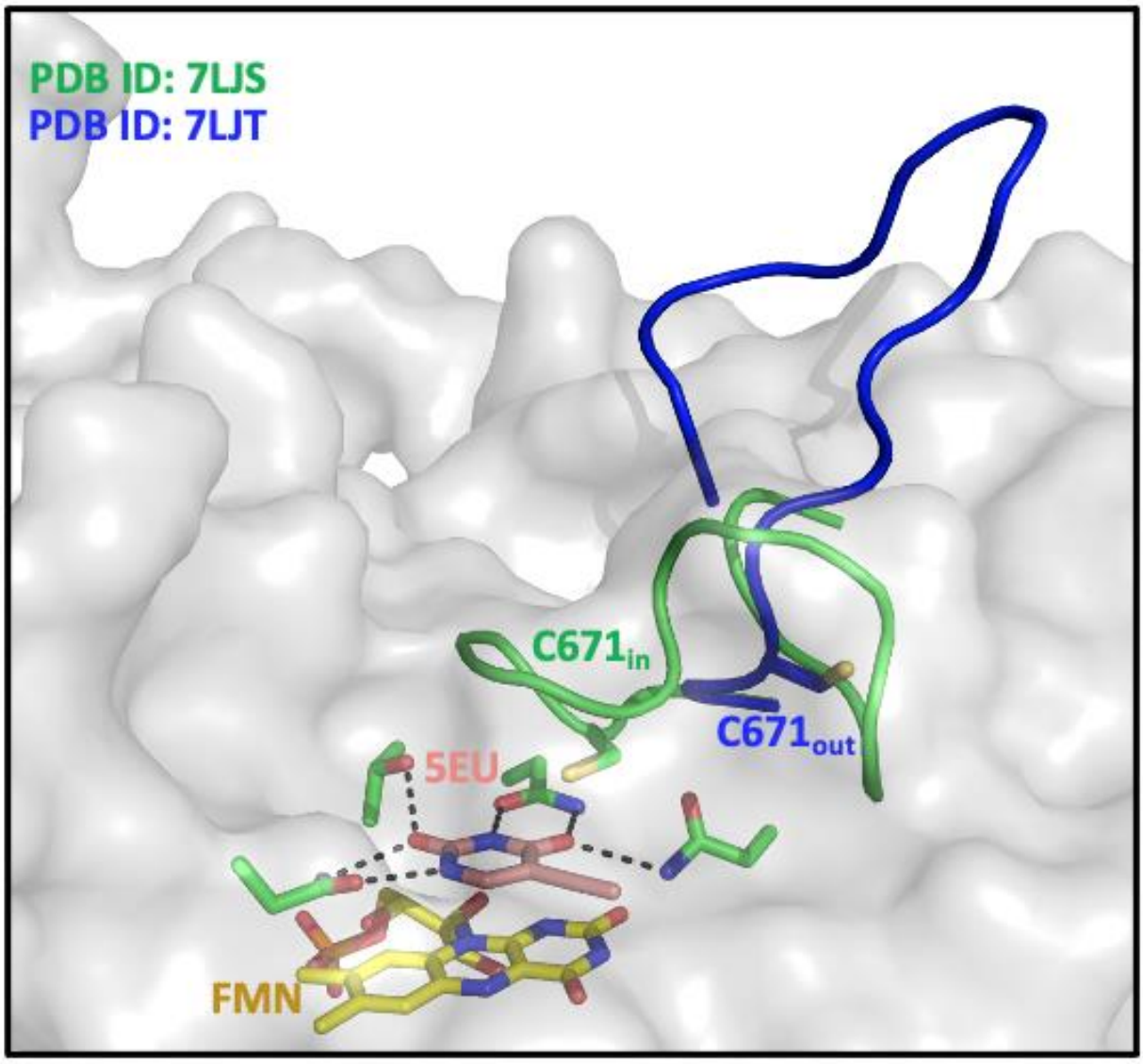

Dashed lines represent groups with hydrogen bonding distances (2.8-3.1 Å)

APPENDIX B

THE NADPH BINDING POSE OF THE DPD•5EU•NADP(H)$_{CLOSED}$ COMPLEX

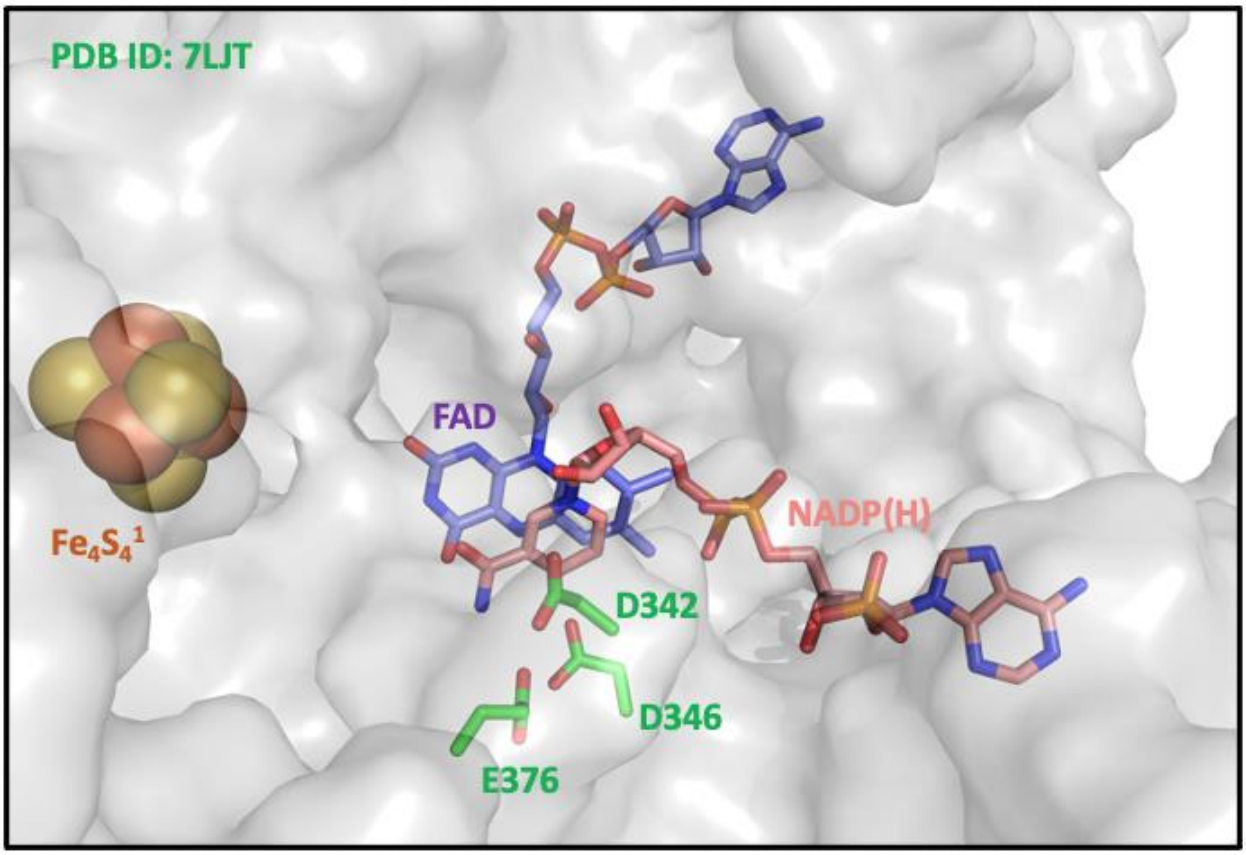
PDB ID: 7LJT
FAD
NADP(H)
Fe_4S_4 [1]
D342
D346
E376

APPENDIX C

THE URACIL BINDING ISOTHERM FOR DPD COVALENTLY ACTIVATED BY 5EU

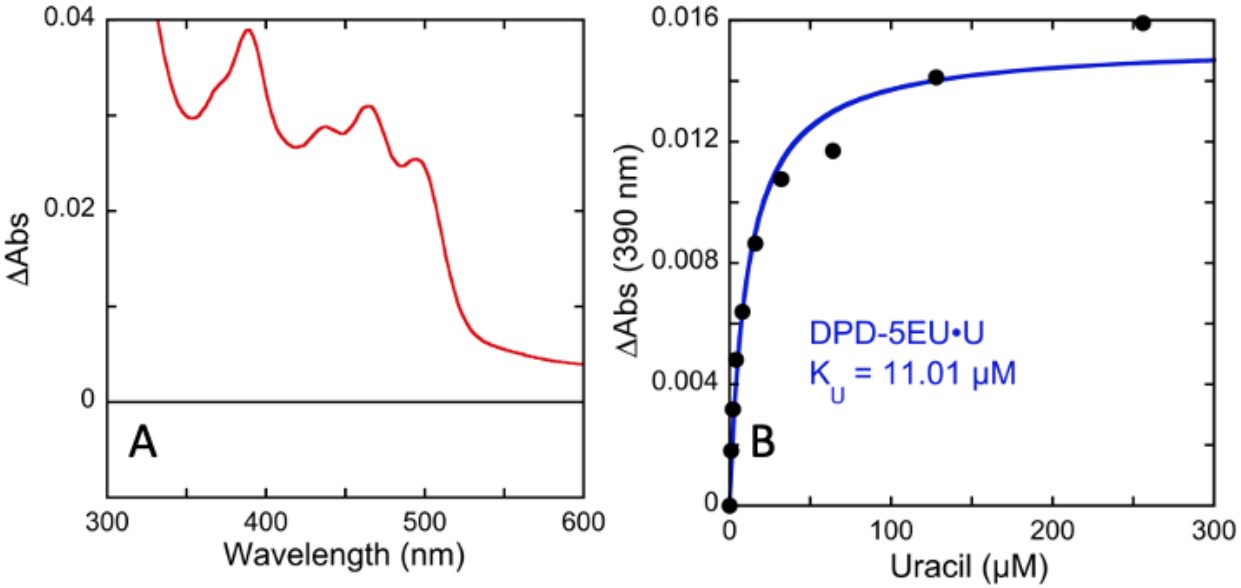

A. The difference spectrum observed when 6.6 μM DPD-5EU was mixed with 112 μM U. **B.** the ligand binding isotherm for 5.5 μM DPD-5EU titrated with U (1-256 μM), fit to the quadratic form of the single site binding equation (Equation 5).

APPENDIX D

CRYSTAL STRUCTURE OF THE ACTIVATED FORM OF THE DPD C671A VARIANT DPD-FMN(H_2) IN THE PRESENCE OF THYMINE AND NADPH

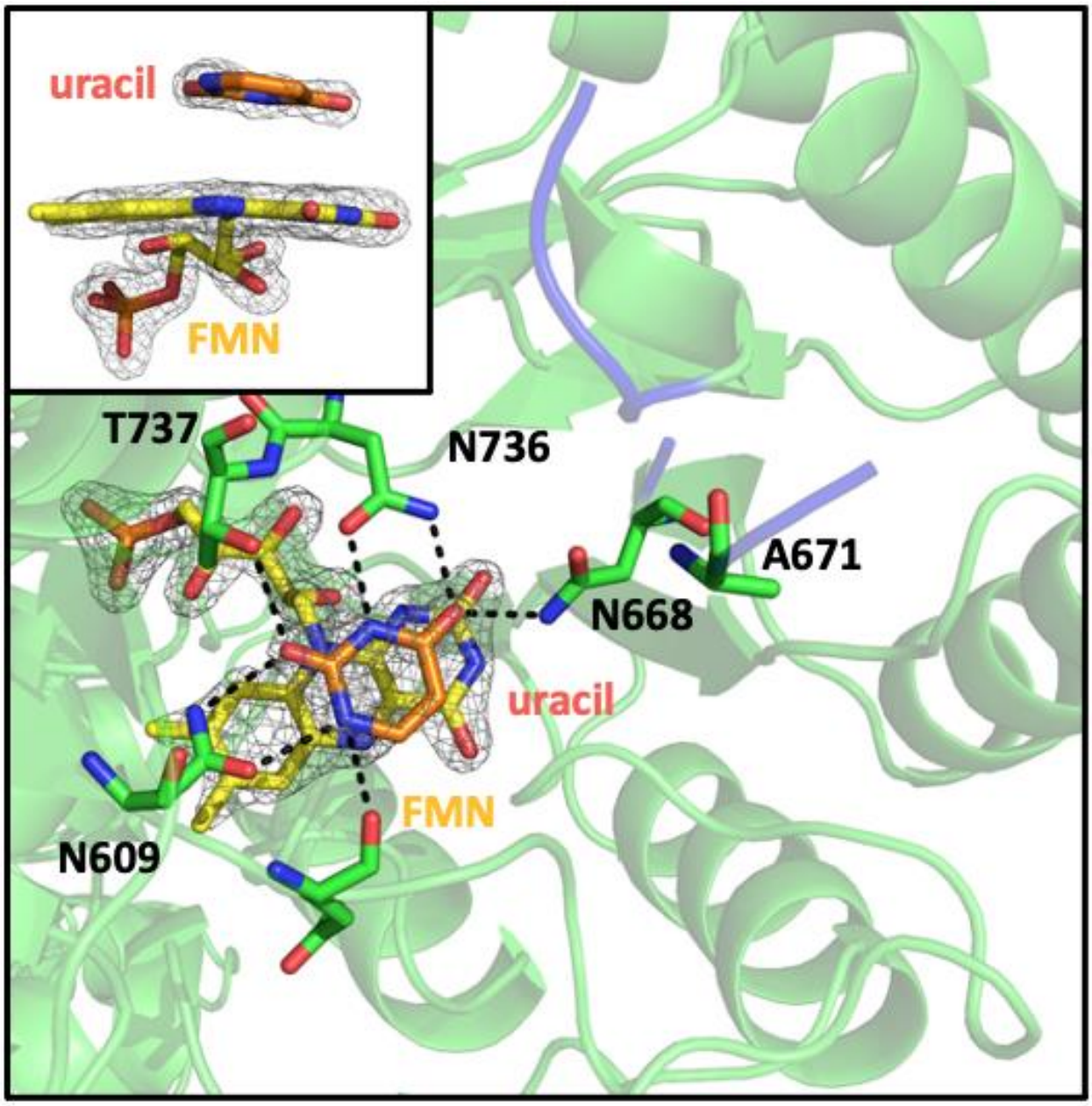

Omit map density was contoured at 2.0σ and generated by excluding, FAD, FMN, NADPH, thymine and A671 for the model.

REFERENCE LIST

[1] Lu, Z. H., Zhang, R., and Diasio, R. B. (1992) Purification and characterization of dihydropyrimidine dehydrogenase from human liver, *J Biol Chem 267*, 17102-17109.

[2] Podschun, B., Jahnke, K., Schnackerz, K. D., and Cook, P. F. (1993) Acid base catalytic mechanism of the dihydropyrimidine dehydrogenase from pH studies, *J Biol Chem 268*, 3407-3413.

[3] Podschun, B. (1992) Stereochemistry of NADPH oxidation by dihydropyrimidine dehydrogenase from pig liver, *Biochem Biophys Res Commun 182*, 609-616.

[4] Schmitt, U., Jahnke, K., Rosenbaum, K., Cook, P. F., and Schnackerz, K. D. (1996) Purification and characterization of dihydropyrimidine dehydrogenase from Alcaligenes eutrophus, *Arch Biochem Biophys 332*, 175-182.

[5] Podschun, B., Cook, P. F., and Schnackerz, K. D. (1990) Kinetic mechanism of dihydropyrimidine dehydrogenase from pig liver, *J Biol Chem 265*, 12966-12972.

[6] Porter, D. J., Chestnut, W. G., Taylor, L. C., Merrill, B. M., and Spector, T. (1991) Inactivation of dihydropyrimidine dehydrogenase by 5-iodouracil, *J Biol Chem 266*, 19988-19994.

[7] Dobritzsch, D., Ricagno, S., Schneider, G., Schnackerz, K. D., and Lindqvist, Y. (2002) Crystal structure of the productive ternary complex of dihydropyrimidine dehydrogenase with NADPH and 5-iodouracil. Implications for mechanism of inhibition and electron transfer, *J Biol Chem 277*, 13155-13166.

[8] Heidelberger, C., Chaudhuri, N. K., Danneberg, P., Mooren, D., Griesbach, L., Duschinsky, R., Schnitzer, R. J., Pleven, E., and Scheiner, J. (1957) Fluorinated pyrimidines, a new class of tumour-inhibitory compounds, *Nature 179*, 663-666.

[9] Rutman, R. J., Cantarow, A., Paschkis, E., and Allanoff, B. (1953) Studies on uracil utilization normal and acetaminofluorene-treated rats, *Science 117*, 282-283.

[10] Rutman, R. J., Cantarow, A., and Paschkis, K. E. (1954) Studies in 2-acetylaminofluorene carcinogenesis. III. The utilization of uracil-2-C14 by preneoplastic rat liver and rat hepatoma, *Cancer Res 14*, 119-123.

[11] Heidelberger, C. (1963) Biochemical Mechanisms of Action of Fluorinated Pyrimidines, *Exp Cell Res 24*, SUPPL9:462-471.

[12] Kent, R. J., and Heidelberger, C. (1972) Fluorinated pyrimidines. XL. The reduction of 5-fluorouridine 5'-diphosphate by ribonucleotide reductase, *Mol Pharmacol 8*, 465-475.

[13] Reilly, R. T., Barbour, K. W., Dunlap, R. B., and Berger, F. G. (1995) Biphasic binding of 5-fluoro-2'-deoxyuridylate to human thymidylate synthase, *Mol Pharmacol 48*, 72-79.

[14] Ludwiczak, J., Maj, P., Wilk, P., Fraczyk, T., Ruman, T., Kierdaszuk, B., Jarmula, A., and Rode, W. (2016) Phosphorylation of thymidylate synthase affects slow-binding inhibition by 5-fluoro-dUMP and N(4)-hydroxy-dCMP, *Mol Biosyst 12*, 1333-1341.

[15] Longley, D. B., Harkin, D. P., and Johnston, P. G. (2003) 5-fluorouracil: mechanisms of action and clinical strategies, *Nat Rev Cancer 3*, 330-338.

[16] Milano, G., and Etienne, M. C. (1994) Dihydropyrimidine dehydrogenase (DPD) and clinical pharmacology of 5-fluorouracil (review), *Anticancer Res 14*, 2295-2297.

[17] Heggie, G. D., Sommadossi, J. P., Cross, D. S., Huster, W. J., and Diasio, R. B. (1987) Clinical pharmacokinetics of 5-fluorouracil and its metabolites in plasma, urine, and bile, *Cancer Res 47*, 2203-2206.

[18] de Bono, J. S., and Twelves, C. J. (2001) The oral fluorinated pyrimidines, *Invest New Drugs 19*, 41-59.

[19] Porter, D. J., Chestnut, W. G., Merrill, B. M., and Spector, T. (1992) Mechanism-based inactivation of dihydropyrimidine dehydrogenase by 5-ethynyluracil, *J Biol Chem 267*, 5236-5242.

[20] Baccanari, D. P., Davis, S. T., Knick, V. C., and Spector, T. (1993) 5-Ethynyluracil (776C85): a potent modulator of the pharmacokinetics and antitumor efficacy of 5-fluorouracil, *Proc Natl Acad Sci U S A 90*, 11064-11068.

[21] Spector, T., Harrington, J. A., and Porter, D. J. (1993) 5-Ethynyluracil (776C85): inactivation of dihydropyrimidine dehydrogenase in vivo, *Biochem Pharmacol 46*, 2243-2248.

[22] Porter, D. J., Harrington, J. A., Almond, M. R., Lowen, G. T., Zimmerman, T. P., and Spector, T. (1994) 5-ethynyl-2(1H)-pyrimidinone: aldehyde oxidase-activation to 5-ethynyluracil, a mechanism-based inactivator of dihydropyrimidine dehydrogenase, *Biochem Pharmacol 47*, 1165-1171.

[23] Schnackerz, K. D., Dobritzsch, D., Lindqvist, Y., and Cook, P. F. (2004) Dihydropyrimidine dehydrogenase: a flavoprotein with four iron-sulfur clusters, *Biochim Biophys Acta 1701*, 61-74.

[24] Fagan, R. L., Jensen, K. F., Bjornberg, O., and Palfey, B. A. (2007) Mechanism of flavin reduction in the class 1A dihydroorotate dehydrogenase from Lactococcus lactis, *Biochemistry 46*, 4028-4036.

[25] Reis, R. A. G., Calil, F. A., Feliciano, P. R., Pinheiro, M. P., and Nonato, M. C. (2017) The dihydroorotate dehydrogenases: Past and present, *Arch Biochem Biophys 632*, 175-191.

[26] Stott, K., Saito, K., Thiele, D. J., and Massey, V. (1993) Old Yellow Enzyme. The discovery of multiple isozymes and a family of related proteins, *J Biol Chem 268*, 6097-6106.

[27] Dobritzsch, D., Schneider, G., Schnackerz, K. D., and Lindqvist, Y. (2001) Crystal structure of dihydropyrimidine dehydrogenase, a major determinant of the pharmacokinetics of the anti-cancer drug 5-fluorouracil, *EMBO J 20*, 650-660.

[28] Podschun, B., Wahler, G., and Schnackerz, K. D. (1989) Purification and characterization of dihydropyrimidine dehydrogenase from pig liver, *Eur J Biochem 185*, 219-224.

[29] Rosenbaum, K., Schaffrath, B., Hagen, W. R., Jahnke, K., Gonzalez, F. J., Cook, P. F., and Schnackerz, K. D. (1997) Purification, characterization, and kinetics of porcine recombinant dihydropyrimidine dehydrogenase, *Protein Expr Purif 10*, 185-191.

[30] Rosenbaum, K., Jahnke, K., Curti, B., Hagen, W. R., Schnackerz, K. D., and Vanoni, M. A. (1998) Porcine recombinant dihydropyrimidine dehydrogenase: comparison of the spectroscopic and catalytic properties of the wild-type and C671A mutant enzymes, *Biochemistry 37*, 17598-17609.

[31] Porter, D. J., and Spector, T. (1993) Dihydropyrimidine dehydrogenase. Kinetic mechanism for reduction of uracil by NADPH, *J Biol Chem 268*, 19321-19327.

[32] Shiotani, T., and Weber, G. (1981) Purification and properties of dihydrothymine dehydrogenase from rat liver, *J Biol Chem 256*, 219-224.

[33] Rosenbaum, K., Jahnke, K., Schnackerz, K. D., and Cook, P. F. (1998) Secondary tritium and solvent deuterium isotope effects as a probe of the reaction catalyzed by porcine recombinant dihydropyrimidine dehydrogenase, *Biochemistry 37*, 9156-9159.

[34] Lohkamp, B., Voevodskaya, N., Lindqvist, Y., and Dobritzsch, D. (2010) Insights into the mechanism of dihydropyrimidine dehydrogenase from site-directed mutagenesis targeting the active site loop and redox cofactor coordination, *Biochim Biophys Acta 1804*, 2198-2206.

[35] Porter, D. J. (1994) Dehalogenating and NADPH-modifying activities of dihydropyrimidine dehydrogenase, *J Biol Chem 269*, 24177-24182.

[36] Beaupre, B. A., Roman, J. V., and Moran, G. R. (2020) An improved method for the expression and purification of porcine dihydropyrimidine dehydrogenase, *Protein Expr Purif 171*, 105610.

[37] Moran, G. R. (2019) Anaerobic methods for the transient-state study of flavoproteins: The use of specialized glassware to define the concentration of dioxygen, *Methods Enzymol 620*, 27-49.

[38] Krakow, G., and Vennesland, B. (1961) The equilibrium constant of the dihydroorotic dehydrogenase reaction, *J Biol Chem 236*, 142-144.

[39] Rowland, P., Björnberg, O., Nielsen, F. S., Jensen, K. F., and Larsen, S. (1998) The crystal structure of Lactococcus lactis dihydroorotate dehydrogenase A complexed with the enzyme reaction product throws light on its enzymatic function, *Prot.Sci. 7*, 1269-1279.

[40] Nizam, S., Gazara, R. K., Verma, S., Singh, K., and Verma, P. K. (2014) Comparative structural modeling of six old yellow enzymes (OYEs) from the necrotrophic fungus Ascochyta rabiei: insight into novel OYE classes with differences in cofactor binding, organization of active site residues and stereopreferences, *PLoS One 9*, 1-13.

[41] Nizam, S., Verma, S., Borah, N. N., Gazara, R. K., and Verma, P. K. (2014) Comprehensive genome-wide analysis reveals different classes of enigmatic old yellow enzyme in fungi, *Sci Rep 4*, 1-11.

[42] Fagan, R. L., Nelson, M. N., Pagano, P. M., and Palfey, B. A. (2006) Mechanism of flavin reduction in class 2 dihydroorotate dehydrogenases, *Biochemistry 45*, 14926-14932.

[43] Dobritzsch, D., Persson, K., Schneider, G., and Lindqvist, Y. (2001) Crystallization and preliminary X-ray study of pig liver dihydropyrimidine dehydrogenase, *Acta Crystallogr D Biol Crystallogr 57*, 153-155.

[44] Helsper, J. T., and Demoss, E. V. (1964) Regional Intra-Arterial Infusion of 5-Fluorouracil for Cancer, *Surgery 56*, 340-348.

[45] Almersjo, O., Brandberg, A., and Gustavsson, B. (1975) Concentration of biologically active 5-fluorouracil in general circulation during continuous portal infusion in man: a preliminary report, *Cancer Lett 1*, 113-117.

[46] Amstutz, U., Froehlich, T. K., and Largiader, C. R. (2011) Dihydropyrimidine dehydrogenase gene as a major predictor of severe 5-fluorouracil toxicity, *Pharmacogenomics 12*, 1321-1336.

[47] Diasio, R. B., Beavers, T. L., and Carpenter, J. T. (1988) Familial deficiency of dihydropyrimidine dehydrogenase. Biochemical basis for familial pyrimidinemia and severe 5-fluorouracil-induced toxicity, *J Clin Invest 81*, 47-51.

[48] Harris, B. E., Carpenter, J. T., and Diasio, R. B. (1991) Severe 5-fluorouracil toxicity secondary to dihydropyrimidine dehydrogenase deficiency. A potentially more common pharmacogenetic syndrome, *Cancer 68*, 499-501.

[49] Rivera, E., Chang, J. C., Semiglazov, V., Burdaeva, O., Kirby, M. G., and Spector, T. (2014) Eniluracil plus 5-fluorouracil and leucovorin: treatment for metastatic breast cancer patients in whom capecitabine treatment rapidly failed, *Clin Breast Cancer 14*, 26-30.

[50] Levin, J., and Hohneker, J. (2000) Clinical development of eniluracil/fluorouracil: an oral treatment for patients with solid tumors, *Invest New Drugs 18*, 383-390.

[51] Diasio, R. B. (2002) Can eniluracil improve 5-fluorouracil therapy?, *Clin Colorectal Cancer 2*, 53.

[52] Schilsky, R. L., and Kindler, H. L. (2000) Eniluracil: an irreversible inhibitor of dihydropyrimidine dehydrogenase, *Expert Opin Investig Drugs 9*, 1635-1649.

[53] Baker, S. D. (2000) Pharmacology of fluorinated pyrimidines: eniluracil, *Invest New Drugs 18*, 373-381.

[54] Rowinsky, E. K. (1995) The suitability of selected new anticancer agents for infusional therapy and the effects of others on infusional therapy practices, *J Infus Chemother 5*, 173-178.

[55] Milano, G., Etienne, M. C., and Fischel, J. L. (1995) [Intratumoral dihydropyrimidine dehydrogenase and its inhibition: a new approach in the pharmacokinetics of 5-fluorouracil], *Ann Gastroenterol Hepatol (Paris) 31*, 103-105.

[56] Cao, S., Baccanari, D. P., Joyner, S. S., Davis, S. T., Rustum, Y. M., and Spector, T. (1995) 5-Ethynyluracil (776C85): effects on the antitumor activity and pharmacokinetics of tegafur, a prodrug of 5-fluorouracil, *Cancer Res 55*, 6227-6230.

[57] Baker, S. D., Diasio, R. B., O'Reilly, S., Lucas, V. S., Khor, S. P., Sartorius, S. E., Donehower, R. C., Grochow, L. B., Spector, T., Hohneker, J. A., and Rowinsky, E. K. (2000) Phase I and pharmacologic study of oral fluorouracil on a chronic daily schedule in combination with the dihydropyrimidine dehydrogenase inactivator eniluracil, *J Clin Oncol 18*, 915-926.

[58] Grem, J. L., Harold, N., Shapiro, J., Bi, D. Q., Quinn, M. G., Zentko, S., Keith, B., Hamilton, J. M., Monahan, B. P., Donavan, S., Grollman, F., Morrison, G., and Takimoto, C. H. (2000) Phase I and pharmacokinetic

trial of weekly oral fluorouracil given with eniluracil and low-dose leucovorin to patients with solid tumors, *J Clin Oncol 18*, 3952-3963.

[59] Schilsky, R. L., Bukowski, R., Burris, H., 3rd, Hochster, H., O'Rourke, M., Wall, J. G., Mani, S., Bonny, T., Levin, J., and Hohneker, J. (2000) A multicenter phase II study of a five-day regimen of oral 5-fluorouracil plus eniluracil with or without leucovorin in patients with metastatic colorectal cancer, *Ann Oncol 11*, 415-420.

[60] Skovsgaard, T., Davidson, N. G., Piccart, M. J., Richel, D. J., Bonneterre, J., Cirkel, D. T., Barton, C. M., and Eniluracil/Fluorouracil Breast Cancer Study, G. (2001) A phase II study of oral eniluracil/fluorouracil in patients with anthracycline-refractory or anthracycline- and taxane-refractory advanced breast cancer, *Ann Oncol 12*, 1255-1257.

[61] Leichman, C. G., Chansky, K., Macdonald, J. S., Doukas, M. A., Budd, G. T., Giguere, J. K., Abbruzzese, J. L., and Southwest Oncology, G. (2002) Biochemical modulation of 5-fluorouacil through dihydropyrimidine dehydrogenase inhibition: a Southwest Oncology Group phase II trial of eniluracil and 5-fluorouracil in advanced resistant colorectal cancer, *Invest New Drugs 20*, 419-424.

[62] Heslin, M. J., Yan, J., Weiss, H., Shao, L., Owens, J., Lucas, V. S., and Diasio, R. B. (2003) Dihydropyrimidine dehydrogenase (DPD) rapidly regenerates after inactivation by eniluracil (GW776C85) in primary and metastatic colorectal cancer, *Cancer Chemother Pharmacol 52*, 399-404.

[63] Diasio, R. B. (2002) An evolving role for oral fluoropyrimidine drugs, *J Clin Oncol 20*, 894-896.

[64] Saltz, L., Shimada, Y., and Khayat, D. (1996) CPT-11 (irinotecan) and 5-fluorouracil: a promising combination for therapy of colorectal cancer, *Eur J Cancer 32A Suppl 3*, S24-31.

[65] Kobayashi, K., Shinbara, A., Kamimura, M., Takeda, Y., Kudo, K., Kabe, J., Hibino, S., Hino, M., Shibuya, M., and Kudoh, S. (1998) Irinotecan (CPT-11) in combination with weekly administration of cisplatin (CDDP) for non-small-cell lung cancer, *Cancer Chemother Pharmacol 42*, 53-58.

[66] Rothenberg, M. L., Cox, J. V., DeVore, R. F., Hainsworth, J. D., Pazdur, R., Rivkin, S. E., Macdonald, J. S., Geyer, C. E., Jr., Sandbach, J.,

Wolf, D. L., Mohrland, J. S., Elfring, G. L., Miller, L. L., and Von Hoff, D. D. (1999) A multicenter, phase II trial of weekly irinotecan (CPT-11) in patients with previously treated colorectal carcinoma, *Cancer 85*, 786-795.

[67] Fujishiro, M., Shinkai, T., Fukuda, M., Tamura, T., Ohe, Y., Kunitoh, H., Nishiwaki, Y., Sekine, I., Fukuda, H., and Saijo, N. (2000) Phase I study of a weekly infusion of irinotecan hydrochloride (CPT-11) and a 14-day continuous infusion of etoposide in patients with lung cancer: JCOG trial 9408, *Jpn J Clin Oncol 30*, 487-493.

[68] Spector, T., and Cao, S. (2010) A possible cause and remedy for the clinical failure of 5-fluorouracil plus eniluracil, *Clin Colorectal Cancer 9*, 52-54.

[69] Barr, P. J., Jones, A. S., and Walker, R. T. (1976) Incorporation of 5-substituted uracil derivatives into nucleic acids. Part IV. The synthesis of 5-ethynyluracil, *Nucleic Acids Res 3*, 2845-2849.

[70] Schroeder, A. C., Bloch, A., Perman, J. L., and Bobek, M. (1982) Synthesis and biological evaluation of 6-ethynyluracil, a thiol-specific alkylating pyrimidine, *J Med Chem 25*, 1255-1258.

[71] Beaupre, B. A., Hoag, M. R., Roman, J., Forsterling, F. H., and Moran, G. R. (2015) Metabolic Function for Human Renalase: Oxidation of Isomeric Forms of beta-NAD(P)H that Are Inhibitory to Primary Metabolism, *Biochemistry 54*, 795-806.

[72] Beaupre, B. A., Forouzesh, D. C., and Moran, G. R. (2020) Transient-State Analysis of Porcine Dihydropyrimidine Dehydrogenase Reveals Reductive Activation by NADPH, *Biochemistry 59*, 2419-2431.

[73] Holzer, W., Shirdel, J., Zirak, P., Penzkofer, A., Hegemann, P., Deutzmann, R., and Hochmuth, E. (2005) Photo-induced degradation of some flavins in aqueous solution, *Chemical Physics 308*, 69-78.

[74] Winter, G. (2010) xia2: an expert system for macromolecular crystallography data reduction, *J Appl Crystallogr 43*, 186-190.

[75] Winn, M. D., Ballard, C. C., Cowtan, K. D., Dodson, E. J., Emsley, P., Evans, P. R., Keegan, R. M., Krissinel, E. B., Leslie, A. G., McCoy, A., McNicholas, S. J., Murshudov, G. N., Pannu, N. S., Potterton, E. A., Powell, H. R., Read, R. J., Vagin, A., and Wilson, K. S. (2011)

Overview of the CCP4 suite and current developments, *Acta Crystallogr D Biol Crystallogr 67*, 235-242.

[76] Liebschner, D., Afonine, P. V., Baker, M. L., Bunkoczi, G., Chen, V. B., Croll, T. I., Hintze, B., Hung, L. W., Jain, S., McCoy, A. J., Moriarty, N. W., Oeffner, R. D., Poon, B. K., Prisant, M. G., Read, R. J., Richardson, J. S., Richardson, D. C., Sammito, M. D., Sobolev, O. V., Stockwell, D. H., Terwilliger, T. C., Urzhumtsev, A. G., Videau, L. L., Williams, C. J., and Adams, P. D. (2019) Macromolecular structure determination using X-rays, neutrons and electrons: recent developments in Phenix, *Acta Crystallogr D Struct Biol 75*, 861-877.

[77] McCoy, A. J., Grosse-Kunstleve, R. W., Adams, P. D., Winn, M. D., Storoni, L. C., and Read, R. J. (2007) Phaser crystallographic software, *J Appl Crystallogr 40*, 658-674.

[78] Emsley, P., Lohkamp, B., Scott, W. G., and Cowtan, K. (2010) Features and development of Coot, *Acta Crystallogr D Biol Crystallogr 66*, 486-501.

[79] Lowe, A. B. (2014) Thiol-yne 'click'/coupling chemistry and recent applications in polymer and materials synthesis and modification, *Polymer 55*, 5517-5549.

[80] Hoag, M. R., Roman, J., Beaupre, B. A., Silvaggi, N. R., and Moran, G. R. (2015) Bacterial Renalase: Structure and Kinetics of an Enzyme with 2- and 6-Dihydro-beta-NAD(P) Oxidase Activity from Pseudomonas phaseolicola, *Biochemistry 54*, 3791-3802.

[81] Lowry, O. H., Passonneau, J. V., and Rock, M. K. (1961) The stability of pyridine nucleotides, *The Journal of biological chemistry 236*, 2756-2759.

[82] Rohr, A. K., Hersleth, H. P., and Andersson, K. K. (2010) Tracking flavin conformations in protein crystal structures with Raman spectroscopy and QM/MM calculations, *Angew Chem Int Ed Engl 49*, 2324-2327.

[83] Moloney, M., Faulkner, D., Link, E., Rischin, D., Solomon, B., Lim, A. M., Zalcberg, J. R., Jefford, M., and Michael, M. (2018) Feasibility of 5-fluorouracil pharmacokinetic monitoring using the My-5FU PCM system in a quaternary oncology centre, *Cancer Chemother Pharmacol 82*, 865-876.

[84] Dulchavsky, M., Clark, C. T., Bardwell, J. C. A., and Stull, F. (2021) A cytochrome c is the natural electron acceptor for nicotine oxidoreductase, *Nature chemical biology 17*, 344-350.

[85] Abramovitz, A. S., and Massey, V. (1976) Interaction of phenols with old yellow enzyme physical evidence for charge-transfer complexes, *J.Biol.Chem. 251*, 5327-5336.

[86] Ellis, K. J., and Morrison, J. F. (1982) Buffers of constant ionic strength for studying pH-dependent processes, *Methods Enzymol 87*, 405-426.

[87] Rubinson, K. (2017) Practical corrections for p(H,D) measurements in mixed H2O/D2O biological buffers, *Anal. Methods 9*, 2744-2750.

[88] Cleland, W. W. (1982) The use of pH studies to determine chemical mechanisms of enzyme-catalyzed reactions, *Methods Enzymol 87*, 390-405.

[89] Volk, A., and Kahler, C. J. (2018) Density model for aqueous glycerol solutions, *Exp Fluids 59*, Article 75.

[90] Venkatasubban, K. S., and Schowen, R. L. (1984) The proton inventory technique. 1. Introduction to proton inventories, *CRC Critical Rev.in Biochem. 17*, 1-44.

[91] Kohen, A., and Limbach, H. (2006) *Isotope Effects in Chemistry and Biology*, Vol. 1096, CRC Press.

[92] Kresge, A. (1964) Solvent isotope effect in H2O-D2O mixtures, *Pure and Appl. Chemistry 8*, 15.

[93] Holzerm, W., Shirdel, J., Zirak, P., Penzkoferm, A., Hegemann, P., Deutzmann, R., and Hochmuth, E. (2005) Photo-induced degradation of some flavins in aqueous solution, *Chemical Physics 308*, 69-78.

[94] Forouzesh, D. C., Beaupre, B. A., Butrin, A., Wawrzak, Z., Liu, D., and Moran, G. R. (2021) The Interaction of Porcine Dihydropyrimidine Dehydrogenase with the Chemotherapy Sensitizer: 5-Ethynyluracil, *Biochemistry 60*, 1120-1132.

[95] Yalloway, G. N., Mayhew, S. G., Malthouse, J. P., Gallagher, M. E., and Curley, G. P. (1999) pH-dependent spectroscopic changes associated

with the hydroquinone of FMN in flavodoxins, *Biochemistry 38*, 3753-3762.

[96] Gadda, G., and Sobrado, P. (2018) Kinetic Solvent Viscosity Effects as Probes for Studying the Mechanisms of Enzyme Action, *Biochemistry 57*, 3445-3453.

[97] Massey, V., and Ghisla, S. (1974) Role of charge transfer interactions in flavoprotein catalysis, *Annals of the New York Academy of Sciences 227*, 446-465.

[98] Forouzesh, D. C., Beaupre, B. A., Butrin, A., Wawrzak, Z., Liu, D., and Moran, G. R. (2021) The Interaction of Porcine Dihydropyrimidine Dehydrogenase with the Chemotherapy Sensitizer: 5-Ethynyluracil, *Biochemistry*.

[99] Mhaidat, N. M., Bouklihacene, M., and Thorne, R. F. (2014) 5-Fluorouracil-induced apoptosis in colorectal cancer cells is caspase-9-dependent and mediated by activation of protein kinase C-delta, *Oncol Lett 8*, 699-704.

[100] Ponce-Cusi, R., and Calaf, G. M. (2016) Apoptotic activity of 5-fluorouracil in breast cancer cells transformed by low doses of ionizing alpha-particle radiation, *Int J Oncol 48*, 774-782.

[101] Goirand, F., Lemaitre, F., Launay, M., Tron, C., Chatelut, E., Boyer, J. C., Bardou, M., and Schmitt, A. (2018) How can we best monitor 5-FU administration to maximize benefit to risk ratio?, *Expert Opin Drug Metab Toxicol 14*, 1303-1313.

[102] Tuchman, M., Stoeckeler, J. S., Kiang, D. T., O'Dea, R. F., Ramnaraine, M. L., and Mirkin, B. L. (1985) Familial pyrimidinemia and pyrimidinuria associated with severe fluorouracil toxicity, *N Engl J Med 313*, 245-249.

[103] van Kuilenburg, A. B., Haasjes, J., Richel, D. J., Zoetekouw, L., Van Lenthe, H., De Abreu, R. A., Maring, J. G., Vreken, P., and van Gennip, A. H. (2000) Clinical implications of dihydropyrimidine dehydrogenase (DPD) deficiency in patients with severe 5-fluorouracil-associated toxicity: identification of new mutations in the DPD gene, *Clin Cancer Res 6*, 4705-4712.

[104] Baker, S. D., Khor, S. P., Adjei, A. A., Doucette, M., Spector, T., Donehower, R. C., Grochow, L. B., Sartorius, S. E., Noe, D. A.,

Hohneker, J. A., and Rowinsky, E. K. (1996) Pharmacokinetic, oral bioavailability, and safety study of fluorouracil in patients treated with 776C85, an inactivator of dihydropyrimidine dehydrogenase, *J Clin Oncol 14*, 3085-3096.

[105] Desmoulin, F., Gilard, V., Malet-Martino, M., and Martino, R. (2002) Metabolism of capecitabine, an oral fluorouracil prodrug: (19)F NMR studies in animal models and human urine, *Drug Metab Dispos 30*, 1221-1229.

[106] Diasio, R. B. (2000) Oral DPD-inhibitory fluoropyrimidine drugs, *Oncology (Williston Park) 14*, 19-23.

[107] Beinert, H., Holm, R. H., and Munck, E. (1997) Iron-sulfur clusters: nature's modular, multipurpose structures, *Science 277*, 653-659.

[108] Ziegler, G. A., Vonrhein, C., Hanukoglu, I., and Schulz, G. E. (1999) The structure of adrenodoxin reductase of mitochondrial P450 systems: electron transfer for steroid biosynthesis, *J Mol Biol 289*, 981-990.

[109] Muller, J. J., Lapko, A., Bourenkov, G., Ruckpaul, K., and Heinemann, U. (2001) Adrenodoxin reductase-adrenodoxin complex structure suggests electron transfer path in steroid biosynthesis, *J Biol Chem 276*, 2786-2789.

[110] Vanoni, M. A. (2021) Iron-sulfur flavoenzymes: the added value of making the most ancient redox cofactors and the versatile flavins work together, *Open biology 11*, 210010.

[111] Lolis, E., Alber, T., Davenport, R. C., Rose, D., Hartman, F. C., and Petsko, G. A. (1990) Structure of yeast triosephosphate isomerase at 1.9-A resolution, *Biochemistry 29*, 6609-6618.

[112] Beaupre, B. A., Forouzesh, D. C., Butrin, A., Liu, D., and Moran, G. R. (2021) Perturbing the Movement of Hydrogens to Delineate and Assign Events in the Reductive Activation and Turnover of Porcine Dihydropyrimidine Dehydrogenase, *Biochemistry 60*, 1764-1775.

[113] Rowland, P., Nielsen, F. S., Jensen, K. F., and Larsen, S. (1997) The crystal structure of the flavin containing enzyme dihydroorotate dehydrogenase A from Lactococcus lactis, *Structure 5*, 239-252.

[114] Hagen, W. R., Vanoni, M. A., Rosenbaum, K., and Schnackerz, K. D. (2000) On the iron-sulfur clusters in the complex redox enzyme dihydropyrimidine dehydrogenase, *Eur J Biochem 267*, 3640-3646.

[115] Pai, E. F., and Schulz, G. E. (1983) The catalytic mechanism of glutathione reductase as derived from x-ray diffraction analyses of reaction intermediates, *J Biol Chem 258*, 1752-1757.

[116] Fink, K., Henderson, R. B., and Fink, R. M. (1952) -Aminoisobutyric acid in rat urine following administration of pyrimidines, *J Biol Chem 197*, 441-452.

[117] Fink, R. M., Fink, K., and Henderson, R. B. (1953) beta-amino acid formation by tissue slices incubated with pyrimidines, *J Biol Chem 201*, 349-355.

[118] Dorsett, M. T., Morse, P. A., Jr., and Gentry, G. A. (1969) Inhibition of rat dihydropyrimidine dehydrogenase by 5-cyanouracil in vitro, *Cancer Res 29*, 79-82.

[119] Gibson, Q. H., Swoboda, B. E. P., and Massey, V. (1964) Kinetics and mechanism of action of glucose oxidase, *J.Biol.Chem. 239*, 3927-3934.

[120] Paff, M. T., Baccanari, D. P., Davis, S. T., Cao, S., Tansik, R. L., Rustum, Y. M., and Spector, T. (2000) Preclinical development of eniluracil: enhancing the therapeutic index and dosing convenience of 5-fluorouracil, *Invest New Drugs 18*, 365-371.

[121] Yip, D., Karapetis, C., Strickland, A. H., Steer, C., Holford, C., Knight, S., and Harper, P. (2003) A dose-escalating study of oral eniluracil/5-fluorouracil plus oxaliplatin in patients with advanced gastrointestinal malignancies, *Ann Oncol 14*, 864-866.

[122] Czito, B. G., Hong, T. J., Cohen, D. P., Tyler, D. S., Lee, C. G., Anscher, M. S., Ludwig, K. A., Seigler, H. F., Mantyh, C., Morse, M. A., Lockhart, A. C., Petros, W. P., Honeycutt, W., Spector, N. L., Ertel, P. J., Mangum, S. G., and Hurwitz, H. I. (2004) A Phase I trial of preoperative eniluracil plus 5-fluorouracil and radiation for locally advanced or unresectable adenocarcinoma of the rectum and colon, *Int J Radiat Oncol Biol Phys 58*, 779-785.

VITA

Dr. Dariush Forouzesh grew up in Elmwood Park, Illinois. He attended Loyola University Chicago for an undergraduate degree, obtaining a Bachelor of Science in Biochemistry and graduating with honors in 2016 before returning to begin his research career in the laboratory of Dr. Graham R. Moran in 2018. Over the next 5 years Dr. Forouzesh studied the chemical mechanism of the antineoplastic desensitizer, dihydropyrimidine dehydrogenase and published three research articles and one review that collectively redefine the understanding of how this enzyme operates. In that time, he presented seven posters on the topic at the Midwest Enzyme Chemistry Conference, the Southeast Enzyme Conference, the Enzyme Mechanisms Conference and the Gordon Research Conference. He also assisted in teaching several general chemistry labs and an introductory biochemistry lab in addition to mentoring undergraduates in research techniques. Dr. Forouzesh was awarded the 2022 Arthur J. Schmitt Fellowship in recognition of exceptional leadership qualities and skill within his field.